THE UNIVERSITY OF CHICAGO

WITHDRAWAL OF β-CATENIN IN AN INDUCIBLE GENETICALLY ENGINEERED MOUSE MODEL RESTORES T CELL INFILTRATION BUT NOT CHECKPOINT BLOCKADE EFFICACY

A DISSERTATION SUBMITTED TO
THE FACULTY OF THE DIVISION OF THE BIOLOGICAL SCIENCES
AND THE PRITZKER SCHOOL OF MEDICINE
IN CANDIDACY FOR THE DEGREE OF
DOCTOR OF PHILOSOPHY

COMMITTEE ON IMMUNOLOGY

BY
ALEXANDRA CABANOV

CHICAGO, ILLINOIS
JUNE 2024

To mom, my first and forever inspiration - you were not only my pillar of strength but also my best friend and most ardent supporter. From a very young age, you fostered my curiosity and ignited a passion for scientific exploration by setting up my first home laboratory. You nurtured my love for science with the same tenderness with which you nurtured me. I carry your spirit in every step of my journey and in every line of this thesis.

Mi-e dor de tine, mami.

The speed of your success is limited only by your dedication and what you're willing to sacrifice. **- Nathan W. Morris**

TABLE OF CONTENTS

LIST OF FIGURES

LIST OF TABLES

ACKNOWLEDGMENTS

The journey to complete this dissertation has been filled with countless hours of hard work, endless curiosity, and invaluable lessons. Throughout this time, I've been fortunate to be supported by many individuals who offered their wisdom, encouragement, and belief in my potential. Their contributions have not just shaped the work presented in this thesis, but have also profoundly shaped me as a person and a scientist.

To my mentor, Tom Gajewski, your boundless enthusiasm for scientific inquiry is nothing short of infectious, and I am deeply grateful for the privilege of having such a motivating mentor. Throughout these years, I have accrued an immense debt of gratitude to you, not only for your support on both personal and professional fronts but also for your unyielding belief in my abilities, consistently driving me to become a more proficient scientist. Your relentless dedication to honing my skills as a storyteller has imparted the invaluable lesson that clear and articulate communication is perhaps one of the most vital aspects of the scientific pursuit.

To my fellow lab members, both past and present, thank you for creating an environment that feels more like a second home than just a workplace. Blake, Jess, Kyle, and Emily, your readiness to assist and your camaraderie made those long days and nights in the lab so much more enjoyable. Jay, your kindness and patience have left a lasting impact on me, and your presence at my wedding in Romania was a gesture I hold close to my heart.

To Andrea and Jon, your mentorship played a major role in making my PhD journey smoother and more rewarding. Your guidance and countless hours of engaging scientific discussions have been instrumental in my success. I cannot thank you enough for your mentorship, and I am confident that both of you will excel as future principal investigators.

To the emerging talents within the Gajewski lab, Ruxandra, Cole, Yaoping, Anna and Stephen. You all not only breathed life back into our lab after the pandemic but also fearlessly plunged into late-night experiments, your courage and determination is nothing

short of awe-inspiring. A special shout out to Ruxandra, our Romanian roots lead to an instant bond. You are incredibly talented and hardworking, and I cannot wait to see what you achieve because you will be unstoppable.

To Vyara, Shuyin, Santiago, and Tyler, you guys are an amazing group of scientists and have all become dear friends. Last but not least, to Athalia, words cannot convey the gratitude I feel for having met you. I never imagined finding a sister during this Ph.D., but I would not have made it without you and I cannot wait for our kids to grow up together.

To my friends outside academia, I thank you all for your support. Andrey and Reni, I am so thankful for always being there for me with a kind word or just to listen when I was yet again down about an experiment not working. I could always count on you, and I do not take that for granted.

To my incredible family, thank you for the countless hours you've spent on the phone with me, keeping me company through many long nights in the lab. I owe you an immeasurable debt of gratitude for your boundless love and unwavering support throughout this journey. Moni, un intreg ocean ne desparte dar nici nu simt. Esti mereu in inima mea, in gandul meu si esti mereu acolo cu o vorba calda sau o gluma. Nu stiu ce m-asi face fara tine. Tati, iti multumesc din toata inima pentru ca mereu mi-ai fost alaturi si m-ai sustinut. David, de abia astept sa te vad realizat. Ai tot ce-ti trebuie sa fii successful!

During my thesis journey, I experienced the loss of my mother, married my best friend, and welcomed the most beautiful and kind-hearted child into our lives. This journey has been both long and arduous, but with you by my side, it has also been profoundly beautiful.

To my incredible husband, I never thought I would be so fortunate to marry my best friend. Your kindness and patience know no bounds and I am immensely grateful for all that you do for our little family. Words cannot adequately convey the depth of gratitude I feel for your support. To my sweet Lillian, you have been a beacon of light and happiness in a time of much pain and struggle. Your smiles and unconditional love motivate me every day,

and I aspire to be the role model you deserve. My little family, I could not imagine life any differently, and I am thankful for you both every day.

ABSTRACT

Checkpoint blockade immunotherapy (CBI) is a cornerstone of modern cancer treatment, but efficacy is not universal, partly due to a wide variation in baseline immune cell infiltration in the tumor microenvironment (TME). One mechanism contributing to this variability is tumor cell-intrinsic activation of the β-catenin signaling pathway, which has been shown to drive a non-T cell-inflamed TME leading to a loss of therapeutic efficacy of a range of immunotherapies. There is great interest in drugging the Wnt/β-catenin pathway in an effort to restore immune interactions in β-catenin-active tumors. As a proof-of-concept, we reasoned that a genetic experiment eliminating β-catenin expression after establishment of a non-T cell-inflamed TME would illustrate the maximal biologic effect that could be expected with total blockade of the pathway. We developed a genetically engineered mouse (GEM) model that allows for dynamic regulation of β-catenin on and off via doxycycline. We observed that administration of doxycycline resulted in robust nuclear accumulation of melanocyte-specific β-catenin which was accompanied by a reduction in $CD3^+$ T cell infiltration. Discontinuing doxycycline treatment led to loss of nuclear β-catenin expression, associated with a substantial return of $CD3^+$ T cells into the TME. However, despite the re-infiltration of $CD3^+$ T cells, the tumors previously expressing β-catenin did not regain therapeutic responsiveness to anti-CTLA-4 plus anti-PD-L1 therapy. Single cell RNA sequencing of the ex-β-catenin tumors indicated the enrichment of an immunosuppressive-like macrophage population, characterized by the expression of Ccl8, Gas6, Cd163 and Cd209g. Moreover, spatial transcriptomic analysis demonstrated that $CD3^+$ T cells are in close contact with these M2-like macrophages, likely resulting in their inhibition. This finding suggests that the prior presence of β-catenin may induce long-lasting changes in the TME that continue to suppress the immune response even after β-catenin levels are reduced, having important therapeutic implications.

CHAPTER 1

INTRODUCTION

1.1 From melanocyte activation to metastatic progression

Melanoma accounts for only 1.7% of all skin cancers, however it is the leading cause of all skin cancer-related deaths. With a five-year survival rate seen in approximately 94% of all patients with localized primary melanoma, this prognosis has been reported to drop to less than 18% once the disease progresses to metastasis [1].

1.1.1 UV radiation and melanoma

Melanoma emerges from melanocytes, a cell type that resides within the skin's basal layer and gives our skin its color. Ultraviolet (UV) radiation is a major player in the development of melanoma and the factor responsible for approximately half of all skin cancers. Exposure to UV radiation initiates a cellular cascade that induces carcinogenesis, but also protection via melanin production [2]. UV radiation activates keratinocyte which in turn activates melanocytes via the melanocyte-stimulating hormone (MSH)/melanocortin receptor 1 (MC1R) signaling pathway. This signaling cascade kick-starts the production and release of melanin within melanocytes. While melanin is responsible for skin pigmentation, it also plays a major role as a photoprotective agent by absorbing and dispersing UV radiation [3]. Melanin acts as a shield to help protect cellular DNA from UV-induced damage. Melanin's multiple roles within the cell emphasize its essential part in maintaining skin health and preventing melanoma [4, 5].

Downstream from the activation of the MSH/MC1R pathway, the activation of the microphthalmia-associated transcription factor (MITF) has been demonstrated to be essential for melanocyte development and is also linked to melanoma progression [6, 7]. MITF is involved in regulating the expression of key survival proteins in melanocytes and melanoma

cells, such as anti-apoptotic proteins BCL2 and BCL2A1, and the cell cycle regulator CDK2. Additionally, MITF overexpression has been shown to increase the risk of developing melanoma [8].

1.1.2 The path to malignant melanoma

BRAF and NRAS mutations rank among the most prevalent genetic alterations in primary tumors, with BRAF playing a leading role in melanoma generation [9]. Activating mutations in BRAF are detected in up to 80% of benign nevi; however, alone these are not sufficient to gain a malignant phenotype [4]. It is the acquisition of further mutations, particularly the loss-of-function alterations in tumor suppressor genes, that triggers transformation into malignant melanoma. Among these, the inactivation of the tumor suppressor genes PTEN and p53 are some of the frequent mutations strongly linked to the aggressive and invasive characteristics of metastatic melanoma (MM) [10, 11]. It has been reported that the second most common genetic change linked to the non-T-cell inflamed phenotype in MM is the loss of PTEN. [12].

Approximately 50% of both primary and metastatic melanomas present with BRAF mutations, with over 90% consisting of a specific mutation - a valine to glutamate change at position 600 - which significantly increases the enzyme's activity [13, 9]. Moreover, activating mutations in BRAF typically occur early in the development of melanoma, whereas loss of PTEN has been shown to accumulated over the course of the disease making it more common in advanced stages of melanomas and metastasis [14, 15]. Interestingly, mutations in both PTEN and BRAF have been shown to co-occur, suggesting that PTEN silencing is a potential predicting factor of BRAF inhibitor therapy resistance [16].

1.2 The tumor microenvironment

In both the clinic and in laboratory settings, solid tumors are often classified into distinct categories based on their spontaneous immune infiltration at baseline. This categorization is primarily into two main groups: the T cell-inflamed and the non-T cell-inflamed tumors [17, 18]. Characterization of 31 solid tumor types using the TCGA dataset, identified approximately one third of all human tumor samples as non-T-cell-inflamed. Similarly, approximately one third of the remaining tumors were identified as T-cell-inflamed [19]. This baseline immune infiltrate within solid tumors has been shown to not only be a critical predictor of overall survival but is also predictive of responsiveness to checkpoint blockade immunotherapy.

1.2.1 The T cell-inflamed tumor microenvironment

The T cell-inflamed tumor microenvironment is characterized by a complex immune landscape. Central to the T cell-inflamed tumor is the spontaneous infiltration of $CD8^+$ T cells at baseline. This phenotype usually is accompanied by an augmented expression of cytokines and chemokines necessary for a successful adaptive immune response [20, 21]. Furthermore, these tumors are often characterized by a dominant type I interferon (IFN) transcriptional signature, indicative of innate immune pathway activation. As a consequence of this ongoing tissue-based adaptive immune response, many immunosuppressive mechanisms become upregulated such as augmented PD-L1 expression on tumor cells and increased infiltration of regulatory $FoxP3^+$ T cells, apparently as a negative feedback loop to control chronic inflammation [22].

Preclinical mouse studies combined with correlative data from human tumor samples have identified several key steps involved with the spontaneous generation of a T cell-inflamed tumor microenvironment. One critical cell population is Batf3-lineage dendritic cells (DCs). These cells acquire tumor antigens and subsequently migrate to the tumor-draining lymph

node, where they prime and activate naïve $CD8^+$ T cells. This leads to their activation and differentiation into cytotoxic effector cells, which exit the lymph node an have the opportunity to traffic back into the tumor site (Fig 1.1). Batf3 DCs are also pivotal in this step, as they produce chemokines such as CXCL9 and CXCL10 that facilitate recruitment of activated $CD8^+$ T cells within the tumor microenvironment (TME) [23, 24]. However, once these T cells infiltrate, they become functionally dampened by negative regulatory pathways that ultimately enable tumor growth.

Nonetheless, the presence of these mechanisms within T cell-inflamed tumors forms the basis of their sensitivity to immunotherapy. Immunotherapies take advantage of the pre-existing immune response by re-engaging the immune system to recognize and destroy cancer cells, currently by blockade of negative regulatory pathways. The responsiveness of the T cell-inflamed tumors to checkpoint inhibitions can be attributed to the immune activities facilitated by the action of Batf3 DCs, infiltration with $CD8^+$ T cells, and the complex network of chemokines and cytokines already present within the tumor which can be leveraged against the tumor. This complex interplay of immune responses within the TME reflects a significant effort by the immune system to counteract the tumor, despite the ultimate evasion from immune detection and destruction via inhibitory pathways (Fig 1.3).

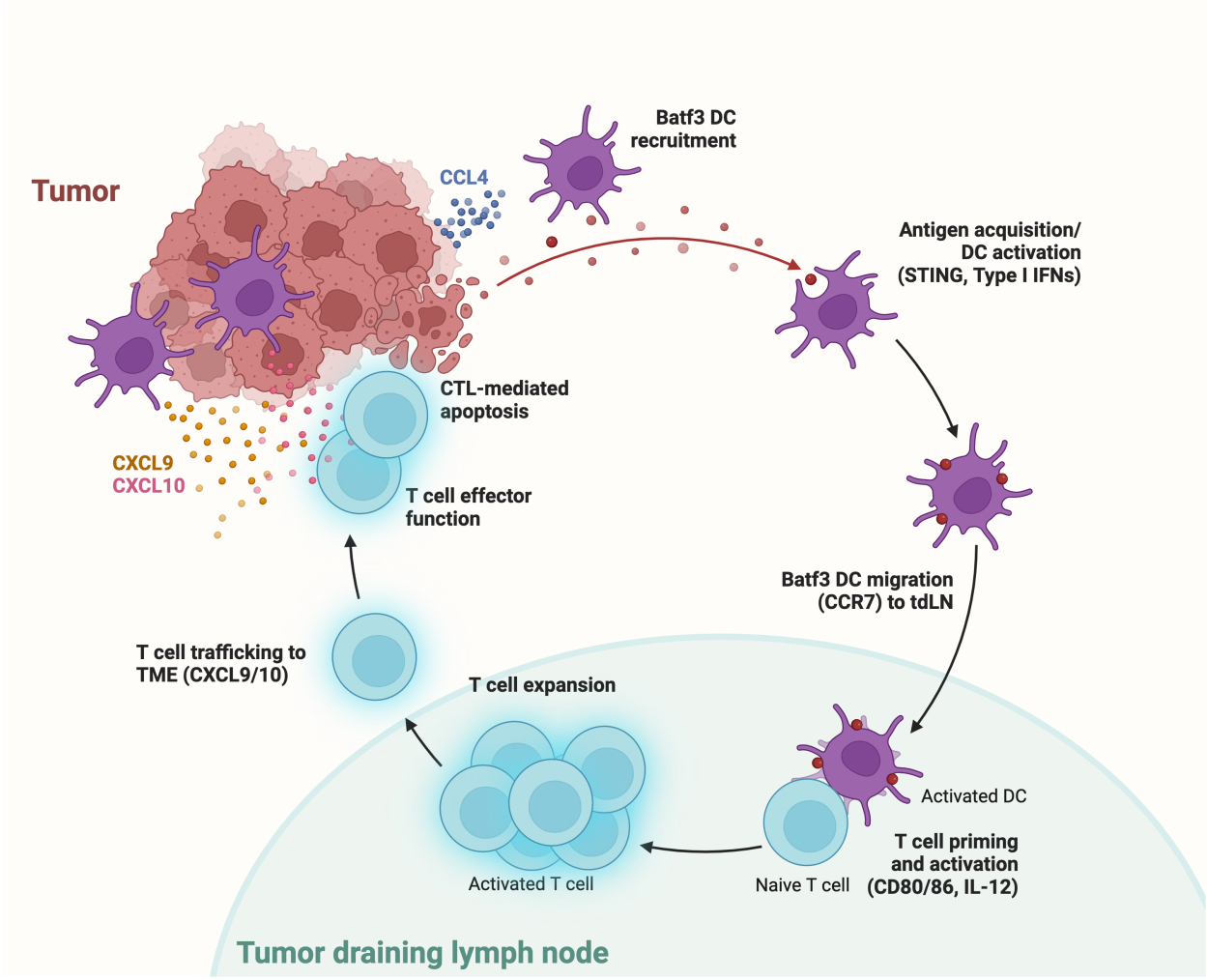

Figure 1.1: **The anti-tumor immune response.** In a successful, spontaneous immune response, Batf3 DCs get recruited to an early malignancy where they acquire antigen and become activated via STING and type I IFN. Subsequent to their activation, these Batf3 DCs migrate to the tumor-draining lymph node where they interact with $CD8^+$ T cells. Productive interactions between these two cell populations, result in $CD8^+$ T cell priming and activation. The effector $CD8^+$ T cells then traffic back into the TME via a CXCL9/CXCL10 chemokine gradient. In addition to the priming and activation of $CD8^+$ T cell, Batf3 DCs are also major producers of chemoattractants CXCL9 and CXCL10, which help effector T cells home to the TME.

1.2.2 The non-T cell-inflamed tumor microenvironment

In contrast to T cell-inflamed tumors, the non-T cell-inflamed tumors are characterized by a marked decrease in $CD8^+$ T cell infiltration as well as lower numbers of cDC1 cells. Additionally, these exhibit lower expression of type I IFN gene signatures [21]. Despite a lack of baseline $CD8^+$ T cell infiltration, these tumors are highly infiltrated by tumor-associated macrophages (TAMs) which have been associated with immune suppression and play a critical role in tumor promotion and progression [25, 26]. Since checkpoint blockade immunotherapy acts on the existing immune compartment within solid tumors, the marked reduction of $CD8^+$ T cells and cDC1 cell infiltrates in the non-T cell-inflamed tumors renders them relatively resistant to checkpoint blockade therapies [27, 28, 29].

Investigation into potential tumor cell-intrinsic mechanisms leading to a non-T cell-inflamed tumor phenotype revealed activation of the Wnt/β-catenin signaling pathway in a major subset of human cancers [27, 19, 30]. Mechanistic studies in mice revealed that β-catenin induces expression of the transcriptional regulator ATF3, which suppresses of CCL4, a chemokine crucial for the recruitment of Batf3 DCs to the tumor microenvironment. This impaired recruitment of Batf3 DCs results in a failed adaptive immune response as these cDC1s are essential for $CD8^+$ T cell priming and also contribute to effector T cell recruitment (Fig 1.2) [23].

In addition to the tumor cell-intrinsic activation of β-catenin signaling pathway, another mechanism implicated in driving the non-T cell-inflamed TME is loss of tumor suppressor gene PTEN. [31, 32].

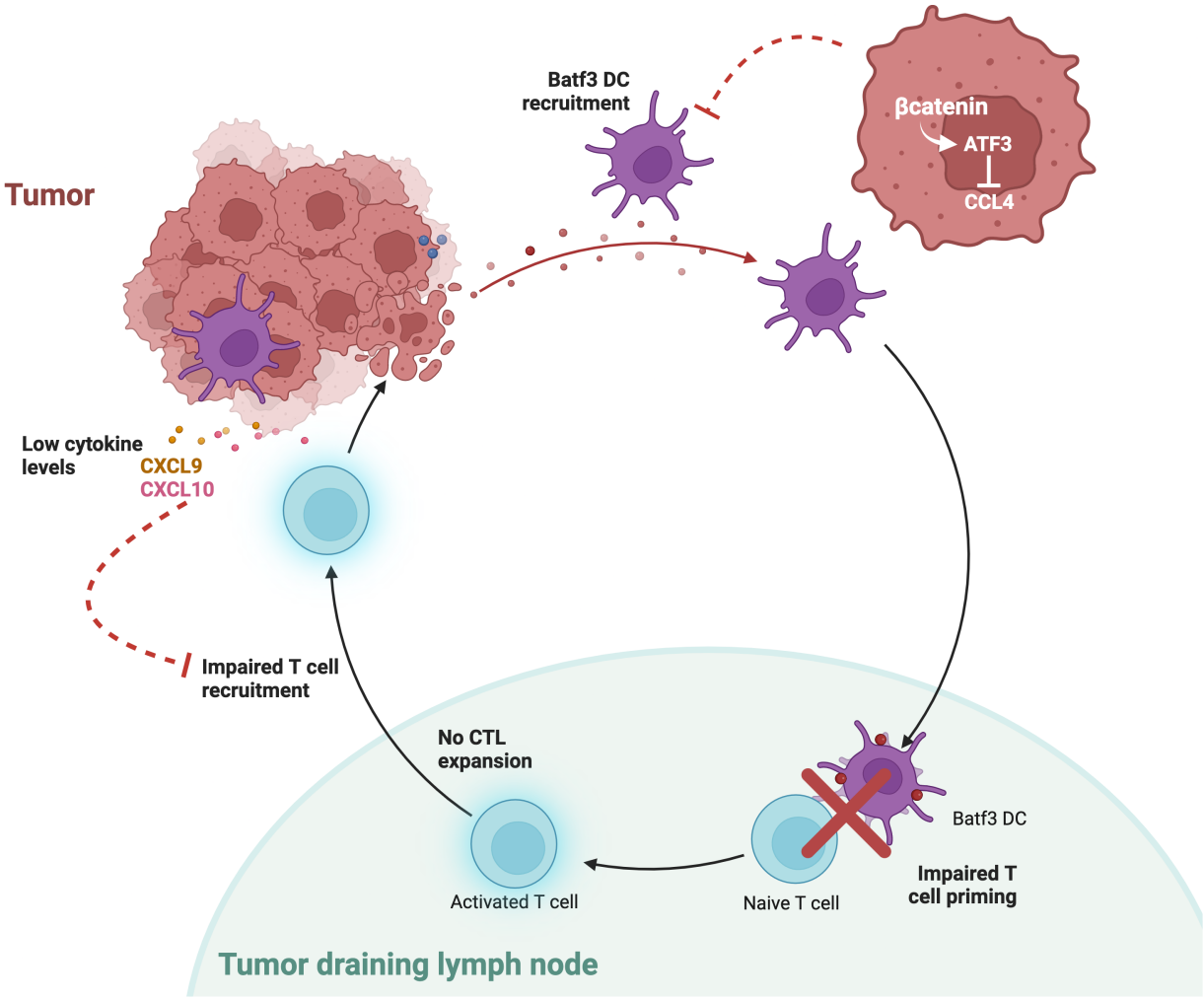

Figure 1.2: **Mechanisms for immune exclusion.** One mechanism for the immune exclusion of melanoma tumors is tumor-cell intrinsic activation of β-catenin signaling. Activation of the β-catenin signaling pathway results in activation of ATF3. ATF3 suppresses the production of chemokine CCL4 by tumor cells, which is crucial in recruiting Batf3 DCs to the TME. Tumors with reduced abundance of Batf3 DCs exhibit impaired effector T cell priming and activation. As a result, these tumors exhibit no effector T cell expansion or recruitment into the TME.

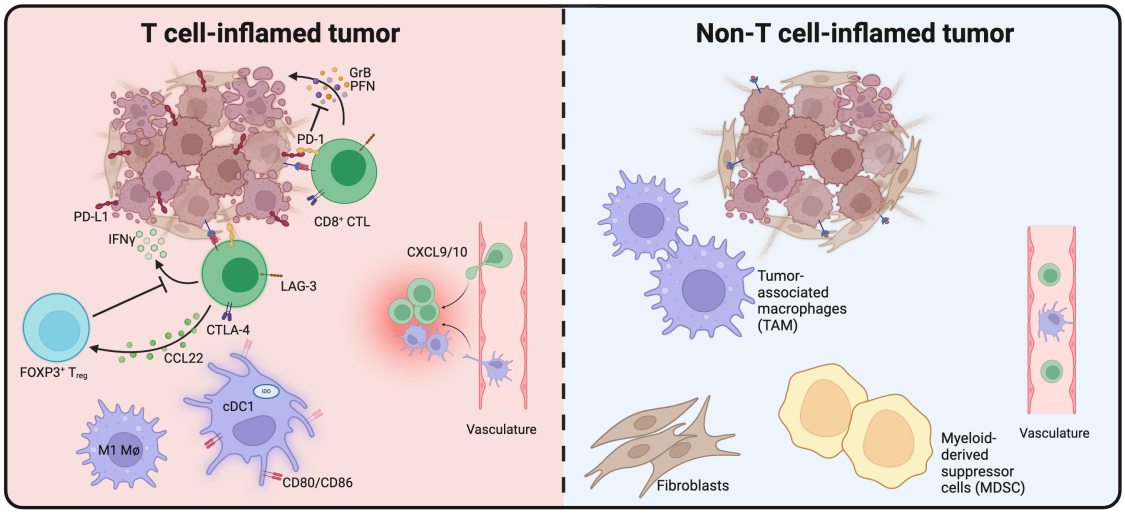

Figure 1.3: **The T cell-inflamed vs the non-T cell-inflamed tumor microenvironment.** The T cell-inflamed microenvironment (left) is characterized by the presence of $CD8^+$ T cells and cytokine and chemokines associated with a productive anti-tumor immune response and recruitment of other immune subsets within the TME. Additionally, these tumors exhibit increased type I IFN gene signatures. As consequence to the pro-inflammatory mechanisms observed, the T-cell inflamed tumors upregulate immune inhibitory mechanisms such as the upregulation of PD-L1 on tumor and myeloid cells and increased presence of regulatory T cells. The non-T cell-inflamed tumor (right) is characterized by the absence of $CD8^+$ T cell infiltration and an overall diminished inflammatory signature. These tumors show evidence of increased TAM and MDSC presence.

1.2.3 Immune profiles and therapy outcomes

Beyond assessing immune infiltration status, consideration of the activation and spatial arrangement of these cells within the tumor microenvironment has become paramount for understanding immunotherapy efficacy. Gene expression profiles that enrich for inflamed and non-inflamed tumors have aided in predicting therapy response rates to single agent anti-PD-1 treatment. This gene signature includes transcripts related to activated T cells, chemokines for immune cell recruitment, type I IFN-induced transcripts indicative of innate immune signaling, as well as transcripts associated with DCs and macrophages [33]. While the immune-infiltrated phenotype enriches for responders due to the presence of $CD8^+$ T cells and DCs in the TME, the non-T cell-inflamed phenotype is associated with primary resistance to anti-PD-1 [34].

In addition to these two well-established categories of solid tumor types, recent analysis of human tumor samples has revealed a third intermediate category, termed immune-excluded tumors. These tumors are characterized by the presence of immune cells on the periphery of the tumor mass, spatially segregated from the tumor cells themselves. This observation suggests a defective immune cell infiltration and activity within the tumor, rendering these tumors also resistant to immunotherapies [35].

1.3 The multifaceted role of β-catenin

β-catenin, an evolutionarily conserved molecule, is involved in several critical functions within the cell. It is not only vital for the integrity of the epithelial barrier and serves as a fundamental structural element of cadherin-based adherens junctions, but β-catenin also plays a key role in the Wnt signaling pathway. [36, 37].

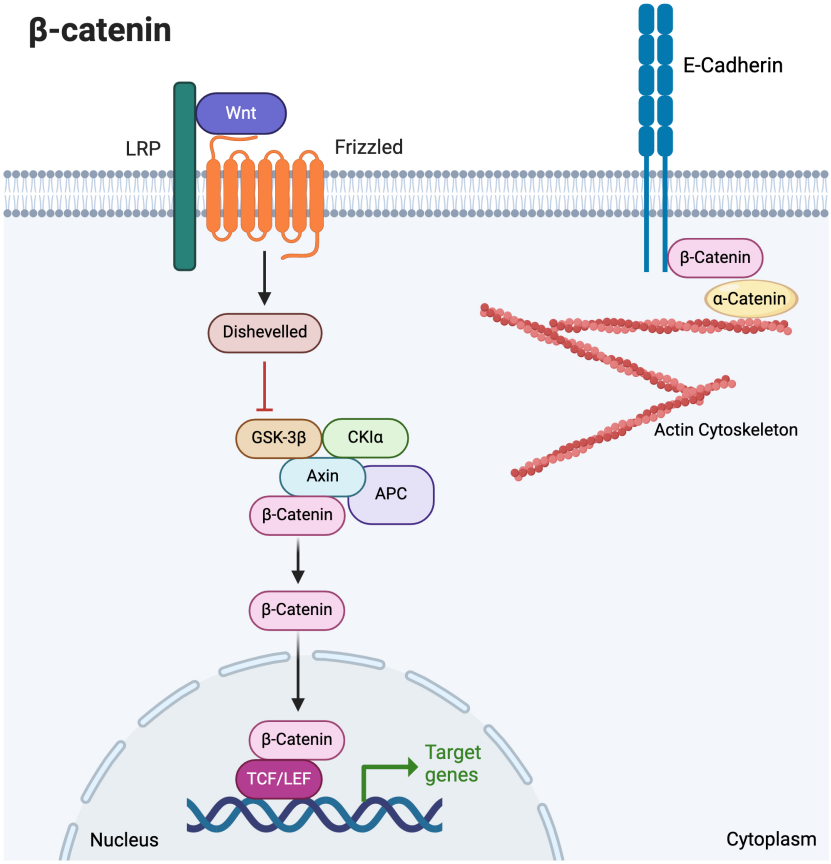

Figure 1.4: **The multifaceted role of β-catenin.** β-catenin is a multifunctional molecule involved in both structural support as well as signaling pathways within the cell. As a structural protein, β-catenin mediates the attachment to actin filaments by anchoring to the cytoplasmic tail of E-Cadherin on one side and to α-Catenin on the other side. The formation of this cadherin/catenin complex is crucial in maintaining cellular integrity and architecture. As a signaling molecule, β-catenin plays a key role within the Wnt signaling pathway. Engagement of Frizzled/LRP receptors activates the Wnt signaling pathway and recruits the destruction complex to the plasma membrane. Without the destruction complex to sequester and target for degradation, β-catenin accumulates in the cytoplasm. This accumulation of β-catenin in the cytoplasm enables its nuclear translocation. Once in the nucleus, β-catenin interacts with TCF/LEF transcription factors and initiates the transcription of multiple downstream target genes, which have been linked to be involved in essential cellular responses. The dual role of β-catenin in both maintaining cellular structure and transcriptional regulation, underscores its unique role in cellular physiology.

1.3.1 β-catenin structure

The β-catenin protein consists of a core region containing 12 Armadillo repeats which are flanked by distinct N-terminal (NTD) and C-terminal (CTD) domains. Both the NTD and CTD exhibit structural flexibility, allowing for diverse interactions. However, the central region forms a relatively rigid scaffold essential for the interaction of β-catenin with various binding partners. This central scaffold is where most interactions occur and facilitates its roles across different cellular locations, including the membrane, cytosol, and nucleus [38, 39].

Many studies have demonstrated that β-catenin's dual roles in cell adhesion and nuclear signaling are mediated by its two molecular forms, both of which possess unique binding capabilities. β-catenin exists as a monomer or a dimer. When activated by Wnt signaling, the monomeric form of β-catenin does not bind cadherins. However, the principal cadherin-binding variant of β-catenin is a dimer, partnering with α-catenin. This reveals a competitive dynamic between the two forms of β-catenin, with their respective roles in cell adhesion and transcriptional activities being governed by these specific molecular configurations [40]. Additionally, the spatial distribution of β-catenin's binding partners within the cell likely plays a crucial role in facilitating the distinct functions of these proteins.

1.3.2 β-catenin in cell adhesion

As a structural protein, β-catenin collaborates with α-catenin and E-cadherin to form the cadherin/catenin complex. The formation of this scaffold is critical in maintaining the cohesion and adhesive characteristics of epithelial cells. On one side, β-catenin attaches to the intracellular domain of E-cadherin, while on the other it binds to α-catenin facilitating the interaction and linking to actin filaments. This complex triggers the additional clustering of adherens junctions and enhances the stability of cellular adhesion.[41].

1.3.3 β-catenin in the Wnt signaling pathway

The Wnt signaling pathway is a complex pathway that has been studied for over 40 years. The Wnt signaling pathway can be categorized into two major arms: the canonical, also known as the Wnt/β-catenin dependent pathway, and the non-canonical or the β-catenin-independent pathway. The non-canonical Wnt pathway has been primarily implicated in cell polarity and mobility, while the β-catenin-dependent pathway is involved in cell proliferation and migration [42, 43].

The Wnt ligands themselves are cysteine-rich glycoproteins which are key mediators of cell-to-cell communication. Thus far, there have been 19 secreted glycoproteins identified [44, 45]. These proteins interact with at least 15 types of cell membrane receptors and co-receptors (Frizzled or LRP5/6) to initiate downstream signaling cascades [46].

The canonical, β-catenin-dependent signaling pathway is the most studied of the two. The activation of this signaling pathway begins with the stabilization of β-catenin which subsequently results in its transcription-promoting activities. In the absence of Wnt activation, the concentration of β-catenin is kept at low levels by the destruction complex, which is constituted by APC, GSK3-β, Axin and CK1. In this scenario, β-catenin gets phosphorylated at a preferential site, Ser33 and Ser37, by GSK-3 which in turn marks it for proteolytic degradation [47]. However, when Wnt ligands bind their cognate surface receptors, the destruction complex gets recruited to the membrane allowing for β-catenin to escape degradation and accumulate in the cytoplasm. Accumulation of β-catenin in the cytoplasm allows for its translocation into the nucleus where it binds TCF/LEF and controls downstream target gene expression such as myc, Mift, Axin2, and cyclinD1 [48, 49, 50, 51].

1.3.4 β-catenin signaling pathway dysregulation in melanoma

Recent studies have identified mutations in the Wnt/β-catenin signaling pathway in many types of solid cancers such as melanoma, colorectal cancer, breast cancer, hepato-

cellular carcinoma, and others. Furthermore, activating mutations in the Wnt/β-catenin signaling pathway or inhibitory mutation in negative regulators of this pathway have been linked to aberrant cellular functions such as proliferation, apoptosis, cell renewal, migration, and differentiation [52]. Tumor cell-intrinsic β-catenin activation in melanoma has been causally linked to lack of immune infiltration, specifically $CD8^+$ T cells and Batf3-lineage dendritic cells (cDC1s). The underlying mechanism demonstrated was that activation of β-catenin signaling pathway drives expression of ATF3, a transcriptional repressor. Furthermore, ATF3 has been shown to inhibit the expression CCL4, a crucial chemokine recruiting Batf3 DCs. The reduced expression of tumor-intrinsic CCL4 impaired the recruitment of Batf3 DCs to these tumors resulting in a failed spontaneous immune response [53]. Furthermore, β-catenin-expressing melanomas have been shown to be resistant to checkpoint blockade therapy with anti-PD-L1 plus anti-CTLA-4, likely due to the lack of spontaneous immune cell engagement. Collectively, these data suggest that tumor cell-intrinsic β-catenin pathway activation can mediate primary resistance to checkpoint blockade immunotherapy.

In addition to priming an anti-tumor immune response, Batf3 DCs were also shown to be major producers of chemokines CXCL9 and CXCL10. These key chemokines are responsible for successful effector $CD8^+$ T cell recruitment [23]. These additional data implicate β-catenin pathway activation in a secondary mechanism in which activated T cells fail to be recruited into the TME.

1.3.5 Therapeutic targeting of β-catenin in cancer

The involvement of Wnt signaling in carcinogenesis has been most studied in the context of colorectal cancer. Aberrant Wnt signaling has been implicated in many aspects of oncogenesis, from driving cancer stem cell maintenance all the way to metastasis [54]. The main driver of colon cancer is loss of function mutations within the adenomatous polyposis coli (APC) gene. This tumor suppressor gene has been shown to interact not only with β-catenin

but also with TCF and LEF leading to the regulation of the TCF/β-catenin pathway. Loss of APC activity has been demonstrated to be positively correlated with augmented β-catenin signaling. These findings suggest APC plays a major role in the pathogenesis of colorectal cancer [55].

In addition to colorectal cancer, tumor-intrinsic aberrant β-catenin signaling has been observed in more than half of all breast cancer and melanoma cases, as well as multiple other cancer types. As previously mentioned, tumor cell-intrinsic activation of β-catenin signaling pathway has been shown to be sufficient in driving resistance to checkpoint blockade therapy in metastatic melanoma [27]. Furthermore, activation of the β-catenin signaling pathway has been associated with the onset, progression and spread in pancreatic ductal adenocarcinoma (PDAC). In the context of ovarian cancer, the interplay between Wnt/β-catenin and STAT3 signaling pathways has been shown to support the growth, mobility, and invasion of ovarian cancer cells [56, 57]. These data collectively highlight the widespread involvement of the Wnt/β-catenin pathway in cancer onset, development and progression.

Despite its involvement in the pathology of multiple types of cancers, the Wnt/β-catenin signaling pathway also plays a critical role in both embryonic development and adult physiology. While there has been great interest in developing therapeutic interventions aimed at inhibiting the pathogenic effects of β-catenin, its role in cellular and tissue homeostasis have made this endeavor quite difficult [58]. There have been many promising results in preclinical animal models, however, the transition of these therapeutics into humans has not yet been successful. Many therapeutic agents fail to advance beyond early phase clinical trials due to the severe adverse effects observed as a consequence of global Wnt/β-catenin signaling blockade [59].

1.4 Breakthroughs in melanoma therapies

Metastatic melanoma has traditionally been relatively resistant to standard chemotherapies. For many years, overall survival rates remained unchanged due to a lack of truly effective treatments [60, 61]. Early chemotherapies and the development of cytokines as therapeutics (IFN-α and IL-2) demonstrated minimal benefit, increasing the five-year survival rate by only a few percent [62].

1.4.1 B-Raf-targeted therapies

The discovery that activated B-Raf serves as a driver oncogene in approximately 50% of melanomas led to the development of targeted small molecule inhibitors of this kinase [63]. The B-Raf^{V600E} mutation, present in over 90% of all human melanomas, is particularly notable [64]. Research has demonstrated that the B-Raf^{V600E} mutation promotes ERK activation, essential for cell proliferation [65]. *In vitro* studies targeting B-Raf^{V600E} have shown a marked reduction in tumor cell proliferation [66, 67].

Vemurafenib was the first BRAF inhibitor developed, and was FDA approved in 2011, followed by dabrafenib in 2013 [68]. Vemurafenib demonstrated remarkable efficacy, with approximately 50% of patients exhibiting tumor reduction and an overall survival rate of 84% at 6 months. Although dabrafenib also showed positive outcomes, phase III clinical trials demonstrated that treatment with vemurafenib resulted in superior progression-free survival [69, 70].

Interestingly, secondary resistance was found to develop in a median time of around 6 months, and these tumors were characterized as having re-activation of the Ras/MAPK pathway [68]. Therefore, inhibitors of MEK were developed, to target the same pathway at a second node. Combination B-Raf/MEK inhibitors demonstrate potent, long-lasting responses as well as decreased toxicity compared to BRAF inhibitors alone [71, 72, 73, 74]. For this reason, combination B-Raf/MEK inhibitors are now a standard of care for treating

metastatic melanoma. However, cures are uncommon, which prompted continued evaluation of immunotherapeutic strategies against this disease.

1.4.2 Immune checkpoint blockade

The realization that activated T cells can be functionally held in check by negative regulatory receptors has led to a collection of novel therapeutics referred to as immune checkpoint blockade. These are monoclonal antibodies (mAbs) that block engagement of specific inhibitory receptors by their cognate ligands.

The anti-CTLA-4 mAb ipilimumab was the first checkpoint blockade mAb to gain recognition for the treatment of solid cancers and was FDA approved in 2011. Anti-CTLA-4 monotherapy showed remarkable tumor control, even rejection in several transplantable murine tumor models, including colon carcinoma, fibrosarcoma, prostatic carcinoma, lymphoma and renal carcinoma [75, 76, 77]. Furthermore, anti-CTLA-4 mediated rejection in preestablished tumors as well as demonstrated effective immunological memory to secondary challenge. Mechanistic studies in preclinical animal models revealed that anti-CTLA-4 induces the expansion of two types of tumor-infiltrating T cells. First, an PD-1^+ $ICOS^+$ $TBET^+$ Th1-like $CD4^+$ effector T cell population and second, a phenotypically exhausted-like $CD8^+$ T cell population [78]. These data show that anti-CTLA-4 has a specific effect on a subset of tumor infiltrating T cells within the tumor microenvironment rather than a more generalized activating effect on all tumor infiltrating T cells [79]. In human clinical trials, the inhibition of CTLA-4 showed melanoma tumor control and regression as well as improved overall patient survival. However, single agent anti-CTLA-4 had a relatively low response rate of only 13% [80].

A second mAb approved for human solid tumors, anti-PD-1 (nivolumab or pembrolizumab), was FDA approved in 2014. The inhibition of the programmed cell death protein 1 (PD-1) has demonstrated marked success with promising response rates of around 40%, with signif-

icant durability [81]. PD-1, similar to CTLA-4, is a checkpoint molecule that keeps in check the anti-tumor immune response against many cancers. Early *in vitro* studies demonstrated that PD-1 blunted the effector T cell function by blocking cell proliferation and inhibiting cytotoxic activity and pro-inflammatory cytokine production such as IFN-γ [81]. Anti-PD-1 primarily functions by driving the expansion of specific exhausted $CD8^+$ T cells that are found within the TME [78]. Studies in preclinical animal models demonstrated that tumor cells and antigen presenting cells residing within the TME can upregulate the expression of PD-L1. The increased tumor-specific PD-L1 has been shown to facilitate tumor-immune escape due to negative regulation of T cells expressing PD-1 [82]. Inhibiting the PD-1/PD-L1 axis in humans has shown success in the clinic [83]. Moreover, patients with increased baseline $CD8^+$ T cell infiltration or showing evidence for a T cell-inflamed tumor microenvironment by gene expression profiling were more likely to benefit the most from checkpoint blockade therapies [34].

Despite increases in survival rates with single agent checkpoint blockade therapy, the combination of anti-CTLA-4 and anti-PD-1 checkpoint blockade was shown to significantly enhance tumor control and survival rates in many solid cancers, including metastatic melanoma [84]. In clinical trials with advanced melanoma, combination checkpoint blockade with anti-CTLA-4 plus anti-PD-1 resulted in unprecedented survival rates of over 80%. Additionally, more than half of the patient in this trial exhibited robust tumor reduction. The response to combination therapy was substantially enhanced compared to monotherapy, resulting in FDA approval for combined nivolumab and ipilimumab therapy for metastatic melanoma in 2015 [81, 85].

1.4.3 Immunotherapy resistance in melanoma

Even with the remarkable tumor control and enhanced survival rates observed in response to single agent or combination anti-CTLA-4 plus anti-PD-1 therapy, resistance to

these treatments still occurs. Over 50% of melanoma patients demonstrate primary resistance to single agent anti-PD-1 therapy, and approximately 40% show resistance to combined anti-CTLA-4 plus anti-PD-1 therapy. Furthermore, approximately 25% of patients who initially respond develop secondary, acquired resistance to anti-PD-1 therapy [86].

Gene expression profiling of human melanoma samples indicates that an endogenous anti-tumor immune response at baseline is essential for efficacy with combination checkpoint blockade immunotherapy [87, 27]. Additionally, tumor-cell intrinsic activation of β-catenin, which correlates with an absence of spontaneous immune infiltration, is a mechanism of primary resistance to checkpoint blockade immunotherapy in metastatic melanoma. Furthermore, the commensal microbiota has also been reported to have both pro- or anti-tumor effects and be associated with clinical response. The anti-tumor effects of the commensal microbiota have been associated with primary resistance to checkpoint blockade immunotherapy [88, 89].

Secondary resistance to immune checkpoint blockade is incompletely understood, however loss of function mutations in JAK1/JAK2 signaling pathway resulting in impaired immune responses to IFN-γ is one reported mechanism [90]. Furthermore, mutations within beta-2-microglobulin (B2M) resulting in loss of antigen presentation have been associated with acquired resistance to both single agent PD-1 blockade as well as combination anti-CTLA-4 plus anti-PD-1 therapy [91].

Despite the advancements in the way we treat many solid tumors like metastatic melanoma as well as the remarkable response rates that have been achieved, there remains a major fraction of patients which do not respond to most available treatments. Identifying the molecular characteristics of tumors resistant to available treatments is crucial to furthering the field and developing additional strategies to target these non-responders.

1.5 Navigating the dual landscapes of macrophage polarization

Macrophages are critical elements of the immune framework. These cells are distributed in nearly every tissue within the host, where they are involved in tissue homeostasis. These immune cells are highly malleable and exhibit remarkable heterogeneity. Their unique characteristics enable them to execute a variety of functions that extend from innate immune responses in defending against pathogens, to adaptive immune responses in mediating inflammatory responses, to facilitating tissue repair and remodeling [92]. Their remarkable adaptability is further enhanced by their responsive nature to the surrounding environmental cues. This allows them to quickly adjust their activation states in response to the specific molecular context of their environment [93]. Notably, macrophages differentiate into various phenotypes depending on environmental inputs. Two of the most common states macrophages differentiate into are the M1-like or pro-inflammatory macrophages, and the M2-like or anti-inflammatory macrophages. M1-like and M2-like macrophages perform distinct functions and exhibit unique transcriptional profiles showcasing their versatile role in orchestrating immune responses [93].

1.5.1 M1 macrophages: the warriors of inflammation

M1-like macrophages, often labeled as pro-inflammatory or classically activated macrophages, can be generated by polarization *in vitro* by lipopolysaccharide (LPS) alone or in combination with pro-inflammatory cytokines such as IFN-γ. This process is also known to be induced by GM-CSF, [94]. *In vivo*, these M1-like macrophages are thought to play role in innate and adaptive immune responses by producing a range of pro-inflammatory cytokines, including IL-1β, IL-6, IL-12, IL-23, and TNF-α [93]. In addition to cytokine production, M1-like macrophages engage with other immune cells around them and augment the immune response by upregulating co-stimulatory molecules such as CD80 and CD86. The involvement of CD80/86 is crucial for antigen presentation and productive T cell activation [95]. Fur-

thermore, they also secrete chemoattractants such as CXCL1, CXCL2, and CCL5, essential for the recruitment of other immune cell subsets like neutrophils and $CD8^+$ T cells. These collective immune functions highlight the pivotal role of M1-like macrophages in mediating both innate and adaptive immune responses [96].

1.5.2 M2 macrophages: healers and regulators

Alternatively activated macrophages, or M2-like macrophages, have been implicated in immune regulation and tissue repair. This type of macrophage can be induced *in vitro* by exposure to IL-4, IL-13, and M-CSF. In the literature, M2-like macrophages are characterized by specific markers such as upregulation of MRC1 (CD206), Cd163, Arginase 1 (Arg1), and CD209.

Arginase is a molecule primarily associated with wound healing, and was one of the first markers used to characterize anti-inflammatory macrophages. Arginase activity is primarily stimulated by transforming growth factor beta (TGF-β) family proteins, but its expression can be further enhanced by cytokines IL-4 and IL-13. All these molecules have been associated with accelerated wound healing and tissue repair [97]. Moreover, IL-4 not only regulates Arg1 expression, but it has also been linked to increased expression of dendritic cell-specific ICAM-3 grabbing non integrin (DC-SIGN; also called CD209), CD206, as well as CD163 [98]. CD206 is increasingly recognized as a marker for tissue-resident macrophages. Furthermore, CD163 expression is upregulated by growth factor M-CSF, and cytokines IL-6, and IL-10. Conversely, CD163 is downregulated by proinflammatory cytokines such as TNF-α, IFN-γ, and LPS [99]. Furthermore, these M2-like macrophages are known to produce anti-inflammatory cytokines, such as IL-10 and TGF-β, which provide a mechanism maintaining the immune suppressive milieu [94].

From a metabolic standpoint, pro-inflammatory macrophages have been shown to preferentially upregulate glycolysis, while M2-like macrophages utilize fatty acid oxidation and

oxidative metabolism [100].

The stark differences between these two extremes of macrophages and their remarkable ability to switch between activation states has intrigued scientists for decades. It has been demonstrated that macrophages can very quickly and completely revert between phenotypes *in vitro*. This provides evidence for their unique ability to sequentially contribute to both the onset and resolution of inflammation [99].

1.6 Immunosuppression in melanoma

As cancers evolve, they adopt strategies to evade the immune system. A key mechanism of immune evasion involves promoting an immunosuppressive microenvironment that dampens the natural immune response. This environment has been characterized by the presence of high concentrations of immunosuppressive molecules. Increased concentrations of IL-10 and TGF-β as well as increased numbers of immune suppressive cells such as regulatory T cells, myeloid-derived suppressor cells (MDSCs), tumor-associated macrophages (TAMs), and cancer-associated fibroblasts (CAFs) have been all been linked to the immunosuppressive tumor microenvironment. Additionally, while melanoma tumors infiltrated by immune-suppressive populations are also infiltrated by effector T cells, these T cells are often found in dysfunctional states due to increased expression of immune-inhibitory/checkpoint molecules.

1.6.1 Cellular and chemical components of the immunosuppressive TME

A tumor mass is not composed of cancer cells only, but rather is a mix of tumor cells and additional host cells, such as vasculature and immune cells. The immune suppressive component of the TME includes TAMs, cancer-associated fibroblasts (CAFs), and myeloid-derived suppressor cells (MDSCs).

MDSCs are thought to play a crucial role in promoting tumor growth and metastasis

by enhancing cancer cell stemness, proliferation, survival, angiogenesis, and invasiveness. The abundance of MDSCs in solid tumors is correlated with cancer progression. MDSCs contribute to an immune-inhibitory microenvironment that supports immune evasion of cancer cells. This effect is achieved, in part, by stimulating the proliferation and activation of regulatory T cells. Moreover, MDSCs augment cancer stem-cell-like properties and cancer cell survival by upregulating molecules such as the anti-apoptotic factors Bcl-2 and Mcl-1. Furthermore, MDSCs are drawn to pre-metastatic niches, where they establish a cancer-promoting microenvironment that supports the metastasis of solid tumors. [101, 102, 103].

Regulatory T cells are another type of immunosuppressive cell that reside in the TME. Tregs exert their immunosuppressive function via multiple mechanisms: they consume available IL-2 from the TME, thus depriving this cytokine from effector T cells, and they produce immune inhibitory cytokines such as TGF-β, IL-10, and IL-35. Additionally, a key suppressive mechanism is the upregulation of immune checkpoint-related molecules which induce a state of dysfunction in effector T cells [104, 105, 106, 107].

Cancer-associated fibroblasts (CAFs), another major subset of immunosuppressive cells within the TME, also significantly contribute to tumor progression through the secretion of various factors such as hepatocyte growth factor (HGF), TGF-β, stromal-derived factor 1 (SDF-1), platelet-derived growth factor (PDGF), and Sonic hedgehog (Shh). These molecules have been demonstrated to promote tumor cell proliferation and enhancement of stem cell-like properties of cancer cells. In metastatic melanoma, melanoma-associated fibroblasts (MAFs), have been shown to impair cytotoxic T lymphocyte function. *In vitro* studies with T cells exposed to MAF-conditioned media demonstrated a striking dysregulation of the ERK1/2 and NF-κB signaling pathway, reduction in activation marker CD69 and granzyme B production, and impaired cytotoxic activity. Moreover, it has been observed that they can express immune checkpoint receptors such as T cell immunoreceptor with Ig and ITIM domains (TIGIT) and B- and T- lymphocyte attenuator (BTLA). MAFs also dis-

play higher levels of V-domain Ig suppressor of T cell activation (VISTA) and Herpesvirus entry mediator (HVEM) and show increased production and secretion of CXCL12. All of these have been implicated in the disruption of intracellular signaling in cytotoxic T cells, potentially contributing to their dysfunction. [108, 109, 110].

1.7 Tumor-associated macrophages (TAMs) and cancer progression

Another key immunosuppressive cell population identified in the microenvironment of solid tumors are tumor-associated macrophages (TAMs). These are strikingly abundant within the TME, and despite initially thought as being anti-tumor, TAMs are more recently recognized as immune suppressive cells that favor tumor growth. This reconsideration was brought upon by their ability to support the tumor by promoting tumor cell survival, invasion, stem cell viability, and angiogenesis [111]. Furthermore, there is recent evidence that TAMs have the ability to suppress cytotoxic T cells.

1.7.1 TAMs in tumorigenesis

As mentioned in earlier sections, macrophages are involved in many aspects of the host response. They are involved in regulating the development of many tissues, they aid in wound healing, and they contribute to tissue homeostasis. Furthermore, macrophages have been implicated in regulating both innate and adaptive immune responses [112, 113]. Because of their intimate involvement in so many aspects of tissue regulation, macrophages have been linked to a variety of diseases, ranging from inflammation to cancer.

In the context of inflammation, monocytes are recruited from the blood to the site of inflammation, and these will differentiate into pro-inflammatory macrophages at the inflammation site. The pro-inflammatory macrophages have the capability of producing IFN-α/β,

IL-6 and TNF-α that promote inflammation but also kick-start an adaptive immunological cascade. These proinflammatory cytokines engage and recruit additional immune cells to the site of inflammation resulting in the progression of an immune response. However, to avoid harming the host and to keep the immune reaction from going overboard, macrophages have the capability of shifting into a state that supports the resolution of inflammation, which induces immune-suppressive responses to minimize the damage to the host [114]. The macrophages involved in wound healing have been shown to produce Wnt ligands that are involved tissue repair [115].

Within established tumors, TAMs are usually educated away from a pro-inflammatory phenotype towards immune-suppressive phenotypes. These TAMs have been demonstrated to promote tumor progression via induction of tumor cell migration, invasion and angiogenesis [116]. Additionally, immunosuppressive TAMs have been shown to remodel the tumor microenvironment via the increased production of matrix metalloproteinases (MMPs) and cathepsins. These molecules come together to form a scaffold/conduit type of system which allows for the intentional release of growth factors aiding in tumor cell invasion and metastasis [117, 118]. These TAMs have been shown to further support the TME by secreting angiogenic factors that enhance the tumor vasculature such as VEGF family members, IL-8, PDGF, and FGF [119].

Interestingly, the site where a specific type of tumor will metastasize has also been linked to the presence of macrophages. Finding a suitable microenvironment, also known as a pre-metastatic niche, is crucial for the tumor's ability to leave the primary location, disseminate, and establish at another site. Data suggest that pre-metastatic niches show a type of "priming" of the area prior to tumor cell arrival. These areas are characterized by an increase in growth factors that recruit tumor-associated cells to those sites. These cells, many of which are macrophages, cluster to these areas and create an environment suitable for tumor cell adhesion and invasion [120, 121, 122].

1.7.2 Targeting TAMs for cancer therapy

The dominant current view in is that tumor-associated macrophages (TAMs) play a tumor-promoting role. This nuanced understanding of TAMs has made them attractive targets for therapeutic intervention. The two current strategies being explored for targeting TAMs include to either reprogram them from an anti-inflammatory phenotype to a pro-inflammatory one, or to ablate them entirely.

Recent studies suggest that TAMs can contribute to chemotherapy resistance. Cathepsin expression within macrophages can contribute to therapy resistance. Additionally, TAMs have been shown to be an active participant in post-chemotherapy recurrence of tumors. This was demonstrated by linking the high expression of Vascular Endothelial Growth Factor (VEGF) on TAMs which is a key molecule in supporting the revascularization of recurrent tumors.

An important focus as a potential therapeutic target has been Colony-Stimulating Factor 1 Receptor (CSF1R), because the inhibition of this myeloid growth factor receptor has been shown to synergize with immune checkpoint inhibitors in preclinical models. Studies have shown that administration of CSF1R inhibitors increased tumor antigen presentation and amplified antigen presentation within macrophages resulting in an improved anti-tumor T cell responses [123]. Importantly, CSF1R inhibition in combination with checkpoint blockade resulted in tumor control in models unresponsive to checkpoint inhibitors alone. Recent findings reveal that the mechanism of action of CSF1R inhibition is not to deplete macrophages but rather it induces a phenotypic shift towards a pro-inflammatory state. This transcriptional and phenotypic change within these macrophages then acts on the immune system already present in the TME by engaging natural killer cells and dendritic cells for a reinvigorated immune response. [123, 124].

An additional molecule of interest is CD40, often expressed on a subset of TAMs. Activation of CD40 has shown encouraging outcomes due to its ability to induce a phenotypic shift

TAMs. Treatment with anti-CD40 in animal models has demonstrated that engaging this receptor induces a shift from anti-inflammatory TAMs to pro-inflammatory macrophages. Moreover, these exhibit augmented production of proinflammatory cytokine IL-12. This fundamental transition within macrophages also leads to the activation of $CD8^+$ T cells and DCs, ultimately potentiating an anti-tumor response [125, 126]. Furthermore, CD40-activated macrophages have been shown to infiltrate and degrade tumor stroma. These data provide evidence for immune therapies that do not directly involve T cells [127]. Intriguingly, combining CSF1R inhibition with CD40 stimulation synergizes to induce a striking effect on TAMs. The combination of these therapies promotes a highly proinflammatory microenvironment further enhancing checkpoint blockade therapy efficacy [128].

These early findings provide evidence that TAM-targeted therapies have the potential to be developed towards clinical translation, with the aim of expanding the efficacy of immunotherapy in patients. However, clinical results have been limited to date.

CHAPTER 2

MATERIALS AND METHODS

2.1 Genetically engineered mouse model

Our animal model was created by crossing two established genetically engineered mouse models. The first, contains a tyrosinase driven Cre recombinase, an activation mutation within the BRAF gene, $BRAF^{V600E}$, and a bi-allelic deletion of the tumor suppressor gene PTEN. The last two are integrated in their respective loci. To this background, we integrated a TET-ON system for the regulation of an active variant of β-catenin. This second genetically engineered animal was altered to include the expression of a reverse transactivator (rtTA) under the Rosa26 promoter, and a mutated β-catenin gene (β-$catenin^{S33Y}$) under the collagen type I alpha 1 (Col1a) promoter.

The final mouse model harbored the active $BRAF^{V600E}$, deletion of PTEN, and the expression of the reverse transactivator and the β-$catenin^{S33Y}$. This was achieved by breeding these animals across several generations to ensure homozygosity of the critical alleles ($BRAF^{V600E}$, PTEN, rtTA, and indβ-$catenin^{S33Y}$), thereby guaranteeing that the genetic modifications were uniformly present in every cell. A comprehensive genotyping protocol followed the breeding program (Table 2.1), confirming the presence of the Cre-ER transgene in all offspring, which is crucial for the constitutive activation of the oncogenes and the model's overall functionality.

2.2 Tumor induction and measurement

Preparation of 4-OH-Tamoxifen: A solution of 4-hydroxytamoxifen (catalog number H7904-25MG) was prepared by reconstituting it in 100% ethanol to a final concentration of 2.5 μg/mL. If there was visible precipitate, the 4-hydroxytamoxifen plus ethanol was placed

on a shaker at 37°Celsius for 15 minutes to ensure everything dissolved and the solution was the proper concentration.

All experiments were performed on animals aged between 8 to 14 weeks. We prepared the animals by shaving their dorsal surface using an electric shaver. 5μL of the 4-hydroxytamoxifen was applied to the prepared area on each animal using a micro-pipette. This application is performed under ambient conditions, with the animals awake and minimally restrained.

The tumor growth was monitored by measuring the volume of the induced autochthonous tumors starting three weeks after the tumor induction. The height, width and length of all tumors was measured using calipers every other day for the last three weeks of tumor development. All animals were awake and minimally restrained while measuring the tumor volume.

2.3 Checkpoint blockade therapy administration

Starting on the 21st day post tumor induction, the animals were treated with combined anti-PD-L1 (Catalog Number BE0101) and anti-CTLA-4 (Catalog Number BE0131) therapy. The monoclonal antibodies were diluted in Dulbecco's Phosphate Buffered Saline (DPBS) (Catalog Number 14190-144) and administered intraperitoneally (i.p.), at a concentration of 100 μg/mL. The control group was treated with DBPS only. The mAb therapy was administered every other day, mirroring the schedule of tumor volume measurements, for the remainder of the experiment.

2.4 Euthanasia and tumor harvesting

At the experimental endpoint, animals were euthanized by CO_2 inhalation for 5 minutes, followed by cervical dislocation as a secondary mode of euthanasia. The fur overlying and

around the tumor site was removed using Nair Hair Removal Cream, and the area was cleaned and sterilized with 70% ethanol. Tumors were excised with micro-scissors, ensuring separation from adjacent non-tumorous/healthy tissue.

2.5 Preparation of histological samples

For histological examination, each tumor was bisected to obtain a central, cross-section. Each tissue section was fixed in 5 mL of 10% Neutral Buffered Formalin (NBF) (Catalog Number HT501128-4L) for 24 hours at room temperature. After fixation, samples were transferred to 70% ethanol for long-term preservation or sent to the University of Chicago Human and Tissue Research Center for embedding in paraffin, sectioning, and slide preparation for microscopic examination.

2.6 Tumor digestion for flow cytometry

Tumor samples intended for flow cytometric analysis were chemically and mechanically digested into single-cell suspensions. First, all tumors were placed in Miltenyi Biotec OctoMacs tubes (Catalog Number 130096334) containing 2 mL of a homemade digestion buffer and manually minced using micro-scissors. The digestion buffer used was a mixture of Collagenase Type IV (Catalog Number C5138-1G), Dnase I (Catalog Number 18-068-015) and Hyaluronidase V (Catalog Number H6254-1G) diluted in Dulbeccos Modified Eagle Medium (DMEM) (Catalog Number 11885084). The minced tissue was then mechanically dissociated using the OctoMacs system followed by a 30-minute incubation at 37°Celsius with rotation. This step was repeated one more time. The resulting material was strained through a 70 μm cell strainer and washed once with 30 mL of cold 1x DPBS.

2.6.1 Lymphocyte isolation and immunostaining

To isolate lymphocytes, the single cell suspension obtained from the digested tumors was centrifuged, and the pellet was re-suspended in 10 mL of cold DPBS. A layer of Ficoll-Paque PLUS (4 mL) (Catalog Number 17144003) was added beneath the single cell suspension, and the mixture was centrifuged at 500 xg without brake or acceleration for 30 minutes. The interphase was collected and washed in 10 mL of DPBS to remove any residual Ficoll.

For $CD45^+$ cell sorting: samples were re-suspended in 1 mL of 0.04% Bovine Serum Albumin (BSA) (Catalog Number 9998S) with 1x EDTA (Catalog Number J15694.AP) and incubated for 30 minutes on ice with Fixable Viability Dye eFluor 780 (Catalog Number 65-0865-14) at a dilution of 1:1000 and APC anti-mouse CD45 (Catalog Number 103112, clone 30-F11) at a dilution of 1:200. Following the staining protocol, samples were washed with 10 mL of 0.04% BSA solution to remove excess stain and unbound antibodies. After washing, the cells were re-suspended in 2 mL of 0.04% BSA solution and filtered once more using a 70 μm cell strainer, prior to fluorescence-activated cell sorting (FACS). Gating strategies using Fluorescence Minus One Controls (FMOs) were determined and $CD45^+$ cells were sorted (as determined by APC positive stain) and exhibiting viability (as determined by exclusion of eFluor 780 stain) were sorted from the mixture. The cells were sorted in the same 0.04% BSA solution and processed for downstream analysis (Table 2.2).

2.7 Histological slide preparation and multiplex immunofluorescence staining

All murine FFPE tissue samples were stored at room temperature. Slides were baked at 65°Celsius for one hour. After baking, the slides underwent a rehydration sequence:

1.Xylene Immersion: The slides are immersed in xylene three times for 10 minutes each.

2.Ethanol Washes and Rehydration: A series of graded ethanol washes followed, with

concentrations decreasing from 100%, 95%, to 75%, for 10, 10, and 2 minutes respectively.

3.Rinsing: All slides were rinsed in deionized (DI) water to remove any residual ethanol and xylene.

All slides were then immersed in 10% NBF for 20 minutes to fix the tissue. For the antigen retrieval step, the slides were placed in a 1x AR9 buffer (Catalog Number AR600250ML) and subjected to pressure cooking for 20 minutes, breaking the cross-links formed during fixation and exposing the antigens.

Post-antigen retrieval, samples were blocked using a Akoya blocking solution (Catalog Number ARD1001EA) for 10 minutes at room temperature to prevent non-specific antibody binding. This was followed by the primary antibody incubation: all primary antibodies were diluted in the provided blocking buffer and samples were incubated with diluted primary antibody for one hour at room temperature or overnight at 4°Celsius (Table 2.3). After the primary antibody incubation, the samples were washed three times in 1X Tris-buffered saline with Tween 20 (TBST) (Catalog Number L10K124) to remove unbound antibodies, each wash lasting 2 minutes. Next, the slides were incubated with a secondary-HRP antibody (Catalog Number ARH2001EA), diluted at a ratio of 1:2 in HRP buffer (catalog Number ARD2001EA), for 10 minutes at room temperature. This was followed by another series of TBST washes.

Then all samples were incubated with an Opal fluorophore-conjugated antibody diluted 1:200 in Opal Buffer (Catalog Number 220110012) for 10 minutes at room temperature (Table 2.4). Finally, all samples were stained with DAPI diluted in TBST (1 drop DAPI in 500 uL TBST) (Catalog Number FP1490) for 5 minutes at room temperature to label the nuclei. A final wash with 1X TBST and rinse with DI water was performed prior to the mounting of the slides using ProLong Diamond Anti-Fade Mountant (Catalog Number P36961). The slides were left to dry overnight to ensure the mountant set properly.

2.8 Multiplex immunofluorescent imaging and analysis

Imaging of all samples was performed using the Vectra Polaris microscope. All prepared slides were systematically scanned using this microscope. Following image acquisition, each image was individually checked and 8-10 regions of interest (ROIs) were selected. Because of the heterogeneity of the tumors, we focused on areas that were highly infiltrated by immune cells. Analysis of all ROIs was performed using InForm analysis software. This machine learning algorithm requires initial training specific to the experiment at hand to accurately differentiate and identify targeted markers. This training involves teaching the software to recognize patterns and features that distinguish positive marker expression from background noise or non-specific staining.

For the analysis of β-catenin status, which was sometimes complicated by the presence of melanin pigment in the samples, a dual-segmentation approach was adopted. This strategy involved using both DAPI staining, which labels nuclei, and comparison of β-catenin status with control samples known to exhibit positive nuclear β-catenin staining. This dual reference enabled the software to precisely segment the images and confidently identify cells positive for β-catenin, overcoming the challenge posed by melanin interference.

The assessment of CD3 status relied solely on DAPI staining for segmentation. CD3, a plasma membrane marker, presents a distinct staining pattern that does not require additional references for accurate segmentation. This approach simplifies the analysis by focusing on the nuclear staining to delineate cell boundaries and identify the presence of CD3 within the samples.

2.9 Marker quantification process

Preliminary Training: First, the InForm software was trained using control samples. These controls were manually classified as either positive or negative for the markers of

interest, based on visual inspection by the researcher. This step calibrates the software, ensuring it can accurately recognize and differentiate the targeted markers in subsequent analyses.

Batch Analysis: Following the preliminary training, a batch analysis of all slides was conducted. This phase processes multiple slides simultaneously, utilizing the trained machine learning model to maintain consistency and accuracy across all samples. This automated analysis significantly enhances efficiency and reduces the potential for human error, ensuring reliable quantification of the targeted markers across the study.

2.10 Single cell sequencing analysis

Raw reads were processed using Cell Ranger (v6.1.2) from 10X Genomics, and downstream analysis, including quality control, was carried out in R. Cells were quality filtered to retain only cells with at least 500 total counts and at least 250 unique features. Cells were also removed if over 10% of their reads were from mtRNA. Lastly, doublets were identified and removed using the package DoubletFinder (v2.0.3). The counts were then normalized with Seurat's SCTransform function (Seurat v4.1.3), and the cells were integrated following the standard workflow for the Seurat package. The final integrated data were visualized as a Uniform Manifold Approximation and Projection (UMAP), and clusters were identified at a range of resolutions and visualized with clusters (v0.5.0). This indicated resolution 1.0 would provide high quality separation of cells into 25 distinct clusters. Markers defining each cluster were identified using the function FindConservedMarkers() grouping by the sample identity. The conserved markers were compared to canonical markers to annotate the clusters wherever possible, and clusters not conforming to known cell types were instead labeled by their top distinguishing genes.

Four samples obtained from two independent experiments were submitted for sequencing (experimental conditions: ex-βcatenin and water), each consisting of CD45+ cells iso-

lated as described in the previous section and pooled from 5-6 murine tumors. 10,000 cells for each sample were loaded into the 10x Genomics Sequencer and sequencing was performed by the 10x Genomics Core at University of Chicago. Reads were aligned and feature-barcode matrices were generated using the 10x Genomics Cell Ranger software. For the pre-processing step, cells with a percentage of counts coming from mitochondrial RNA higher than 15 and all genes expressed in less than 3 cells were removed. Outliers in the distribution of the number of genes in a cell vs. the number of mRNA counted in a cell were also excluded. Data was normalized using Seurats SCTransform function [129]. Principal component analysis (PCA) was performed, followed by dimensionality reduction using RunUMAP on the top 40 principal components (PCs). The k-nearest neighbors were calculated and the SNN graph was constructed using Seurats FindNeighbors function (https://satijalab.org/seurat/reference/findneighbors). Clustering was performed using Seurats FindClusters function (https://satijalab.org/seurat/reference/findclusters). Pseudo-bulk differential expression via DESeq2-LRT method (https://hbctraining.github.io/scRNA-seq/lessons/pseudobulk_DESeq2_scrnaseq.html) was performed to identify the top differentially expressed genes in each cluster. Based on the top differentially expressed genes in each cluster, the different immune cell types present were identified. Pseudo-bulk differential expression via DESeq2-LRT method (https://hbctraining.github.io/scRNA-seq/lessons/pseudobulk_DESeq2_scrnaseq.html) was also performed within each cell type comparing the ex-β-catenin and control samples. The F480+ Cd11b+ macrophage cluster was subsetted and the process described above (PCA, identification of k-nearest neighbors, dimensionality reduction using UMAP, and clustering) was repeated for this cluster only. Pseudo-bulk differential expression was performed between the macrophage subclusters which allowed identification of the top genes representative for each of them.

2.11 Spatial transcriptomics

Spatial transcriptomic analysis (10x Genomics Visium FFPE kit, catalog no. 1000338) was performed on archived formalin-fixed paraffin-embedded (FFPE) tissue sections from murine metastatic melanoma samples. Spatial transcriptomics was performed according to manufacturer protocol. Briefly, tissue RNAs were isolated using Allprep DNA/RNA FFPE kit (Qiagen, catalog no. 80234) and quality controlled (DV200 greater than or equal to 50%). Then, 5 μm tissue sections were cut and placed onto Visium slides and dried at 42°Celsius for 3 hours. After keeping the slide with desiccant overnight, slides were dried again for 2 hours at 60°Celsius. All slides were deparaffinized and stained for Hematoxylin and Eosin (H&E). First, slides were covered in 1 mL Hematoxylin (Millipore Sigma, catalog no. MHS16) for 3 minutes at room temperature. After intermittent washing steps, the slides were then covered in 1 mL Bluing reagent (Agilent, catalog no. CS70203-2) for 1 minute at room temperature and washed. Last, slides were submerged in Eosin (Millipore Sigma, catalog no. HT110116) for 1 minute. H&E-stained slides were imaged on a Evos M7000 Microscope. Probe hybridization, probe ligation, probe release, extension, elusion and library construction were done according to the manufacturer's protocol. The spatial transcriptome library was prepared following the manufacturer's instruction and sequenced on the NovaSeq 6000 system at the University of Chicago Genomics core facility.

2.11.1 Spatial transcriptomics data processing

Raw reads were processed using Space Ranger (v1.3.0) from 10X Genomics using the Mouse Transcriptome Probe Set v1.0 as a reference. Downstream analyses were carried out in R. All spots were retained for analysis, as all spots across samples had sufficient reads and features. All samples were imported and merged in R using the Seurat package.

2.11.2 Spot summaries by gene combinations

To visualize expression of different gene combinations across each tissue, features were built for each gene or set of genes and added to the metadata for the merged Seurat object and then visualized using the function SpatialDimPlot with custom color schemes defined for each set of genes. The same features were used to estimate the number of spots in each sample corresponding to each set of gene combinations.

2.11.3 Distances between spots

We used the package Giotto (v1.1.2) to estimate distances between spots defined by the expression of specific genes. We first converted the merged Seurat object into a Giotto object by providing the Seurat count matrix and the combined image coordinates to the function createGiottoObject. We then used createSpatialNetwork with maximum_distance_delaunay set to 400 to build a network representation of the adjacency between spots in each tissue. In order to estimate the distance between spots, such as the distance from each $M2^+$ spot to the nearest $CD3^+$ spot, we used the function findNetworkNeighbors to first find the intersection between all M2 spots and all direct neighbors to a $CD3^+$ spot. We then grew the list of neighbors iteratively up to a maximum distance of 20 spots (all M2 were actually within 6 spots of a $CD3^+$ spot). A custom R function was written to simplify this iterative process to directly add the estimated distance to the Seurat object, including the reciprocal calculation of the distance from a $CD3^+$ to the nearest $M2^+$ spot. This process was repeated for different subsets of $M2^+$ spots (e.g. $Ccl8^+$ M2 spots) or $CD3^+$ spots (e.g. $Cd3^+$ $Cd4^+$ $Foxp3^+$ spots), and the results were summarized in a data.frame object and visualized with ggplot2 (v3.4.4).

2.11.4 Pseudobulk differential expression analysis

Differential expression analysis was carried out using a pseudobulk approach with edgeR (v3.40.2) and limma (v3.54.1). Prior to building pseudobulk samples, we first identified all $CD3^+$ $M2^+$ and $CD3^+$ DC^+ spots. $M2^+$ spots were defined as $Adgre1^+$ $SiglecF^-$ spots expressing at least one of Ccl8, Gas6, Cd163, or Cd209g, and DC^+ spots were defined as $Itgax^+$ spots expression at least one of Batf3, Xcr1, or Clec9a. Due to the size of macrophages and dendritic cells, we excluded any $M2^+$ spots that were adjacent to a DC^+ spot and vice versa. We also excluded any $M2^+$ spots that were adjacent to an $M1^+$ spot, with $M1^+$ spots defined as spots expressing $Adgre1^+$ $SiglecF^-$ and either CD14 or IL-1β. Adjacency was identified using findNetworkNeighbors as above. Given the exclusion criteria, we then created $CD3^+$ $M2^+$ and $CD3^+$ DC^+ subsamples within each tissue, normalized the expression of each gene by the expression of Actb or CD3ϵ, CD3γ and CD3δ, and then summed the normalized expression across spots within each group to build pseudobulk samples. In the case of slides 2C and 5A, only 1 $CD3^+$ DC^+ spot remained after exclusions, and these samples were not included for downstream comparisons.

After preparing the pseudobulk samples, the data were processed following standard bulk RNA workflows, including filtering to remove genes with low expression (performed with filterByExpr from edgeR), log-cpm normalization with the cpm function, and finally TMM normalization with calcNormFactors. DEGs were then identified with voomWithQualityWeights from the limma package, with the design model.matrix defined to identify either treatment effects (ex-β-catenin vs water comparisons) or cell type effects (DC vs M2 comparisons).

2.11.5 Heatmaps

Summary heatmaps were created to show the mean scaled expression for genes of interest across $CD3^+$ DC^+ and $CD3^+$ $M2^+$ spots in each sample. To build these values, we

normalized expression by Actb or CD3ϵ, CD3γ and CD3δ and then applied the functions NormalizeData and ScaleData from Seurat. The latter two functions were applied to each sample separately. The final result are values akin to Z-scores for each gene when compared to the expression of that gene across all spots in a given tissue. Finally, we subset the data to only the DC^+ and $M2^+$ spots that meet the exclusion criteria applied to the differential expression analysis. Within each sample, we then estimated the mean of the scaled expression for each gene. Results were also summarized further by averaging the sample-level mean expression at the treatment or cell type levels. (These means were simply the mean of values shown in the sample-level heatmaps, rather than recalculating the means from a pool of all appropriate spots across samples. This choice is made to prevent samples with more spots from having a disproportionate impact on the final mean.)

Target	Primer 1	Primer 2	Primer 3
Braf	CTC TGC TGG GAA AGC GGC	TGA GTA TTT TTG TGG CAA CTG C	n/a
Cre:ER	CAG GGT GTT ATA AGC AAT CCC	CCT GGA AAA TGC TTC TGT CCG	n/a
Pten	AAC ATG CAA CAC TGT AAA TTC AAC TG	TCC TGC AGC CCG GGG G	GCT ACC AGG ATG CTT CTG AC
Ctnnb1	ACA TTC ATA AAG GAC TTG GGA GGT GT	AGA ATC ACG GTG ACC TGG GTT AAA	n/a
Ind-Ctnnb1	GCA CAG CAT TGC GGA CAT GC	GCA GAA GCG CGG CCG TCT GG	CCC TCC ATG TGT GAC CAA GG
rtTA	AGC CTG CCC AGA AGA CTC C	AGA CTG CCT TGG GAA AAG CG	CTG GCT TCT GCG GAC CG

Table 2.1: Mouse Primers.

Marker	Fluorophore	Clone	Dilution	Vendor	Cat. No.
CD45	APC	30-F11	1:200	BioLegend	103112
F4/80	Pacific Blue	BM8	1:200	BioLegend	123124
Siglec-F	PE	E50-2440	1:200	BD	552126
Fixable Viability Dye	eFluor 780	n/a	1:1000	Invitrogen	65-0865-14

Table 2.2: Antibodies for Sorting $CD45^+$ and $F4\text{-}80^+$.

Marker	Clone	Dilution	Duration	Temperature	Vendor	Cat. No.
Anti-β-Catenin	D10A8	1:30	Overnight	4°Celsius	Cell Signaling	8480S
Anti-CD3ϵ	n/a	1:60	1 hour	ambient	Abcam	Ab16669
Anti-Sox10	SD204	1:1000	1 hour	ambient	Novue	NBP2-67812

Table 2.3: Antibodies for Multiplex ImmunoFluorescence.

Marker	Dilution	Duration	Temperature	Vendor	Cat. No.
Opal 520	1:200	1 hour	ambient	AKOYA	OP-001001
Opal 570	1:200	1 hour	ambient	AKOYA	OP-001003
Opal 690	1:200	1 hour	ambient	AKOYA	OP-001006
Opal 620	1:200	1 hour	ambient	AKOYA	OP-001004

Table 2.4: Opal Antibodies.

CHAPTER 3

RESULTS

3.1 The development of a novel genetically engineered mouse model of inducible β-catenin

Previous findings from our laboratory demonstrated that constitutive activation of β-catenin in a genetically engineered mouse model of melanoma resulted in a reduced immune cell infiltrate within the TME, which was accompanied by a loss of efficacy of anti-CTLA-4 and anti-PD-L1 immunotherapy [27, 23]. These collective observations led us to ask a new question: Would genetic elimination of β-catenin in established tumors reinvigorate the immune system resulting in re-infiltration by immune cells and restoration of checkpoint blockade efficacy?

To approach this question and investigate the impact of tumor cell-intrinsic β-catenin modulation, we developed a novel genetically engineered mouse model (GEMM) that allows for the dynamic regulation of tumor cell-intrinsic β-catenin expression both on and off. The ability to modulate tumor cell-intrinsic β-catenin within an animal model provides us with a unique tool to investigate the direct effects of β-catenin modulation on the tumor immune microenvironment.

This GEMM employs a tyrosinase-driven, tamoxifen-regulated Cre-recombinase model system, which was designed to drive the expression of an active form of Braf ($Braf^{V600E}$), and the bi-allelic deletion of the tumor suppressor gene PTEN. The combination of these two alterations within tumor cells has been established as sufficient to generate melanomas in mice and are frequently seen alterations in human tumors. Furthermore, these mutations were studied in our previously established constitutive mouse model in which the activation of $Braf^{V600E}$ and the PTEN deletion in autochthonous murine tumors serves as a foundational model to mimic the genetic landscape of human metastatic melanoma.

To enable dynamic regulation, we incorporated a reverse transactivator system that, upon administration of doxycycline, initiates the expression of a mutant, non-degradable form of β-catenin (β-catenin^{S33Y}). This addition enables the doxycycline inducible regulation of active β-catenin expression, providing a versatile tool for dissecting the role of tumor cell-intrinsic activation of β-catenin signaling pathway in modulation of the host immune response [130] (Fig 3.1).

Thus, creating this model involved crossing mice harboring the tyrosinase-Cre-ER, Braf^{V600E} and PTEN$^{-/-}$ background with animals expressing the reverse transactivator and inducible β-catenin^{S33Y}. All experimental animals were selected to be homozygous for Braf^{V600E}, the reverse transactivator, and the inducible β-catenin construct, ensuring uniformity in genetic modification across the study cohort. Additionally, the bi-allelic deletion of the PTEN gene was confirmed in all mice, alongside the Cre^{+} genotype, guaranteeing the expression of the targeted genes and the fidelity of the experimental model.

3.2 Genetic expression of β-catenin allows detection of nuclear accumulation

Our first goal was to explore assays that would enable detection of nuclear β-catenin in tissue sections. To address this initial question, we began with inducing tumors in the original Braf^{V600E} / PTEN$^{-/-}$ (BP) and Braf^{V600E} / PTEN$^{-/-}$ / CAT-STA (BPC) animals by topically applying 4-HO tamoxifen to the freshly shaved dorsal skin. Topical application favors localized activation of the Cre-recombinase system, thereby triggering the genetic modifications designed to simulate in situ melanoma development. Following a six-week period, a timeframe chosen based on preliminary studies from our laboratory indicating optimal tumor growth, we harvested the tumors for analysis (Figure 3.2.a).

Focusing first on assessing the status of β-catenin expression within the tumor cells, we used Immunohistochemistry (IHC) to stain tissue samples from tumors in which we

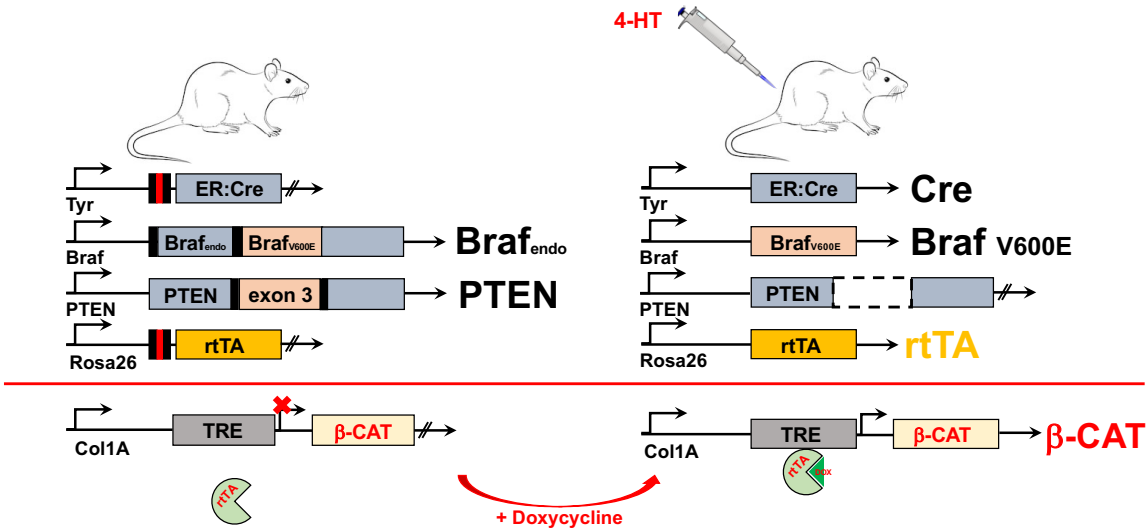

Figure 3.1: **Genetically engineered mouse model.** The genetically engineered animal model we developed contains Cre-recombinase restricted to the tyrosinase promoter, a mutant $Braf^{V600E}$ in the Braf locus, lox-STOP-lox PTEN in the PTEN locus, and a reverse transactivator under the Rosa26 promoter. A final β-$catenin^{S33Y}$ was inserted under the control of the Col1a promoter. The β-$catenin^{S33Y}$ expression is controlled by the presence of doxycycline in the system.

induced constitutive activation of β-catenin compared to control samples. We detected clear nuclear expression of β-catenin at the protein level in tumor samples from BPC animals when compared to litter mate BP controls (Fig 3.2.b). Upon choosing regions of interest and quantifying the amount of nuclear β-catenin, we observed a meaningful increase in the nuclear levels of β-catenin expression in the BPC animals (Fig 3.2.c). This finding confirmed the model's functionality and highlighted the potential for active signaling via β-catenin in

this melanoma context.

A noteworthy observation was that the tumors expressing active β-catenin also showed a marked increase in melanin production. This increase in melanin presented a challenge, as its presence interfered with the IHC staining process and thereby complicating the interpretation of our results. The increase in melanin production did not fully interfere with our analysis of BPC tumor samples and we were able to detect clear differences between the BPC and BP samples, but it did prompt the consideration of alternative techniques.

3.3 Doxycycline administration in the inducible GEMM results in the nuclear accumulation of β-catenin

With an assay for β-catenin detection in hand, we sought to ascertain whether it was feasible to activate the tumor cell-intrinsic β-catenin^{S33Y} using the TET-ON system. Tumors were induced by topical 4-OH tamoxifen on day zero in the Braf^{V600E} / PTEN$^{-/-}$ / indβ-catenin^{S33Y} (BPiC) model, at which time we introduced either sucrose alone or a combination of doxycycline and sucrose in their drinking water which was maintained throughout the tumor progression period (Fig 3.3.a). In these initial experiments we included historical GEM controls, namely the Braf^{V600E} / PTEN$^{-/-}$ (BP) and Braf^{V600E} / PTEN$^{-/-}$ / CAT-STA (BPC) models.

In the preliminary stages of our investigation, IHC images (Fig 3.3.b) and subsequent quantification (Fig 3.3.c) aimed at assessing nuclear β-catenin localization in BPiC tumors yielded inconclusive results. This ambiguity was attributed to the augmented melanin production observed in these tumors, which interfered with the accurate evaluation and quantification of β-catenin's nuclear translocation.

In an effort to address the technical challenges encountered due to the enhanced melanin production within these tumors, we shifted multiplex immunofluorescence (mIF) staining. To this end, tumor induction in BPiC animals was performed as before (Fig 3.4.a). Following a

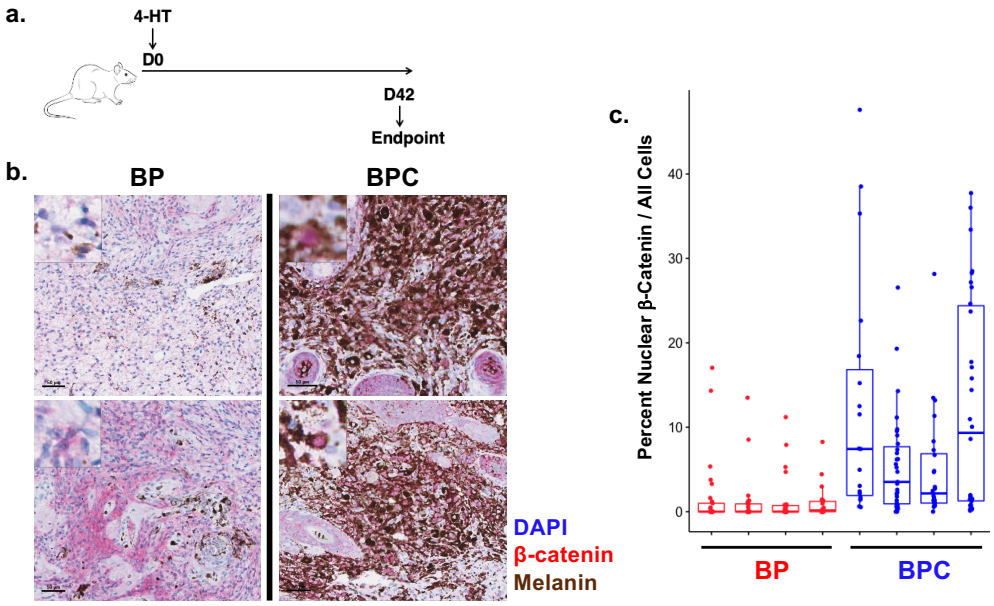

Figure 3.2: **Genetic expression of β-catenin enables detection of nuclear accumulation.** a. Experimental design: Tumors were induced at day zero using 4-hydroxytamoxifen and allowed to develop until day 42 (experimental endpoint). b. Immunohistochemistry images of representative samples for $Braf^{V600E}$ / $PTEN^{-/-}$ (BP) and $Braf^{V600E}$ / $PTEN^{-/-}$ / CAT-STA (BPC) tumors showing β-Catenin staining. Blue = DAPI, red = β-Catenin, brown = melanin. c. Quantification of nuclear expression of β-catenin in $Braf^{V600E}$ / $PTEN^{-/-}$ (red, n=4) and $Braf^{V600E}$ / $PTEN^{-/-}$ / CAT-STA (blue, n=4) tumor samples. One dot = one region of interest, 8-10 regions of interest were selected per tumor.

six-week period to allow for tumor development, these tumors were excised, fixed in formalin, and subsequently processed for immunostaining.

Representative mIF images (Fig 3.4.b) demonstrate a pronounced punctate pattern, indicative of nuclear localization, exclusively in animals exposed to doxycycline. This increased nuclear translocation of β-catenin was absent in the control animals maintained on

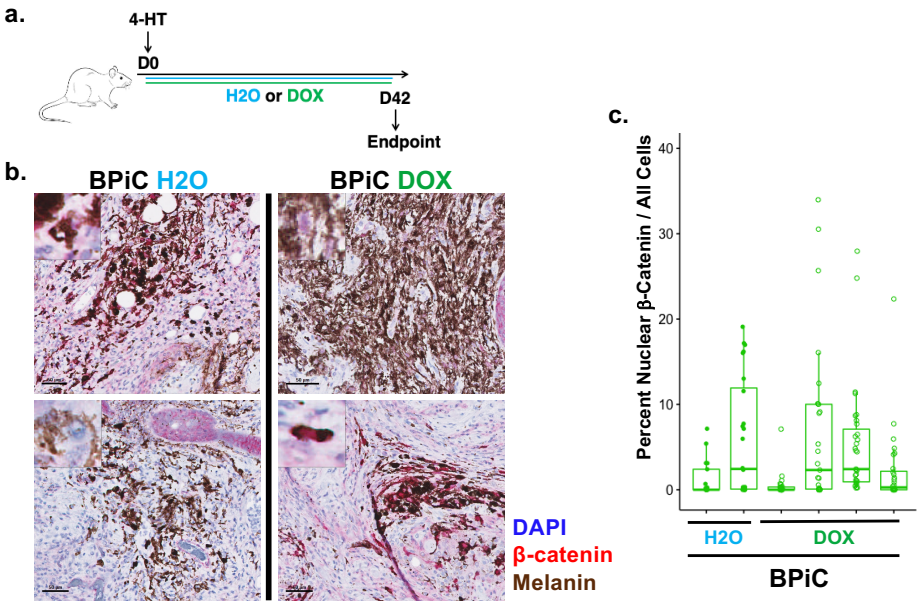

Figure 3.3: **Doxycycline administration in the inducible GEMM results in the nuclear accumulation of β-catenin.** a. Experimental design: Tumors were induced at day zero using 5uL of 4-hydroxytamoxifen at which time the animals were placed on sucrose only or sucrose plus doxycycline water until day 42 (experimental endpoint). b. Immunohistochemistry images of representative samples for $Braf^{V600E}$ / $PTEN^{-/-}$ / indβ-$Catenin^{S33Y}$ (BPiC) maintained on sucrose only water (left) or on sucrose plus doxycycline water (right). Blue = DAPI, red = β-Catenin, brown = melanin. c. Quantification of nuclear expression of β-catenin in tumor samples from $Braf^{V600E}$ / $PTEN^{-/-}$ / indβ-$Catenin^{S33Y}$ (green) exposed to sucrose (n=2) or sucrose plus doxycycline (n=4). One dot = one region of interest, 8-10 regions of interest were selected per tumor.

sucrose water only. A statistical examination of both groups revealed a significant increase in nuclear translocation of β-catenin specifically within the doxycycline-exposed group (Fig 3.4.c). These results demonstrate the successful induction of tumor cell-intrinsic β-catenin expression and nuclear translocation in this model.

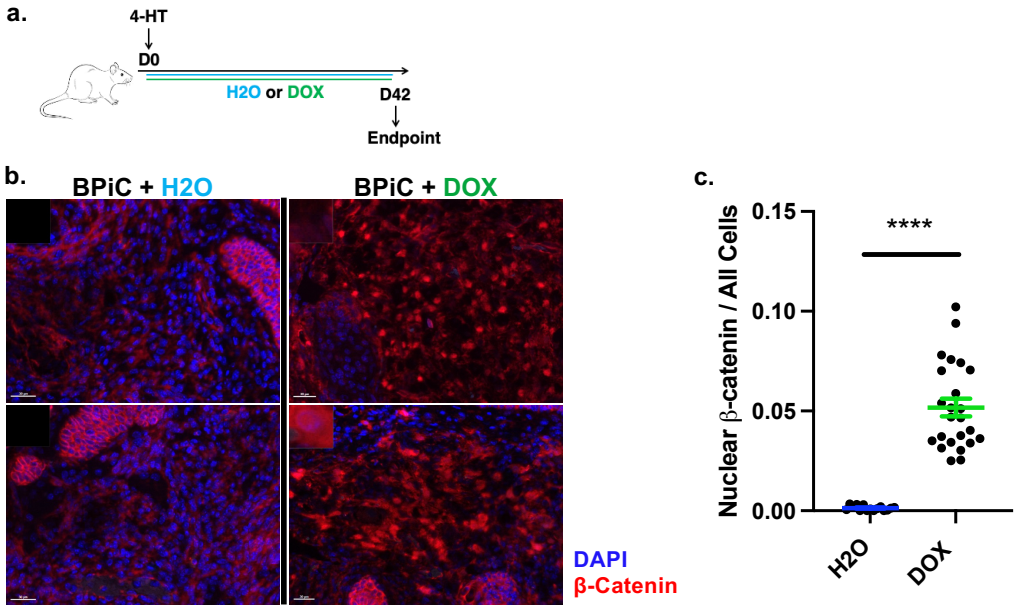

Figure 3.4: **Administration of doxycycline in the inducible mouse model results in nuclear accumulation of β-catenin.** a. Experimental design: Tumors were induced at day zero using 4-hydroxytamoxifen at which time the animals were placed on sucrose only or sucrose and doxycycline water until day 42 (experimental endpoint) b. Multiplex Immunofluorescence images of representative tumor samples from $Braf^{V600E}$ / $PTEN^{-/-}$ / indβ-$Catenin^{S33Y}$ (BPiC) maintained on on sucrose only or sucrose and doxycycline water. Blue = DAPI, red = β-Catenin. c. Quantification of nuclear β-Catenin staining, one dot = one mouse. All data are mean $\pm$ s.e.m., unpaired Welch's t test **** $P \leq 0.0001$.

3.4 Doxycycline inducible β-catenin tumors have decreased $CD3^+$ T cell infiltration

Our laboratory previously demonstrated that constitutive expression of tumor cell-intrinsic β-catenin was associated with decreased $CD3^+$ T cell infiltration. To explore this

phenomenon in our inducible model, multiplex immunofluorescence (mIF) was employed. We found via mIF an approximate two-fold decrease in $CD3^+$ T cell staining in tumors having doxycycline-induced β-catenin accumulation, confirming our previous observations (Fig 3.5.a,b,c). Thus, inducible β-catenin was capable of leading to diminished T cell accumulation within the TME.

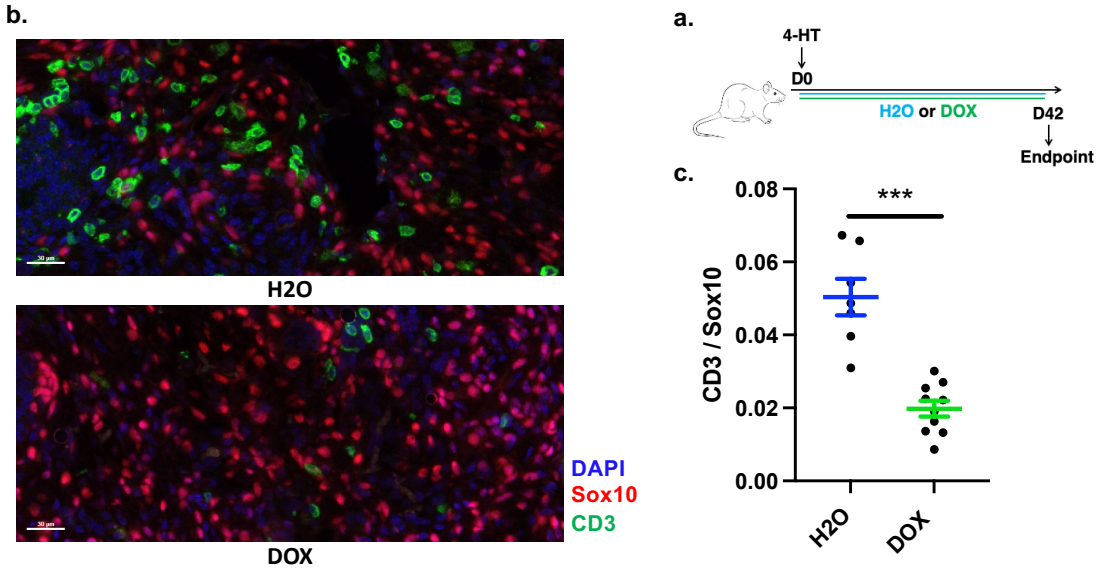

Figure 3.5: **Doxycycline inducible β-catenin tumors have decreased $CD3^+$ T cell infiltration.** a. Experimental design: at day zero, tumors were induced using 4-hydroxytamoxifen and the animals were placed on sugar water or doxycycline water until day 42 (experimental endpoint) b. Multiplex Immunofluorescence images of representative tumor samples from $Braf^{V600E}$ / $PTEN^{-/-}$ / indβ-$Catenin^{S33Y}$ maintained on sucrose only or sucrose plus doxycycline water. Blue = DAPI, red = Sox10, green = $CD3^+$. c. Quantification of $CD3^+$ staining, one dot = one mouse. All data are mean ± s.e.m., unpaired Welch's t test *** $P \leq 0.001$.

3.5 Doxycycline administration itself to baseline GEMMs does not alter the CD3$^+$ T cell infiltration

Prior work in our laboratory had demonstrated that the composition of the gut microbiota could influence anti-tumor immunity and immunotherapy efficacy [88]. Inasmuch as we were administering doxycycline to our mice, it was conceivable that a shift in microbiota composition caused by this antibiotic might have altered T cell accumulation within the TME even without the inducible β-catenin transgene. To this end, we administered either sucrose alone or sucrose plus doxycycline to our GEMMs, including mice without the inducible β-catenin transgene. We observed that despite exposure to doxycycline the entire six-week period of tumor development, animals that did not harbor the reverse transactivator and the inducible β-catenin did not exhibit alterations in the CD3$^+$ T cell compartment (Fig 3.6.a,b,c). These findings substantiate our conclusion that alterations observed within the immune compartment of the inducible animal model are attributed exclusively to β-catenin modulation, independent of any effects from doxycycline administration alone.

3.6 Combination checkpoint blockade fails to control tumors expressing doxycycline-inducible β-catenin

The ultimate goal of our work was to determine whether elimination of tumor cell-intrinsic β-catenin signaling from an established non-T cell-inflamed tumor would restore checkpoint blockade efficacy. To this end, we first investigated the response to immune checkpoint blockade (ICB) of animals lacking β-catenin expression as well as animals with continuous β-catenin expression. Tumors were induced simultaneously with exposure to sucrose alone or sucrose plus doxycycline via the drinking water for a duration of six weeks. Three weeks following tumor induction, the halfway point of tumor development, treatment with combination anti-CTLA-4 and anti-PD-L1 therapy was initiated (Fig 3.7.a). This

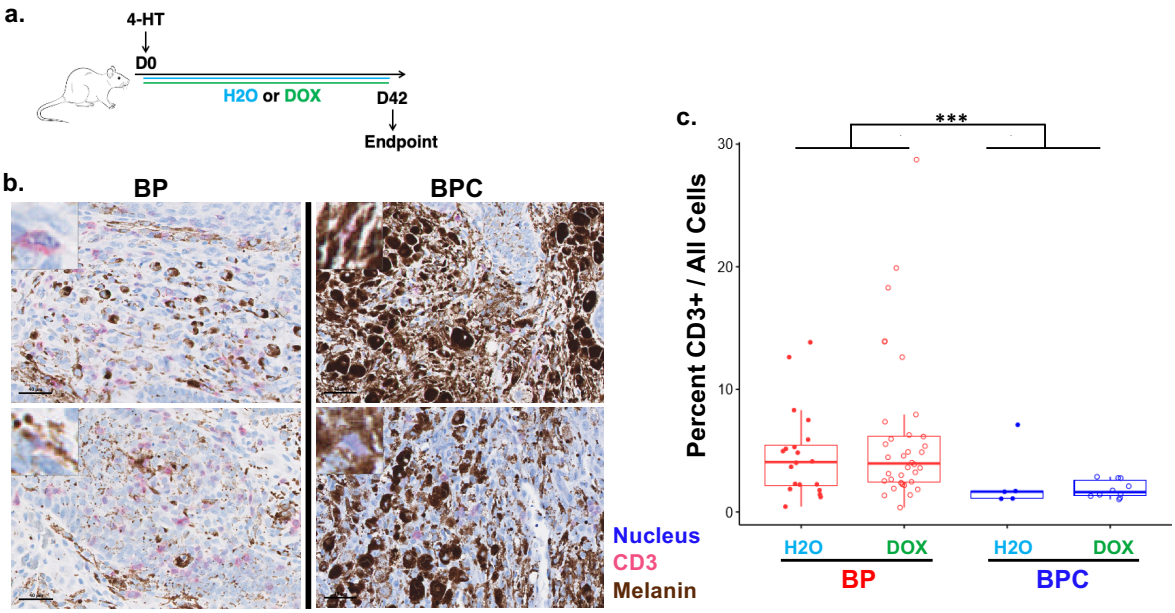

Figure 3.6: **Doxycycline administration itself to baseline GEMMs does not alter the CD3$^+$ T cell infiltration.** a. Experimental design: Tumors were induced at day zero using 4-hydroxytamoxifen at which time we introduced either sucrose alone or a combination of doxycycline and sucrose in their drinking water which was maintained throughout the tumor progression period. b. Immunohistochemistry images of representative samples for Braf^{V600E} / PTEN$^{-/-}$ (BP) and Braf^{V600E} / PTEN$^{-/-}$ / CAT-STA (BPC) tumors showing CD3 staining. Blue = DAPI, red = CD3, brown = melanin. c. Quantification of CD3$^+$ T cell counts in Braf^{V600E} / PTEN$^{-/-}$ (red) exposed to water (H2O) and doxycycline (DOX) and Braf^{V600E} / PTEN$^{-/-}$ / CAT-STA (n=4) exposed to water (H2O) and doxycycline (DOX). One dot = one region of interest. All data are mean ± s.e.m., unpaired Welch's t test *** P $\leq$ 0.001.

treatment was administered every other day for the remainder of the experiment. Animals not subjected to doxycycline, and which did not exhibit detectable levels of nuclear β-catenin accumulation, displayed modest but statistically significant response to combination

anti-CTLA-4 and anti-PD-L1 therapy, as we had observed in our previous studies (Fig 3.7.b) [27]. In contrast, animals maintained on doxycycline, and which exhibited nuclear β-catenin accumulation, demonstrated resistance to ICB treatment (Fig 3.7.c). These findings not only corroborate our previous work but also align with data published by other research groups, reinforcing the interplay between nuclear β-catenin accumulation, immune exclusion, and the efficacy of checkpoint blockade.

3.7 Treating established tumors with doxycycline leads to a rapid increase in nuclear β-catenin accumulation

We next aimed to elucidate the temporal kinetics of β-catenin nuclear accumulation following doxycycline administration. Our experimental design was informed by a reverse engineering approach, due to the necessity of a sizable tumor for experimental evaluation of β-catenin. Given that a full six weeks are required to generate tumors suitable for end-point analysis, and our aim to assess the impact of doxycycline administration over periods of 2, 5, or 7 days, we transitioned the animals from a sucrose only solution to a combined doxycycline and sucrose solution on days 35, 37, and 40 following tumor induction (Fig 3.8.a). This scheduling ensured that the tumors were exposed to doxycycline for the designated duration of 2, 5, or 7 days prior to reaching the experimental endpoint, allowing the examination of β-catenin accumulation within a controlled time-frame. mIF analysis assessing nuclear β-catenin levels revealed that accumulation of nuclear β-catenin was observable as early as 2 days post-doxycycline exposure, with a notable increase by day 5. One week post doxycycline exposure, the levels of nuclear β-catenin mirrored those observed in animals subjected to a continuous six-week doxycycline regimen (Fig 3.8.b,c).

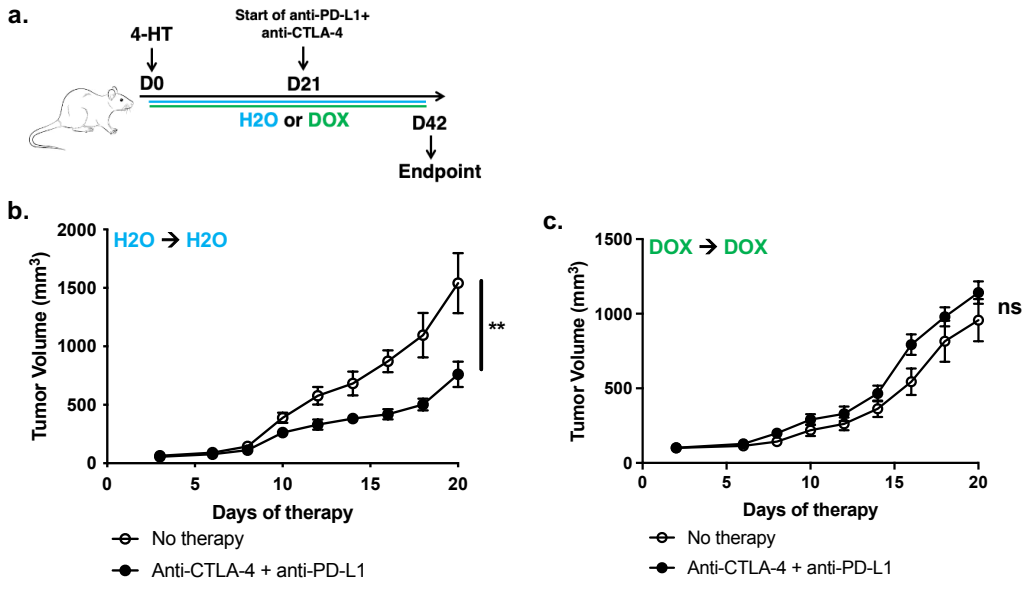

Figure 3.7: **Combination checkpoint blockade fails to control tumors expressing doxycycline-inducible β-catenin.** a. Experimental design: at day zero, tumors were induced using 4-hydroxytamoxifen and the animals were placed on sucrose only or sucrose plus doxycycline water; starting at day 21 post tumor induction, animals were treated with anti-CTLA-4 plus anti-PD-L1 or DPBS every other day until day 42 (experimental endpoint). b. Tumor growth curves in $Braf^{V600E}$ / $PTEN^{-/-}$ / indβ-Cat^{S33Y} animals maintained on sucrose only water (b) ($n \geq 7$) or sucrose plus doxycycline (c) ($n \geq 11$) that were untreated or treated with anti-CTLA-4 plus anti-PD-L1. All data are mean $\pm$ s.e.m., two-way analysis of variance (ANOVA) test. ** $P \leq 0.01$, NS, not significant.

3.8 Removal of doxycycline from the drinking water results in diminished nuclear β-catenin

Following the successful validation of the kinetics of β-catenin induction, we next examined the kinetics of β-catenin reduction following doxycycline removal. Given the increasing

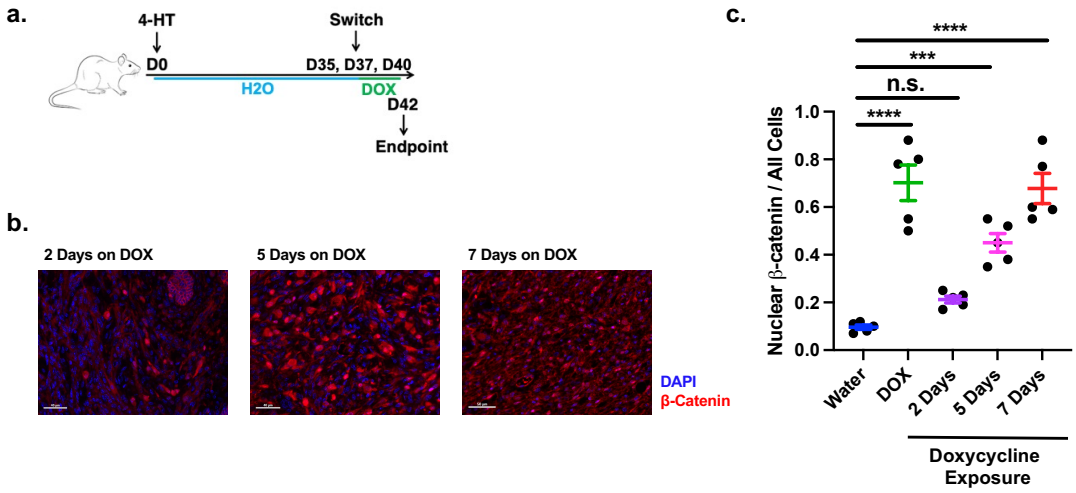

Figure 3.8: **Treating established tumors with doxycycline leads to a rapid increase in nuclear β-catenin accumulation.** a. Experimental design: at day zero, tumors were induced using 4-hydroxytamoxifen and the animals were placed on sucrose water; at day 35, 37 and 40 post tumor induction the animals were switched to sucrose plus doxycycline water until day 42 (experimental endpoint). b. Multiplex Immunofluorescence representative images from $Braf^{V600E}$ / $PTEN^{-/-}$ / indβ-$Catenin^{S33Y}$ tumors that were exposed to doxycycline the last 7, 5 or 2 days of tumor development; blue = DAPI, red = β-Catenin. c. Quantification of nuclear β-Catenin staining, one dot = one ROI. All data are mean $\pm$ s.e.m., one-way analysis of variance (ANOVA) test. **** $P \leq 0.0001$, *** $P \leq 0.001$, NS, not significant.

interest in pharmacologically inhibiting β-catenin within tumors, our novel animal model enables us to genetically deactivate β-catenin, which would simulate the action of a potent pharmaceutical agent targeting the pathway. Because the β-catenin variant expressed in our tumor model likely evades canonical degradation pathways, we reasoned that withdrawal of

doxycycline would not result in an immediate reduction in nuclear β-catenin levels. This hypothesis was based on the assumption that β-catenin degradation in this context would occur primarily through tumor cell proliferation-induced dilution and perhaps through phosphorylation at non-canonical sites. We first conducted experiments in which doxycycline was removed for periods of 2 and 4 days (Fig 3.9.a). These results indicated a clear but non-significant reduction in nuclear β-catenin at day 2, with a more pronounced reduction (approximately 50%) by day 4 (Fig 3.9.b).

Because we saw a clear decrease of nuclear β-catenin at day 4 post doxycycline removal, we evaluated 7 days of doxycycline removal (Fig 3.9.c). Our findings indeed established that, by the seventh day following doxycycline removal from the drinking water, tumors exhibited a near complete absence of nuclear β-catenin expression, in contrast to tumors maintained on a sucrose plus doxycycline water regimen, which displayed robust of nuclear expression (Fig. 3.9.d,e).

3.9 Elimination of nuclear β-catenin re-establishes T cell infiltration within the melanoma TME

Having delineated a temporal window wherein nuclear localization of β-catenin was lost following doxycycline removal, we then assessed whether the loss of β-catenin from established tumors would re-engage the immune system and restore $CD3^+$ T cell infiltration. In our overall study, the genetic ablation of β-catenin was ultimately intended to be paired with combined anti-CTLA-4 and anti-PD-L1 therapy and investigate whether they synergize for effective tumor control. We therefore designed our experiments to allow enough time to ultimately treat with CBI after the potential re-establishment of an immune infiltrate. To this end we administered doxycycline plus sucrose via the drinking water at the time of tumor induction which was continued for one week. After the initial first week of doxycycline exposure, we switched these animals to water containing only sucrose. This would allow one

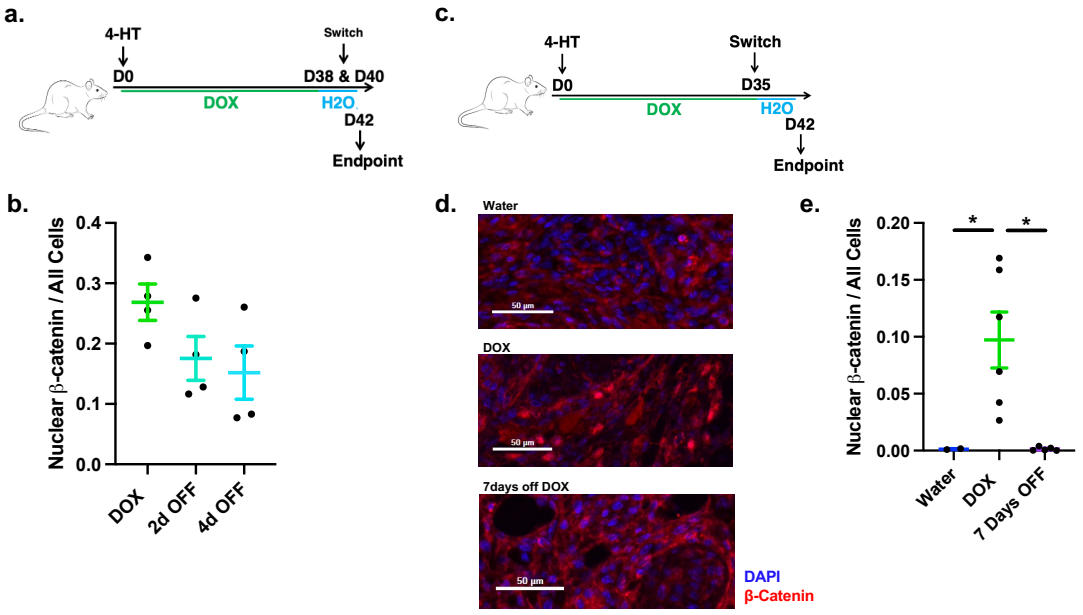

Figure 3.9: **Removal of doxycycline from the drinking water results in diminished nuclear β-catenin.** a. Experimental design: at day zero, tumors were induced using 4-hydroxytamoxifen and the animals were placed on sucrose plus doxycycline water; at day 38 and 40 post tumor induction the animals were switched to sucrose only water until day 42 (experimental endpoint). b. Quantification of nuclear β-Catenin staining, one dot = one mouse. Two independent experiments. All data are mean ± s.e.m., unpaired Welch's t test. NS, not significant. c. Experimental design: at day zero, tumors were induced using 4-hydroxytamoxifen and the animals were placed on sucrose plus doxycycline water; at day 35 post tumor induction the animals were switched to sucrose only water until day 42 (experimental endpoint). d. Immunofluorescence images of representative tumor samples from $Braf^{V600E}$ / $PTEN^{-/-}$ / indβ-$Catenin^{S33Y}$; blue = DAPI, red = β-Catenin. e. Quantification of nuclear β-Catenin staining, one dot = one mouse. Two independent experiments. All data are mean ± s.e.m., one-way analysis of variance (ANOVA) test. * $P \leq 0.05$, NS, not significant.

week for loss of nuclear β-catenin expression, one week for the immune system to become re-engaged, followed by three weeks of combination anti-PD-L1 and anti-CTLA-4 therapy administration (every other day) (Fig 3.10.a).

First, we confirmed that nuclear β-catenin was indeed no longer detected in samples exposed to only one week of doxycycline at the beginning of tumor development. Representative mIF images as well as quantification of nuclear β-catenin display a clear absence of detectable β-catenin in these tumors (Fig 3.10.b,c). In addition to a lack of detectable nuclear β-catenin, the tumors which developed in the presence of β-catenin for the first week had comparable $CD3^+$ T cell infiltration to the tumors which were never exposed to doxycycline. These results indicate that, upon withdrawal of doxycycline and loss of nuclear β-catenin, T cell infiltration was indeed restored (Fig 3.10.c).

3.10 Removal of β-catenin from an established tumor does not restore anti-PD-L1 plus anti-CTLA-4 efficacy

We next evaluated whether genetic elimination of β-catenin from established tumors restores efficacy of checkpoint blockade therapy. Our experimental design was structured to allow sufficient time for immune re-engagement post β-catenin elimination, followed by the administration of checkpoint blockade antibodies. We initiated doxycycline administration simultaneously with tumor induction. After a one-week period, the animals were transitioned to sucrose water alone, hypothesizing that this interval would suffice for the loss of β-catenin, followed by a one-week phase anticipated for the initiation of an immune response. Subsequently, a three-week treatment with anti-PD-L1 and anti-CTLA-4, administered on alternate days, was employed starting at three weeks post-tumor induction (Fig 3.11.a). However, despite the returned $CD3^+$ T cell compartment in the ex-β-catenin tumors, these tumors remained resistant to treatment with anti-CTLA-4 plus anti-PD-L1 (Fig 3.11.b).

These findings were unexpected and suggest that withdrawal of β-catenin alone is not

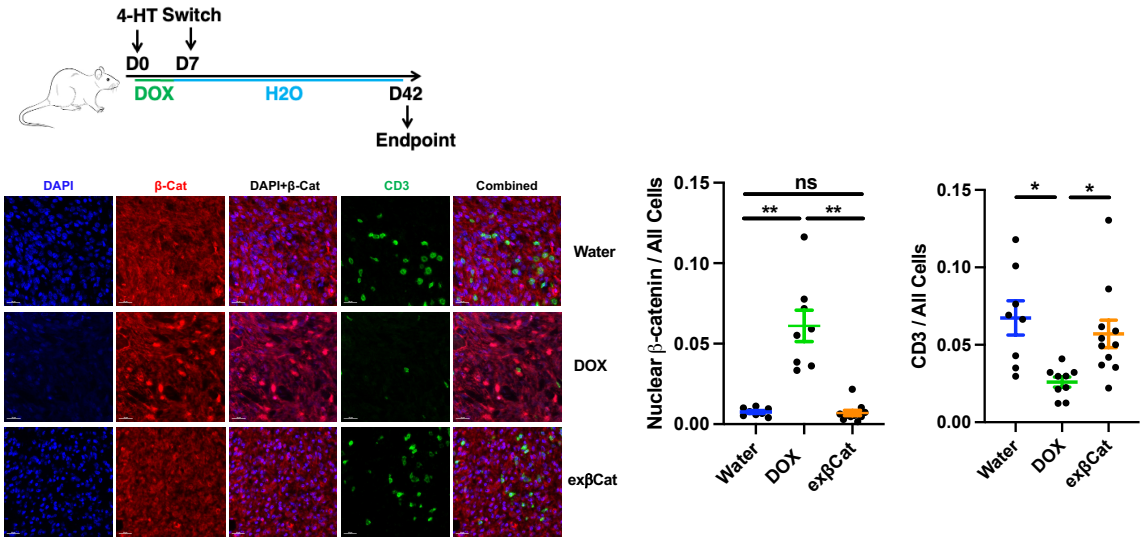

Figure 3.10: **Elimination of nuclear β-catenin re-establishes immune infiltration within the melanoma TME.** a. Experimental design: at day zero, tumors were induced using 4-hydroxytamoxifen and the animals were placed on sucrose plus doxycycline water; at day 7 post tumor induction the animals were switched to sucrose only water until day 42 (experimental endpoint). b. mIF representative images of DAPI, CD3, β-catenin and combined. c,d. Quantification of nuclear β-Catenin staining (c) and CD3^{+} staining (d), one dot = one mouse. All data are mean $\pm$ s.e.m., one-way analysis of variance (ANOVA) test. ** P $\leq$ 0.01, * P $\leq$ 0.05, NS, not significant.

sufficient to sensitize melanoma tumors to CBI. These results imply that pharmacological inhibition of β-catenin signaling pathways in the patients with tumors with β-catenin pathway activation might not be sufficient to engage a therapeutic effect of immunotherapy.

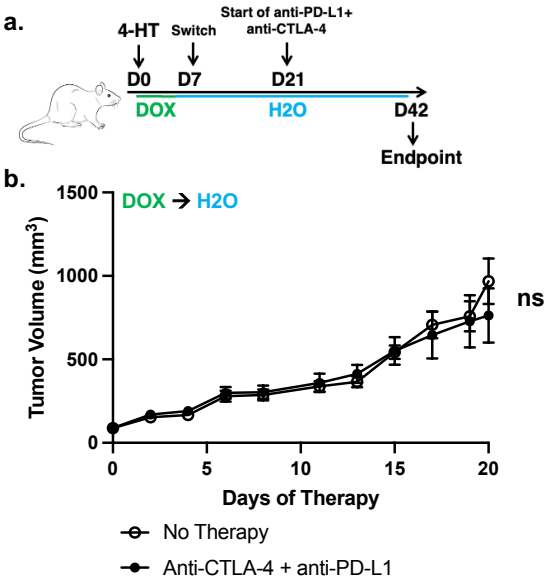

Figure 3.11: **Removal of β-catenin from an established tumor does not restore anti-PD-L1 plus anti-CTLA-4 efficacy.** a. Experimental design: at day zero, tumors were induced using 4-hydroxytamoxifen and the animals were placed on sucrose plus doxycycline water, at day 21 all animals were switched to sugar water. Starting at day 21 post tumor induction, animals were treated with anti-CTLA-4 plus anti-PD-L1 or DPBS every other day until day 42 (experimental endpoint). b. Tumor growth curves in $BRAF^{V600E}$ / $PTEN^{-/-}$ / indβ-Cat^{S33Y} animals ($n \geq 11$) that were untreated or treated with anti-CTLA-4 plus anti-PD-L1. All data are mean $\pm$ s.e.m., two-way analysis of variance (ANOVA) test. ns, not significant.

3.11 Single cell analysis of the immune compartment of ex-β-catenin tumors

Given that tumors with withdrawal of β-catenin remained unresponsive to checkpoint blockade therapy, even with a restored $CD3^+$ T cell presence, our curiosity was piqued

regarding the phenotype and integrity of the $CD3^+$ T cells re-entering these tumors. We also entertained the idea that the tumors' resistance to combined checkpoint blockade might stem from an immune-suppressive microenvironment, distinct from the $CD3^+$ T cell compartment's influence. To explore these varied potential causes, we conducted single-cell RNA sequencing of the immune infiltrate present within the ex-β-catenin tumors. This would allow us to assess the proportion and transcriptional state of the immune cells within the ex-β-catenin tumors. To maximize the impact of β-catenin on the immune compartment, we adopted a modified approach in our experimental design. Tumors were induced on day 0 at which time they were placed on doxycycline plus sugar. Three weeks post tumor induction animals were switched to sugar water, ensuring their development proceeded under continuous exposure to doxycycline/β-catenin for the first three weeks of tumor growth.

After this initial doxycycline/β-catenin exposure, one cohort of mice was transitioned to a sucrose-only drinking solution (Fig 3.12.a). We reasoned that an extended exposure to β-catenin would intensify the immune-resistant phenotype within the ex-β-catenin tumors. Given this alteration in our experimental strategy, we first verified if the immune infiltration was akin to that in tumors not influenced by β-catenin. Our findings indeed demonstrated that ex-β-catenin tumors, which developed in the presence of doxycycline for the initial three weeks prior to doxycycline withdrawal, exhibited restored $CD3^+$ T cell infiltration at levels comparable to our control group (Fig 3.12.b).

We then narrowed our focus to draw comparisons between baseline control tumors and those we termed ex-β-catenin tumors; the tumors exposed to β-catenin for the first 3 weeks only. We omitted tumors that developed under the influence of doxycycline/β-catenin throughout the entire tumor development due to their overall significantly lower immune cell infiltration. Through single-cell comparative analysis of $CD45^+$ lymphocytes from ex-β-catenin tumors, we identified 20 unique clusters, corresponding to 16 distinct immune cell populations (Fig 3.12.c). As expected, this analysis yielded significant numbers of conven-

tional $CD4^+$ and $CD8^+$ T cells, $\gamma\delta$ T cells, and regulatory $FoxP3^+$ T cells. Furthermore, we also detected a notable presence of myeloid-lineage cells, including conventional dendritic cells (DCs) types 1 and 2, macrophage subsets, as well as mast cells and eosinophils.

One challenge within tumors that develop in the skin of genetically engineered mouse models (GEMMs) is the difficulty in digesting these tissues and extracting the majority of immune cells efficiently. Acknowledging these obstacles yet committed to validating our results, we undertook a second single-cell sequencing experiment. In our subsequent attempt, we encountered notable losses in certain cell populations, especially among eosinophils and macrophages subsets. Conversely, we achieved a higher recovery of regulatory $FoxP3^+$ T cells and $\gamma\delta$ T cells (Fig 3.12.c,d). Despite these variations in immune cell recovery, we were confident in our ability to accurately identify the principal immune cell compartments. The uniqueness of each immune population was confirmed through the average expression of selected lineage markers, chosen in alignment with existing literature that characterizes each subpopulation (Fig 3.12.e).

3.12 The immune landscape of ex-β-catenin tumors is permanently altered despite β-catenin removal

Having identified the immune cell subsets present within our inducible melanoma GEMMs, we next focused on the differences between the ex-β-catenin tumors versus control tumors that never had β-catenin expressed. The proportions of immune subsets identified were generally similar across both the experimental and the control groups. Although we noted differential contributions from neutrophils, mast cells, and dendritic cells, given their minor representation among the immune cell populations found in these tumors, we opted to exclude them from our primary analysis. (Fig 3.13.a,b).

Since the ratios of the various immune populations within these tumors exhibited minimal fluctuations, we next investigate potential phenotypic alterations within each immune

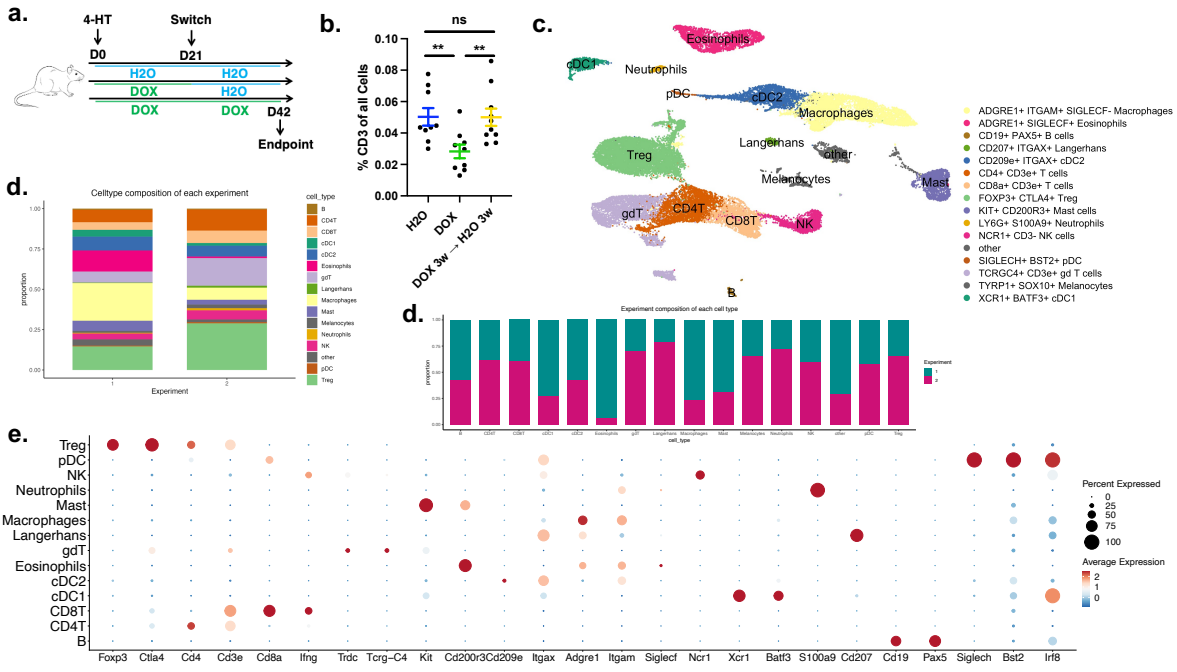

Figure 3.12: **Single cell analysis of the immune compartment of ex-β-catenin tumors.** a. Experimental design: at day zero, tumors were induced using 4-hydroxytamoxifen and the animals were placed on either sucrose or sucrose plus doxycycline water; at day 21 post tumor induction the ex-β-catenin animals were switched to sucrose only water until day 42 (experimental endpoint). b. Quantification of the $CD3^+$ T cell infiltration in ex-β-catenin tumors. One dot = one mouse. The experiment was repeated at least 3 times. All data are mean $\pm$ s.e.m., one-way analysis of variance (ANOVA) test. ** $P \leq 0.01$, ns, not significant. c. UMAP of scRNAseq on all live $CD45^+$ cells isolated from tumors revealed 16 distinct color-coded clusters of cells. General identity of each cell cluster is defined on the right. d. Bar graph of the composition of all immune populations in each single cell RNAseq experimental run. e. Bubble plot displaying the percent and average expression of population defining markers for all relevant immune cell sub-types identified.

cell subset between the two conditions. A comparative analysis of differentially expressed genes between the control tumors and the ex-β-catenin tumors was performed. We employed two distinct analytical approaches: a more conservative method, PseudoBulk, and a less re-

strictive technique, FindMarkers, to rigorously identify the differentially expressed genes in the ex-β-catenin tumors. We identified only a few differentially expressed genes within the T cell or dendritic cell compartments. This outcome was surprising, given our initial hypothesis that we would observe biological differences in these compartments between ex-β-catenin tumors and control samples. However, the majority of the differentially expressed genes were identified within the macrophage subset within these tumors. Specifically, of the 103 differentially expressed genes observed, 89 were exclusive to the macrophage compartment (Fig 3.13.c). Further evaluation revealed a significant enrichment in genes reported to be those associated with M2-like macrophages in ex-β-catenin tumors. Anti-inflammatory genes involved in tissue homeostasis and wound repair were enriched. Of note, genes in this category that have been reported to be linked to an M2-like phenotype in macrophages included Ccl8, Gas6, Mcr1, Cd163, CD209 (f and g), Lyve1 and Vsig4. In contrast, the control tumors displayed an enrichment of pro-inflammatory genes, such as IL6, IL1β, Oas3, Ifi213, Clec4e, and Cxcl3 (Fig 3.13.d). These findings suggest that exposure to β-catenin early during tumor formation results in lasting alterations within the macrophage compartment, with a shift towards an M2-like / anti-inflammatory phenotype that persists even after β-catenin withdrawal.

Building on these initial findings, we delved deeper into the interrelations of these genes using Ingenuity Pathway Analysis. Using this approach, the ex-β-catenin tumors demonstrated pronounced activation of alternative macrophage activation and IL-10 signaling pathways. These pathways are known to contribute to an immune-suppressive microenvironment. In addition, enhanced LXR/RXR activation was observed, which corroborates existing literature indicating that M2-like macrophages elevate cholesterol and fatty acid metabolism processes (Fig 3.14.a).

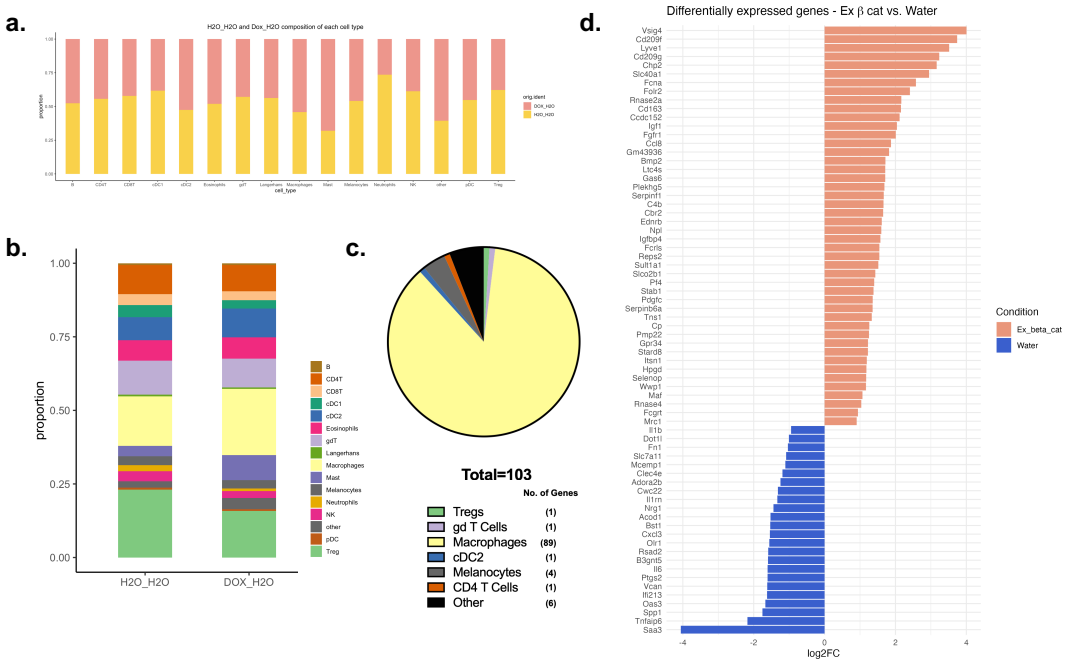

Figure 3.13: **The immune landscape of ex-β-catenin tumors is permanently altered despite β-catenin removal.** a,b. Bar graph of the contribution of all immune population in both the control and the ex-β-catenin tumors. c. Pie chart of the differentially expressed genes between the control and the ex-β-catenin tumors. d. Bar graph of the statistically significant differentially expressed genes within the macrophage cluster comparing the control and the ex-β-catenin tumors.

3.13 Macrophage re-clustering reveals predominance of M2-like phenotypes in ex-β-catenin tumors

Recent studies employing single-cell approaches have revealed multiple subtypes of tumor-associated macrophages, with a range of 5 to 7 distinct subtypes identified within the TME in various studies. The identification of these macrophage subtypes extends beyond the conventional M1/M2 designation typically observed *in vitro*. To explore the macrophages

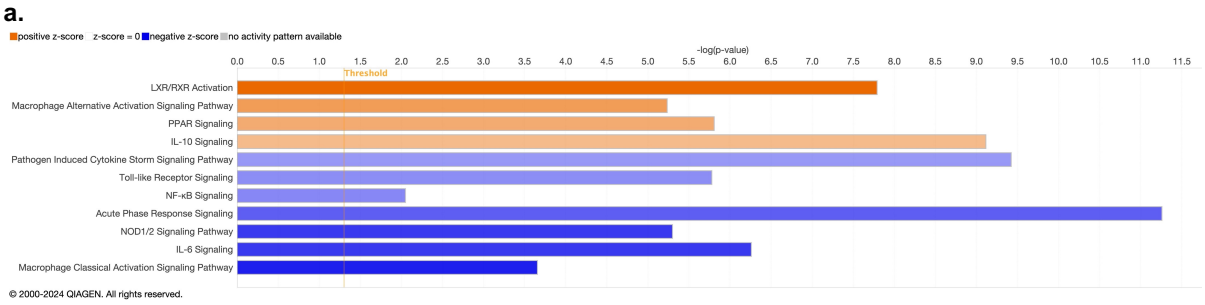

Figure 3.14: **The immune landscape of ex-β-catenin tumors is permanently altered despite β-catenin removal.** a. Ingenuity Pathway Analysis of the differentially expressed genes identified in the macrophage compartment of the scRNAseq analysis.

in our ex-β-catenin tumors in more detail, we sub-clustered all macrophages from our scRNA-seq analyses for increased resolution. This granular examination of macrophages from melanoma GEMMs revealed five distinct macrophage populations.

These populations were discerned based on the average and percentage expressions of 4 to 6 unique genes (Fig 3.15.a). Specifically, Cluster 0 was defined by the expression of genes Clec4e, Il1rn, Olr1, Ptgs2, Flrt3, Il6, and Il1b; Cluster 1 by Ifitm3, Gsr, Plac8, Ifitm6, Hp, and Cd177; Cluster 2 by Cx3cr1, Ciita, Ear2, and Tmem176a; Cluster 3 by Ccl8, Cd163, Cd209g, Gas6, Folr2, and Fcna; and Cluster 4 by Cxcl10, Ccl4, Tnf, Ccl3,

Hspa1b, and Ppp1r15a. Significantly, UMAP visualizations, focusing on the expression patterns of the primary genes defining Clusters 0 and 3, accentuated the distinct functional characteristics of these groups. Cluster 0 was prominently marked by a pro-inflammatory gene expression profile, while in stark contrast, Cluster 3 was defined by a predominance of anti-inflammatory genes. This contrast not only underlines the functional dichotomy within the tumor microenvironment but also emphasizes the nuanced roles these macrophage clusters play in influencing tumor dynamics (Fig 3.15.b).

Notably, UMAPs of the expression of the main genes used to identify clusters 0 and 3 further highlighted that cluster 0 exhibited a marked pro-inflammatory profile, whereas cluster 3 was characterized by predominantly anti-inflammatory gene expression. The UMAP visualizations of each experimental condition provided a visual of the distribution of all five distinct clusters, highlighting a transition from a predominantly M1-like/pro-inflammatory phenotype in the control group to an M2-like/anti-inflammatory phenotype within the ex-β-catenin tumors (Fig 3.15.c). In particular, a marked expansion of Cluster 3 / M2-like macrophages was observed in the ex-β-catenin tumors.

3.14 Spatial examination of ex-β-catenin tumors validates enrichment of immune-suppressive macrophages

It was desirable to sort macrophages out of the ex-β-catenin tumors to evaluate their T cell suppressive functions *in vitro*. However, it was challenging to extract enough cells from these dense GEMM tumors for analysis. Therefore, we opted to pursue spatial transcriptomics, to evaluate T cell activation states in the vicinity of M2-like macrophages compared to T cells adjacent to cDC1s. Our laboratory recently has published that $CD8^+$ T cells in clusters with cDC1 cells show a transcriptional profile predictive of anti-PD-1 efficacy *in vivo* [131]. This approach allows for the assessment of transcripts directly within the tumor microenvironment without necessitating tissue digestion.

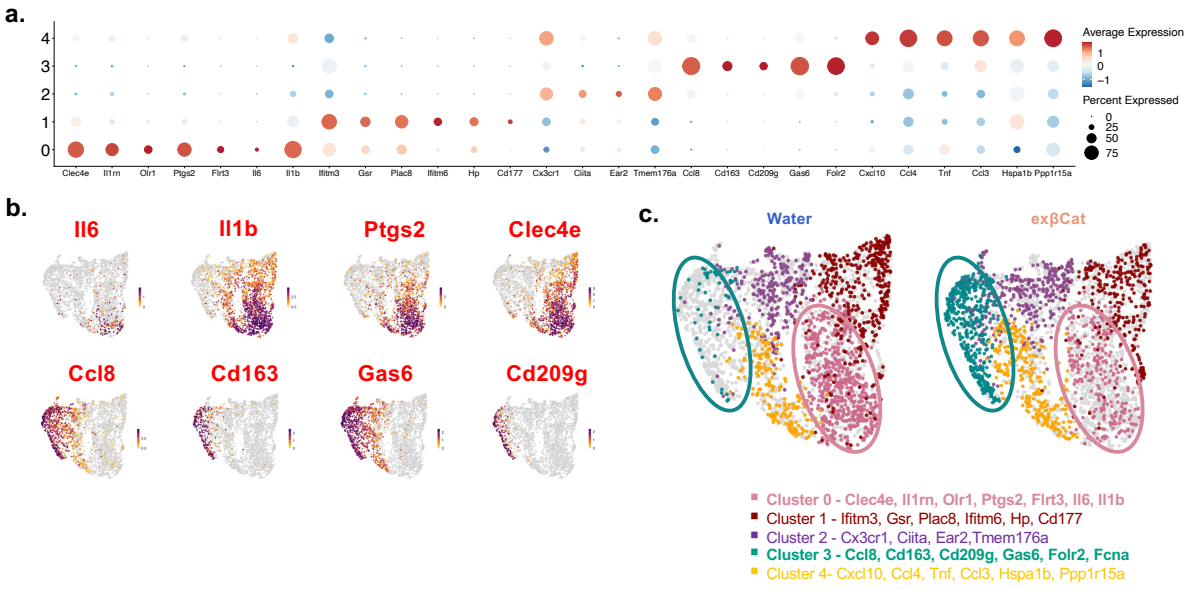

Figure 3.15: **Macrophage re-clustering reveals predominance of M2-like phenotypes in ex-β-catenin tumors.** a. Bubble Plot Analysis depicting average expression and percent expressed of genes used to identify 5 unique macrophage clusters. b. UMAPs showing expression pattern and average expression for selected genes of interest for Cluster 0 and Cluster 3. c. UMAPs exhibiting the gene expression pattern of each unique, color-coded cluster.

We first evaluated the M2 macrophage status in both control and ex-β-catenin tumors, selecting the M2 markers identified in Cluster 3 from our single-cell RNAseq analysis (Ccl8, Gas6, Cd163, and Cd209g). First looking at abundance, ex-β-catenin tumors contained a higher prevalence of these M2-like macrophages compared to control tumors visually confirming our findings using scRNAseq (Fig 3.16.a,b).

We then extended our analysis to evaluate the spatial relationship between these macrophages

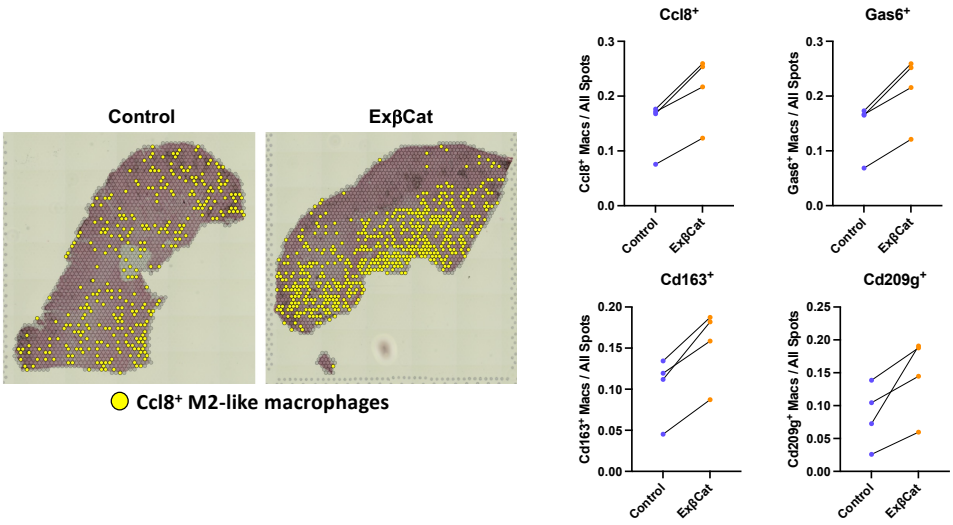

Figure 3.16: **Spatial examination of ex-β-catenin tumors validates enrichment of immune-suppressive macrophages.** a. Representative images of one control tumor (left) and one ex-β-catenin tumor (right) displaying the spots that are F4/80$^+$ and SiglecF$^-$ and Ccl8$^+$ (yellow). b. Ratios of spots that are F4/80$^+$ and SiglecF$^-$ and one M2-like gene (Ccl8$^+$, Gas6$^+$, CD163$^+$, CD209g$^+$) divided by all spots. One-way analysis of variance (ANOVA) test. ns, not significant.

and CD3$^+$ T cells. The analyses revealed that ex-β-catenin tumors exhibited a marked increase in spots that were CD3$^+$ and also expressing one of the selected M2 markers (Fig 3.17.a,b). In aggregate, there was an increase in spots that were CD3$^+$ (identified as Cd3γ^+ or Cd3δ^+ or Cd3ϵ^+) and Adgre1$^+$ Siglecf$^-$ Ccl8$^+$ or Gas6$^+$ or Cd163$^+$ or CD209g$^+$ in the ex-β-catenin tumors (Fig 3.17.c). Although these results did not reach statistical significance because of the challenge of getting enough mice of these complex genotypes and

also the complexity of the analyses, the trend was consistently observed across all analysis methods. These data suggest that ex-β-catenin tumors contain a greater number of M2-like macrophages interacting with T cells within the TME.

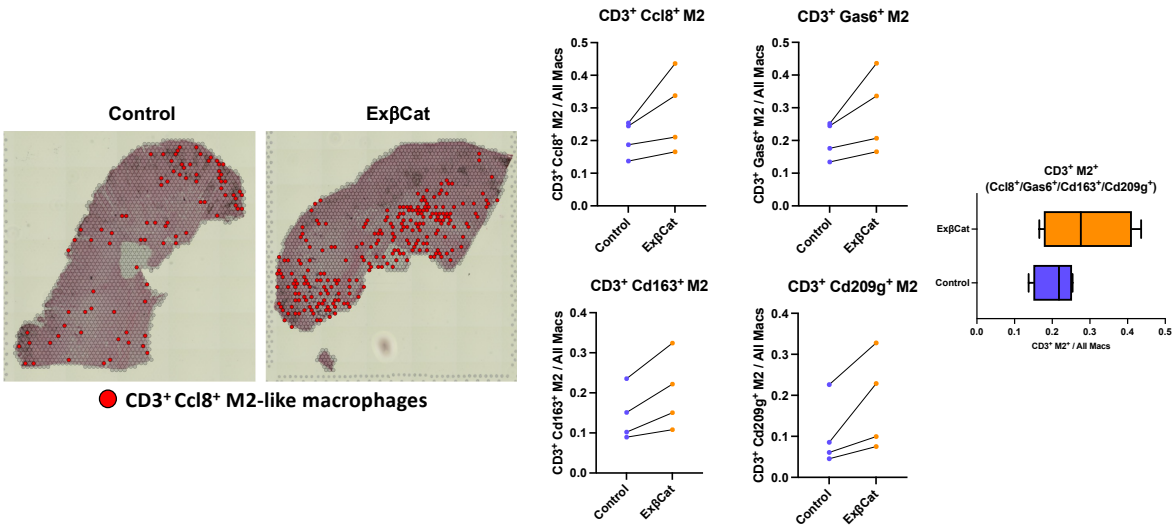

Figure 3.17: **Spatial examination of ex-β-catenin tumors validates enrichment of M2-like macrophages in the vicinity of T cells.** a. Representative images of one control tumor (left) and one ex-β-catenin tumor (right) displaying the spots that are $CD3^+$ $F4/80^+$ and $SiglecF^-$ and $Ccl8^+$ (red). b. Ratios of spots that are $CD3^+$, $F4/80^+$ and $SiglecF^-$ and one M2-like gene ($Ccl8^+$, $Gas6^+$, $CD163^+$, $CD209g^+$) divided by all $F4/80^+$ and $SiglecF^-$ spots. One-way analysis of variance (ANOVA) test. ns, not significant. c. Ratios of spots that are $CD3^+$, $F4/80^+$ and $SiglecF^-$ and $Ccl8^+$ or $Gas6^+$ or $CD163^+$ or $CD209g^+$ divided by all $F4/80^+$ and $SiglecF^-$ spots. One-way analysis of variance (ANOVA) test. ns, not significant.

In addition to investigating the abundance of M2-like macrophages and their co-localization with $CD3^+$ T cells in ex-β-catenin tumors, we analyzed the distances between these two cell

types. By examining the spatial arrangement of M2-like macrophages that were single positive for either Ccl8, Gas6, Cd163, or Cd209g, in relation to the nearest $CD3^+$ T cell, we noted that macrophages from ex-β-catenin tumors were indeed closer to $CD3^+$ T cells (Fig 3.18.a). Moreover, by aggregating data for macrophages positive for any or all of the selected markers, we further validated that these immuno-suppressive macrophages tended to reside nearer to $CD3^+$ T cells in ex-β-catenin tumors compared to control tumors (Fig 3.18.b).

3.15 $CD3^+$ $M2^+$ regions exhibit diminished activation gene expression patterns in ex-β-catenin tumors compared to areas positive for CD3 and cDC1 spots

We next compared the transcriptional profile of spots double positive for CD3 and cDC1 markers to those that were positive for CD3 and M2 markers within ex-β-catenin tumors. We hypothesized that spots positive for CD3 and M2-like macrophages, that were away from any cDC1 positive spots, would display lower T cell activation transcriptional profiles. We recently reported that T cells adjacent to cDC1 cells within the TME represent the subset of T cells showing transcriptional profiles of activation [131]. Indeed, spots positive for CD3 and M2 markers that were spatially segregated from cDC1 markers demonstrated blunted expression of canonical T cell activation molecules, including Il2; Tnfrsf-4, -9, -18; Ctla4; and Gzmk (Fig 3.19). Furthermore, spots that were CD3 and M2-like positive and away from cDC1 exhibited increased expression of markers associated with T cell dysfunction, Tox and Nr4a1 (Fig 3.19). Collectively, these results support the notion that our hypothesis that the persistent presence of M2-like macrophages within ex-β-catenin tumors results in localized suppression of a large fraction of tumor-infiltrating T cells, likely keeping the adjacent $CD3^+$ T cells in check.

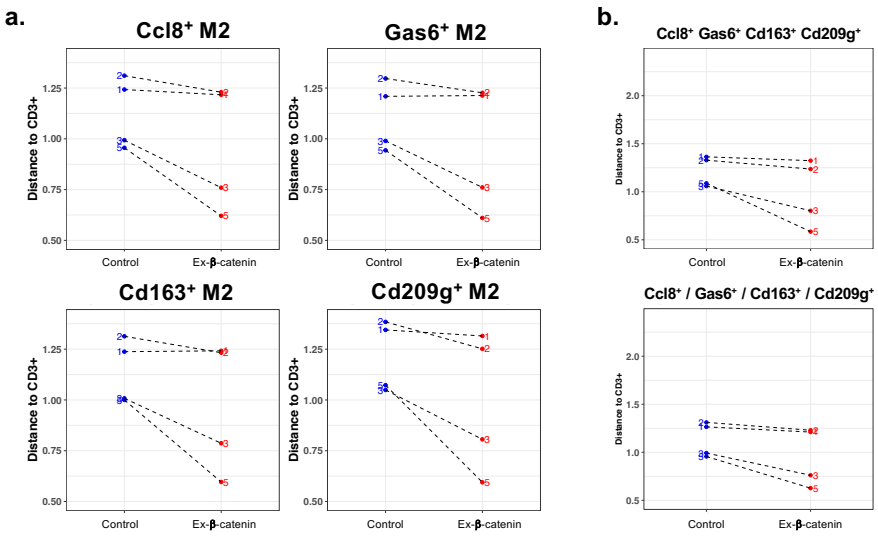

Figure 3.18: **M2-Like macrophages in ex-β-catenin tumors are in closer proximity to CD3$^+$ spots.** a. Average distance of spots that are either F4/80$^+$, SiglecF$^-$ and Ccl8$^+$ to the nearest CD3$^+$ spot; F4/80$^+$, SiglecF$^-$ and Gas6$^+$ to the nearest CD3$^+$ spot; F4/80$^+$, SiglecF$^-$ and CD163$^+$ to the nearest CD3$^+$ spot; and F4/80$^+$, SiglecF$^-$ and CD209g$^+$ to the nearest CD3$^+$ spot. b. Average distance of spots that are either F4/80$^+$, SiglecF$^-$ and Ccl8$^+$ plus Gas6$^+$ plus CD163$^+$ plus CD209g$^+$ to the nearest CD3$^+$ spot (top) and spots that are either F4/80$^+$, SiglecF$^-$ and Ccl8$^+$ or Gas6$^+$ or CD163$^+$ or CD209g$^+$ to the nearest CD3$^+$ spot. Student T test. ns, not significant.

3.16 Areas positive for CD3$^+$ T cells and M2-like macrophages demonstrate reduced proinflammatory pathway activation

To further evaluate the differences between spots that were CD3$^+$ cDC1$^+$ versus spots that were CD3$^+$ M2-like$^+$, we performed Ingenuity Pathway Analysis. When assessing

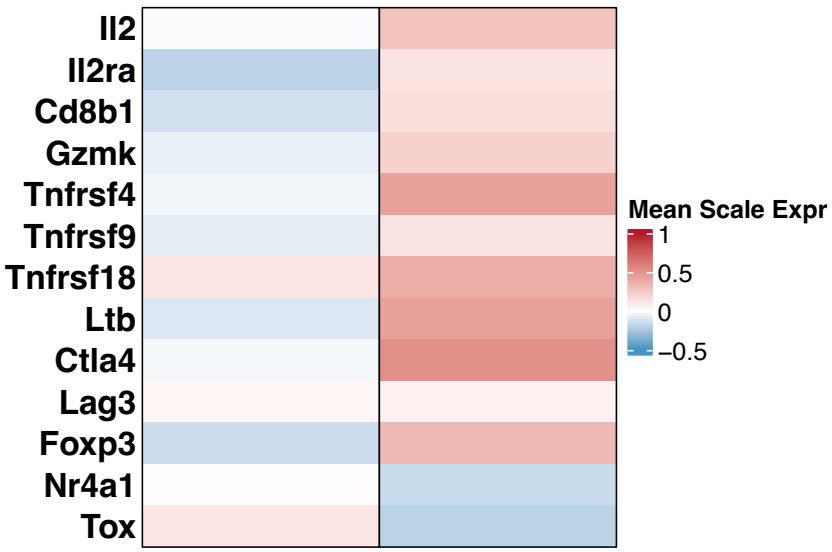

Figure 3.19: **CD3$^+$ M2$^+$ regions exhibit diminished activation gene expression patterns in ex-β-catenin tumors compared to areas positive for CD3 and cDC1 spots.** Heatmap of T cell restricted genes expressed in spots that are CD3$^+$ M2$^+$ compared to spots that are CD3$^+$ cDC1$^+$ in ex-β-catenin tumors.

approximately 1000 DEGs between these spots, we observed a marked reduction of pro-inflammatory pathways such as IFN-γ, TCR, and TNF signaling, as well as reduced acute phase response signaling in CD3$^+$ M2-like$^+$ spots. Furthermore, spots positive for CD3 and M2-like macrophage markers demonstrated increased activation in immune inhibitory pathways such as IL-10 signaling pathway, Wnt/β-catenin, and CLEAR signaling pathway. These data combined suggest an overall blunted immune response in CD3$^+$ M2-like$^+$ areas. Contrastingly, spots positive for CD3 and cDC1 demonstrated transcriptional evidence for increased neutrophil degranulation, antigen processing and presentation, and macrophage

classical activation signaling (Fig 3.20). Based on these findings we conclude that the CD3$^+$ M2-like$^+$ spots were representative of an immune suppressive niche within the TME.

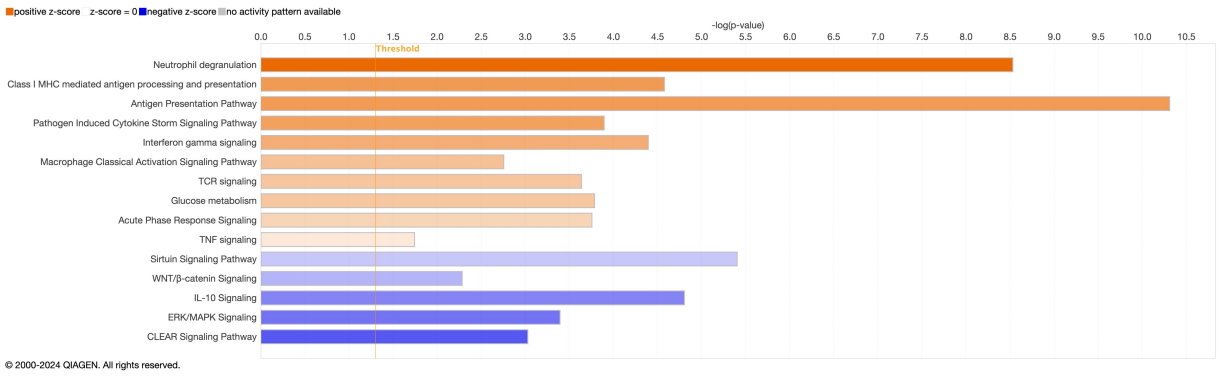

Figure 3.20: **Areas positive for CD3$^+$ T cells and M2-like macrophages demonstrate reduced proinflammatory pathway activation.** Ingenuity Pathway Analysis of the differentially expressed genes identified in CD3$^+$ M2-like$^+$ spots compared to CD3$^+$ cDC1$^+$ spots within ex-β-catenin tumors.

CHAPTER 4

DISCUSSION

4.1 The development of a novel genetically engineered mouse model

Findings from our laboratory previously demonstrated that tumor cell-intrinsic activation of β-catenin signaling pathway is linked to immune exclusion in metastatic melanoma tumors [27, 87]. Since then, several other groups have further corroborated the role of β-catenin pathway activation as one of the potential mechanisms driving immune exclusion [19, 132, 133, 134]. These data collectively have led to the hypothesis that pharmacological inhibition of β-catenin could prove beneficial in the clinic. To this end, there have been many attempts to develop agents targeting the β-catenin signaling pathway. However, pharmacological inhibition of β-catenin has led to significant adverse effects, highlighting the pathway's essential functions in normal cell physiology. β-catenin is not only a major mediator in preserving epithelial cell structure by facilitating E-cadherin and α-catenin interactions and enabling actin filament binding, but it also participates in numerous cellular processes, from proliferation to gene expression regulation [41, 57, 135]. Due to its ubiquitous role in normal cellular and tissue homeostasis, success in inhibiting β-catenin has remained limited [136, 137].

Given that global inhibition of β-catenin pharmacologically is not yet feasible, our study adopted an alternative strategy to explore the consequences of its inhibition within the tumor microenvironment. In this study, we report the development and characterization of a novel genetically engineered animal model designed for the dynamic modulation of tumor cell-intrinsic β-catenin activation. This model emerged from crossing two established genetically engineered mouse models (GEMMs). The first model harbors a tyrosinase-regulated Cre-ER, where Cre activation induces the expression of an activated BRAF variant, $BRAF^{V600E}$,

alongside a bi-allelic deletion of the PTEN tumor suppressor gene - mutations prevalent in human metastatic melanoma [27]. The second GEMM carries a mutant β-catenin under the Col1a promoter, featuring a serine to tyrosine mutation at the S33 phosphorylation site, and a reverse transactivator under the Rosa26 promoter [130]. Crossbreeding these animal models yielded progeny with homozygous alleles for all modifications except Cre-ER, facilitating the induction of autochthonous melanoma tumors with constitutive expression of $BRAF^{V600E}$ and the reverse transactivator, alongside bi-allelic PTEN deletion. Importantly, these tumors were designed to express the active β-$catenin^{S33Y}$ variant conditionally, only in the presence of doxycycline, enabling both the activation and deactivation of this oncogene.

Our first hypothesis was that doxycycline administration would lead to the nuclear accumulation of β-$catenin^{S33Y}$, which is exactly what we observed. The nuclear presence of β-$catenin^{S33Y}$, indicative of an active signaling pathway, was only observed in animals which were exposed to doxycycline. Furthermore, the β-$catenin^{S33Y}$ was also accompanied by a significant reduction in $CD3^+$ T cells within the tumors. These findings not only confirm the connection between β-catenin activation and immune exclusion but also support the validity of our genetically engineered mouse model. This animal model represents, the first example of a melanoma GEMM in which β-catenin can be dynamically regulated to study effects on the host immune response. Our novel animal model represents a powerful tool for studying the intricate dynamics of β-catenin signaling in the context of metastatic melanoma pathogenesis. Importantly, withdrawal of doxycycline led to elimination of tumor cell-intrinsic β-catenin, enabling studies of the host immune compartment upon interruption of β-catenin signaling.

4.2 Dynamic regulation of β-catenin

In the absence of Wnt activation and if found unbound to E-cadherin for structural support, β-catenin is sequestered by the destruction complex and phosphorylated/targeted for

degradation [36, 57]. However, activation of the Wnt pathway results in the recruitment of the destruction complex to the plasma membrane, which allows for the nuclear translocation of β-catenin resulting in subsequent activation of downstream target genes [138]. A notable challenge in our system is that the mutant β-catenin being expressed is resistant to phosphorylation at a critical side. Given that β-catenin^{S33Y} cannot undergo phosphorylation at the S33 site, we hypothesized that inhibition of β-catenin would not result in immediate nuclear clearance [139]. Instead, we proposed a gradual reduction of nuclear β-catenin levels over several days, attributed to the dilution of the signal during tumor growth and potentially due to phosphorylation at non-canonical sites. Our observations confirmed that removal of doxycycline from the drinking water precipitated a gradual decrease in detectable nuclear β-catenin levels so that by day 7 post-doxycycline withdrawal it was no longer detectable. These results demonstrate the feasibility of genetically inhibiting β-catenin signaling specifically within tumor cells.

Upon the development and validation of our animal model, we investigated the temporal regulation of β-catenin within established tumors. Our main focus was to assess whether deactivation of β-catenin would be sufficient to alter the tumor-immune phenotype and render tumors responsive to checkpoint blockade therapy. Specifically, the genetic inhibition of β-catenin at late stages of tumor development would serve as a proof-of-concept, addressing a critical question within the field on cancer immunology: Does blockade of tumor cell-intrinsic β-catenin influence the immune infiltrate and CBI efficacy within melanoma tumors?

4.3 The immune effects of tumor cell-intrinsic β-catenin inhibition

Tumor cell-intrinsic β-catenin activation has been associated with an immune-excluded microenvironment in an array of cancer types. These observations prompted us to ask a new question: would genetic inhibition of nuclear β-catenin restore an immune infiltrate within

melanoma tumors? In line with our hypothesis, genetic inhibition of β-catenin in melanoma tumors (ex-β-catenin tumors) displayed augmented $CD3^+$ T cell infiltration. Moreover, the $CD3^+$ T cell infiltration levels were comparable to those observed in tumors without active β-catenin signaling. These results led us to hypothesize that these tumors, due to a restored immune infiltrate, might regain sensitivity to checkpoint blockade therapy.

To explore this question, we first investigated whether activation of β-catenin signaling within our tumors results in loss of therapeutic efficacy to combination anti-CTLA-4 plus anti-PD-L1. Tumors without β-catenin signaling exhibited a modest, yet statistically significant, therapeutic response to anti-CTLA-4 plus anti-PD-L1. In contrast, tumors with continuous β-catenin signaling were resistant to CBI. Upon withdrawal of doxycycline, ex-β-catenin tumors, despite β-catenin loss and a regained $CD3^+$ T cell infiltrate, remained resistant to CBI. These findings suggest that blockade of the β-catenin signaling pathway alone is not sufficient to re-sensitize previously resistant tumors to immunotherapy.

Having observed a restored immune infiltrate without concurrent immunotherapy efficacy in ex-β-catenin tumors, we investigated the immune cells that were re-infiltrating these tumors. We employed single-cell RNA sequencing to investigate the immune landscape within ex-β-catenin and control tumors. The initial analysis revealed no significant alterations in the composition of immune cell populations between these two conditions, suggesting the possibility of phenotypic rather than quantitative differences. To investigate functional changes between immune cells isolated from ex-β-catenin and control tumors, we conducted a differential gene expression analysis. Remarkably, this analysis detected minimal gene expression changes in most immune cell populations between the two conditions. The majority of differentially expressed genes were identified within the macrophage compartment, indicating a distinct shift in macrophage phenotypes between the two conditions. Control tumors displayed upregulation of genes associated with a pro-inflammatory, M1-like phenotype, including IL1β, IL6, and TLR, in contrast to the ex-β-catenin tumors, which

exhibited an enhanced expression of an anti-inflammatory, M2-like gene signature, with notable upregulation of Mrc1 (Cd206), Cd209g and f, Cd163, Ccl8, and Gas6. This observation marks the first documentation of a direct correlation between tumor cell-intrinsic β-catenin signaling activation and the augmentation of M2-like macrophage phenotypes, representing a significant breakthrough in our understanding. Utilizing Ingenuity Pathway Analysis (IPA), which considers the immunological context and interrelationships among genes, we identified a pronounced enhancement of IL-10 signaling, LXR/RXR pathway activation and alternative macrophage activation pathways in ex-β-catenin tumors. Conversely, control tumors demonstrated enhanced acute phase response signaling, IL-6, toll-like receptor signaling, and macrophage classical activation signaling pathway, providing insightful contrasts in the immunological dynamics between the two tumor types.

The identification of the pronounced M2-like phenotype within the ex-β-catenin tumors prompted a deeper examination of the macrophage subpopulations present in our tumors. By focusing on our F4/80$^+$ SiglecF$^-$ cell populations, we discovered 5 unique macrophage clusters. Specifically, Cluster 0 was characterized by the expression of Clec4e, Il1rn, Olr1, Ptgs2, Flrt3, Il6, and Il1β; Cluster 1 was distinguished by Ifitm3, Gsr, Plac8, Ifitm6, Hp, Cd177; Cluster 2 featured Cx3cr1, Ciita, Ear2, Tmem176a; Cluster 3 was characterized by Ccl8, Cd163, Cd209g, Gas6, Folr2, Fcna; and Cluster 4 was identified by Cxcl10, Ccl4, Tnf, Ccl3, Hspa1b, Ppp1r15a. Each cluster exhibited a spectrum of characteristics, from M1-like to M2-like macrophage attributes. Our focus gravitated towards Cluster 0 and Cluster 3: Cluster 0 was primarily described by M1-like macrophage markers, featuring Il6 and Il1β, whereas Cluster 3 was exhibited more M2-like properties, primarily through the expression of Ccl8, Cd163, CD209g and Gas6. When assessing overall abundance of these macrophage clusters, we observed a marked increase in the M2-like, cluster 3 within the ex-β-catenin tumors when compared to their litter-mate controls.

In summary, this novel mouse model provided a unique and useful tool in which we could

investigate the effects of targeted tumor cell-intrinsic β-catenin inhibition on the immune compartment and therapeutic outcomes in melanoma. These findings not only confirm the connection between tumor cell-intrinsic activation of β-catenin to a diminished $CD3^+$ T cell infiltrate, but further enhance our understanding by providing a link between β-catenin activation and an enhanced prevalence of M2-like macrophages. Remarkably, this shift in the macrophage populations within the melanoma tumors persists despite β-catenin inactivation, indicating a profound alteration within the tumor milieu that confers resistance to combination anti-CTLA-4 plus anti-PD-L1 therapy (Fig 4.1).

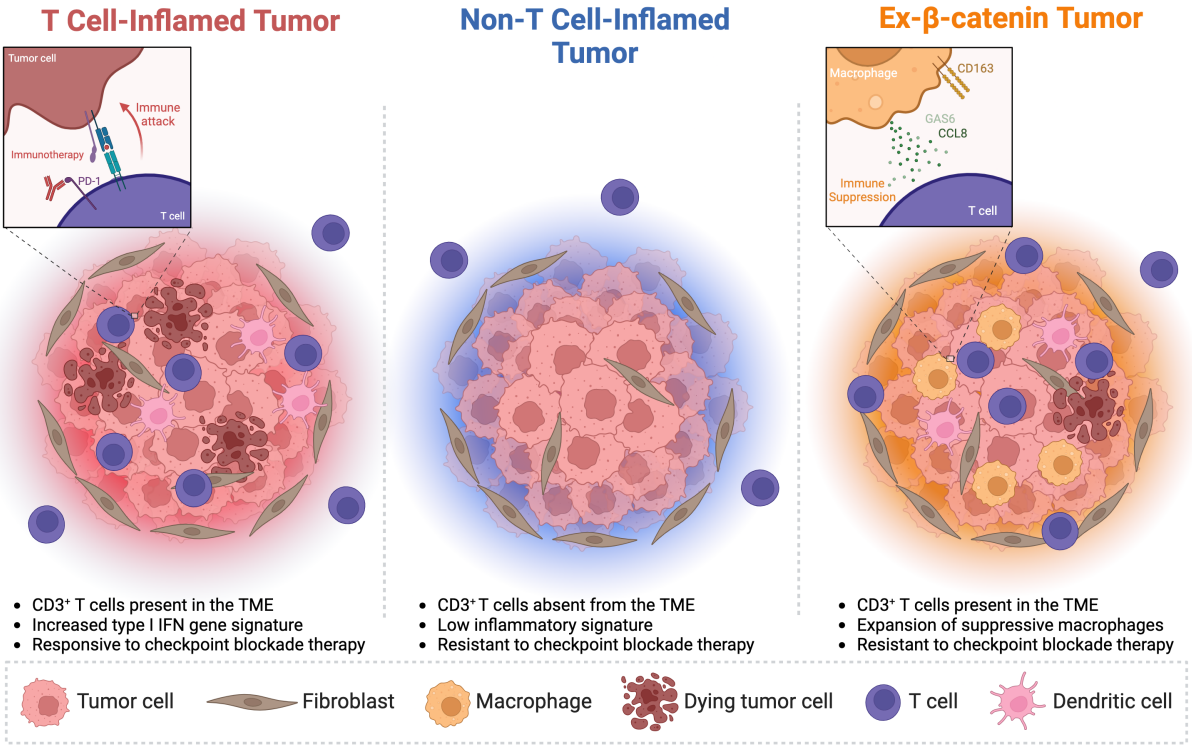

Figure 4.1: **The T cell-inflamed, the non-T cell-inflamed and the ex-β-catenin tumor microenvironment.** Proposed mechanism for checkpoint blockade immunotherapy resistance in ex-β-catenin tumors. Despite a re-gained CD3+ T cell infiltrate, ex-β-catenin tumors remain resistant to anti-CTLA-4 plus anti-PD-L1 due to an enhanced M2-like phenotype within the TME when compared to T cell-inflamed tumors. The predominant M2-like macrophages are likely promoting a pro-tumor microenvironment and keeping the existing T cells in a suppressive milieu.

4.4 Spatial examination of ex-β-catenin tumors suggests an immune-suppressive macrophage phenotype interacting with T cells

While we were interested in isolating macrophages from the TME of ex-β-catenin tumors to understand their functional properties *in vitro*, this proved to be challenging. Particularly with the GEMM tumors, which are very dense and restricted by the skin architecture, obtaining sufficient numbers of cells that are representative of the populations present in situ was not feasible. In addition, the issue of tumor dissociation has further complicated our study because of the intrinsic nature of macrophages, cells that are highly susceptible to environmental cues and disturbances. Handling macrophages, even with the utmost care, can alter their activation status. The cells are highly sensitive to manipulation; thus, *in vitro* studies have reported that even using chemical agents for macrophage release from tissue plates could result in the induction of transcriptional alterations.

We therefore adopted spatial transcriptomics as an innovative approach to evaluate whether M2 macrophages might be adjacent to T cells, and if so whether his resulted in inhibited T cell activation *in situ*.

Indeed, spatial transcriptomic analysis of control and ex-β-catenin tumors confirmed our single cell findings, showing enhanced abundance of M2-like macrophages in the ex-β-catenin tumors. We used markers identified in the single cell experiments to identify these M2-like macrophages, Cd163, Ccl8, CD209g and Gas6. This finding was particularly encouraging as it validated our single-cell observations through an independent and novel technique.

We then investigated he relationship between T cells and M2-like macrophages within the TME. We asked whether ex-β-catenin tumors had an augmented number of spots that were both positive for $CD3^+$ T cells, identified as $Cd3\gamma^+$ or $Cd3\delta^+$ or $Cd3\epsilon^+$, as well as M2-like macrophages, identified as $Adgre1^+$ and $Siglecf^-$ and $Cd163^+$ or $Ccl8^+$ or $Gas6^+$

or Cd209g$^+$. We indeed detected an increased number of double positive spots in the ex-β-catenin tumors. To extend our analysis, we also assessed the distances between any spots that were Adgre1$^+$ and Siglecf$^-$ and Cd163$^+$ or Ccl8$^+$ or Gas6$^+$ or Cd209g$^+$ and the nearest CD3$^+$ T cell. This analysis excluded any M2-like spots that were near M1-like macrophages. When assessing the overall distance from a spot that contains an M2-like macrophage and not an M1-like macrophage to the nearest CD3$^+$ T cell, we observed that in ex-β-catenin tumors CD3$^+$ T cells were overall closer to M2-like macrophages. This discovery is particularly intriguing as it aligns with biological expectations, suggesting that the CD3$^+$ T cells may not be reactivated by combination checkpoint blockade due to their presence within an immunosuppressive niche.

In addition to assessing the spatial organization, we also assessed the transcriptional profiles of spots that were CD3$^+$ and cDC1$^+$ or CD3$^+$ and M2-like$^+$. Our observations were in line with our hypothesis that regions that were CD3$^+$ M2-like$^+$ exhibited diminished expression of pro-inflammatory molecules such as Il2, Ctla4, Tnfrsf 4, 9, 18, and Gzmk. Additionally, spots that were positive for CD3 and M2-like macrophages, and distant from cDC1 cells, had enhanced expression of T cell exhaustion and dysfunction such as Nr4a1 and Tox. To assess these molecules in biological context, ingenuity pathway analysis revealed that spots positive for CD3 and M2-like macrophages had increased immune suppressive pathways such as IL-10 signaling pathway, Wnt/β-catenin signaling pathway and ERK/MAPK signaling pathway. Furthermore, areas away from M2-like macrophages which were positive for CD3$^+$ T cells and and cDC1 displayed robust increase in proinflammatory pathways such as INF-γ signaling pathway, TCR and TNF signaling pathway, classical macrophage activation pathway and antigen presentation signaling pathway.

Overall, these findings link the presence of M2-like macrophages with an anti-inflammatory, pro-tumor phenotype. These M2-like macrophages characterized by Ccl8, Gas6, Cd163 and Cd209g are likely influencing the phenotype and function of CD3$^+$ T cells surrounding them.

4.5 Ccl8 and Gas6 have been implicated in mediating immune suppression and promoting tumor progression

The functional implications of Ccl8 remains incompletely understood, with existing literature reporting varied findings regarding this molecule. One study showed that increased circulating levels of Ccl8 resulted enhanced numbers of $\gamma\delta$ T cells, as Ccl8 is a chemoattractant of $\gamma\delta$ T cells, and the clearance of L. monocytogenes was dependent on $\gamma\delta$ T cells [140]. Furthermore, some studies have linked the expression of Ccl8 to M1-like macrophage recruitment. One group demonstrated that Ccl8 dependent M1 macrophage recruitment enhanced the sensitivity of cutaneous squamous cell carcinoma to photodynamic therapy [141]. More recently, Ccl8 expression was positively correlated with an overall increased immune infiltrate as well as enhanced abundance of M1 macrophages in skin cutaneous human melanoma samples [142]. In addition to its role in cancer and infection, Ccl8 has also been implicated in graft vs host disease (GVHD). Increased serum levels of Ccl8 in human samples were correlated with increased GVHD severity [143] and deficiency of this chemokine was shown to combat early mortality and morbidity in a GVHD mouse study [144].

In contrast to its pro-inflammatory roles, more recent studies in the cancer context have implicated Ccl8 as an immunosuppressive factor. Ccl8 has been linked to metastatic disease where enhanced Ccl8 expression by stromal fibroblasts promote invasion into adjacent stroma, intravasation, extravasation and seeding, crucial steps in the metastasis of breast cancer cells [145]. Furthermore, Ccl8 production by macrophages in the tumor microenvironment acts as a chemoattractant of $CCR5^+$ regulatory T cells, a population of cells which are well established as tumor-promoting. Using a CCR5 inhibitor in a Ccl8 expressing tumor, blockade of CCR5 was shown to result in diminished numbers of regulatory T cells supporting a Ccl8/CCR5 signaling axis in recruiting Tregs [146]. In a study assessing aggressive breast cancer, researchers found that Ccl8 expression by tumor-associated macrophages recruits monocytes into the TME and induces a more aggressive program in cancer cells

allowing for increased motility. This was shown to also correlate with decreased survival in humans [147].

More recently, Ccl8 has been associated with the infiltration of M2-like macrophages in the second phase of mammary gland involution. Researchers showed that Ccl8 accelerated tumor onset and depletion of macrophages counteracted the pro-tumor effects of Ccl8 [148]. Furthermore, podocyte secreted Ccl8 has been implicated in the activation of MSCs which resulted in increased production of immunosuppressive factors such as IL-10, IDO and TGF-β1 by these cells. Interestingly, this study also found that Ccl8 inhibited the IFN-γ production by T cells [149]. Finally, in addition to solid tumors, Ccl8 has also been implicated in hematological malignancies where researchers linked Cd163$^+$ M2-like macrophages with high Ccl8 expression in human DLBCL [150].

Gas6 has been consistently associated with an anti-inflammatory and M2-like macrophage phenotype. Some of the first studies on Gas6 discovered that IL-10 and M-CSF educate TAM to increase production of Gas6 which in turn enhances cancer cell proliferation. Also, IL-10 and M-CSF have been implicated as pro-tumor, M2-like macrophage differentiation factors [151]. More recently, Gas6 has been shown to bind TAM receptors, found on many types of cells. In cancer cells, the engagement of TAM receptors promotes proliferation and migration while inhibiting apoptosis. As a feed forward loop, tumors then increase production of IL-10 and M-CSF which induces more Gas6 expression by tumor associated macrophages. Gas6 binds TAM receptors on NK cells, which in turn inhibits their anti-tumor effects. When Gas6 binds TAM receptors of vascular smooth muscle cells it induces proliferation and angiogenesis transcriptional profile. All of these factors come together to promote tumor development [152]. Additionally, Gas6 engagement of the TAM receptors on macrophages has been shown to polarize these towards a pro-tumor M2-like macrophage phenotype [153].

Gas6 has been reported to be involved in pro-tumor pathways. Gas6 can be highly expressed in pre-invasive lesions and this is accompanied by an increase in macrophages.

Stromal and macrophage Gas6 expression promoted tumor formation and progression [154]. A second study linked Gas6 expression in macrophages to their enhanced resolution of inflammation, a cornerstone marker of M2-like macrophages. Also, exposure to IL-4, a molecule involved in alternative activation of macrophages, resulted in the expression of Gas6 by these M2-like macrophages and defective resolution of injury [155]. Recent studies have also demonstrated that Gas6 blockade in the stroma resulted in augmented NK cell responses and an inhibition in pancreatic cancer cell metastasis. These data showed that Gas6 acts simultaneously on tumor cells and NK cells aiding pancreatic cancer metastasis [156].

In studies outside of cancer, it has been reported that Gas6 induces ATF3 in MerTK$^+$ macrophages after ischemiareperfusion injury. This study also demonstrated the induction of ATF3 prevented apoptosis by repressing type I interferon (Ifih1 and Ifnb1) and apoptosis (Apaf1) gene expression [157].

Our results suggest a scenario in which tumor cell-intrinsic β-catenin signaling induces a gene program in the tumors that is M2-like macrophage promoting. Importantly, inhibition of β-catenin does not reverse this phenotype, and the M2-like macrophages persisted. These M2-like macrophages, identified by Cd163, secrete Ccl8 and Gas6 which are potentially activating many immune suppressive cascades. First these molecules likely activate a feed-forward loop where they instruct the tumor cells to produce more cytokines and chemokines that support an anti-inflammatory milieu and M2-like macrophages. Second, these are likely inhibiting T cell responses because these molecules have been associated with attenuating NK and T cell activation. Lastly, both Ccl8 and Gas6 have been shown to promote invasion and metastasis. Future studies will be necessary to elucidate he precise roles of Ccl8 and Gas6 in the context of this melanoma GEM model.

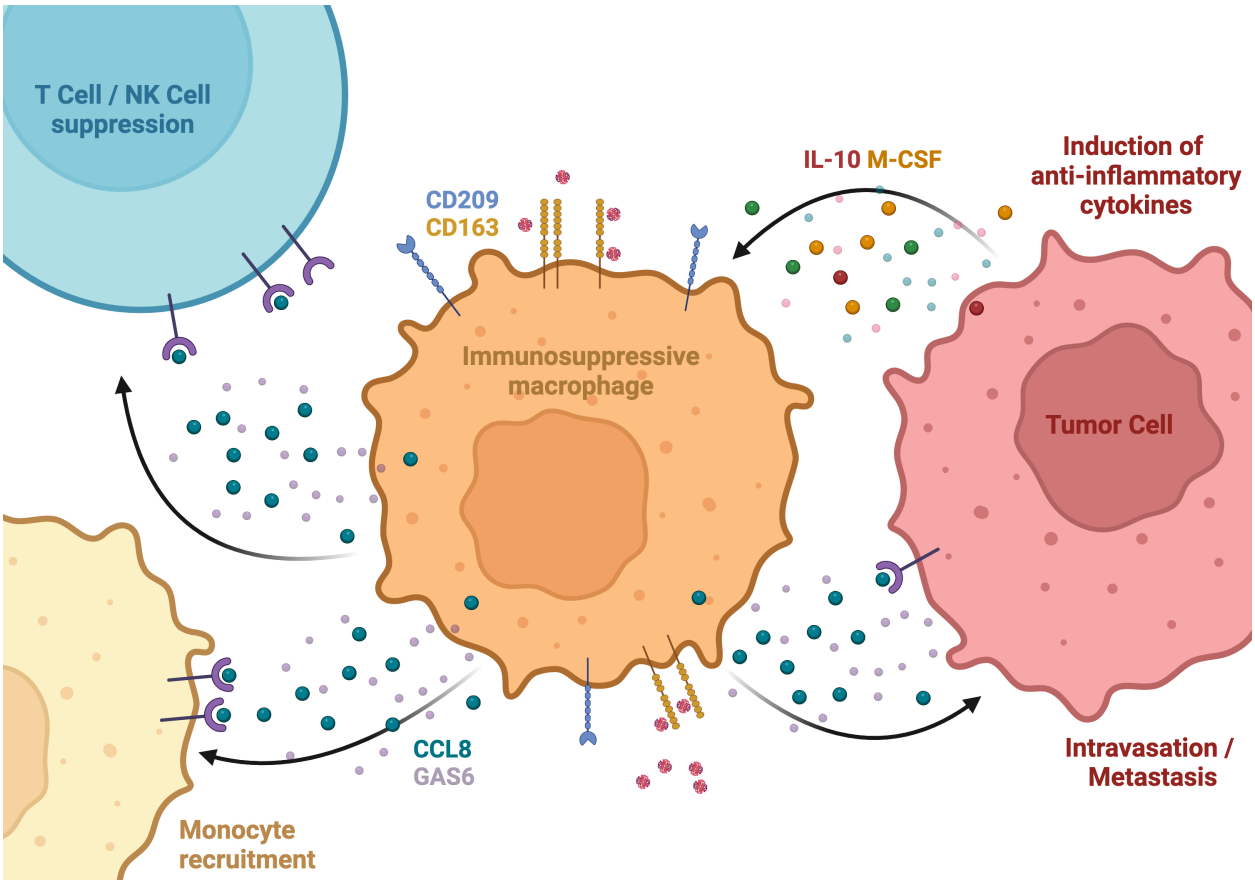

Figure 4.2: **Proposed mechanism of action for Ccl8 and Gas6.** Tumor associated macrophages secrete Ccl8 and Gas6 that affect the tumor microenvironment in 4 ways: First, these molecules are recruit more anti-inflammatory monocytes and regulatory T cells to the tumor, second they kick-start a feed forward loop in adjacent tumor cells to increase the production anti-inflammatory cytokines such as IL-10 and M-CSF that further enhance the immunosuppressive microenvironment, third these molecules play a direct role in promoting invasion and metastasis, and fourth, Ccl8 and Gas6 are likely directly inhibiting the action of T cells.

REFERENCES

[1] Benjamin Switzer, Igor Puzanov, Joseph J. Skitzki, Lamya Hamad, and Marc S. Ernstoff. Managing Metastatic Melanoma in 2022: A Clinical Review. *JCO Oncology Practice*, 18(5):335–351, May 2022. Publisher: Wolters Kluwer.

[2] Ashley Sample and Yu-Ying He. Mechanisms and prevention of UV-induced melanoma. *Photodermatology, Photoimmunology & Photomedicine*, 34(1):13–24, January 2018.

[3] Francisco Solano. Photoprotection and Skin Pigmentation: Melanin-Related Molecules and Some Other New Agents Obtained from Natural Sources. *Molecules*, 25(7):1537, March 2020.

[4] Matthew G Davey, Nicola Miller, and Niall M McInerney. A Review of Epidemiology and Cancer Biology of Malignant Melanoma. *Cureus*, 13(5):e15087.

[5] Stephen M. Ostrowski and David E. Fisher. Biology of Melanoma. *Hematology/Oncology Clinics of North America*, 35(1):29–56, February 2021.

[6] Gaël G. McGill, Martin Horstmann, Hans R. Widlund, Jinyan Du, Gabriela Motyckova, Emi K. Nishimura, Yi-Ling Lin, Sridhar Ramaswamy, William Avery, Han-Fei Ding, Siobhán A. Jordan, Ian J. Jackson, Stanley J. Korsmeyer, Todd R. Golub, and David E. Fisher. Bcl2 Regulation by the Melanocyte Master Regulator Mitf Modulates Lineage Survival and Melanoma Cell Viability. *Cell*, 109(6):707–718, June 2002.

[7] Pakavarin Louphrasitthiphol, Alessia Loffreda, Vivian Pogenberg, Sarah Picaud, Alexander Schepsky, Hans Friedrichsen, Zhiqiang Zeng, Anahita Lashgari, Benjamin Thomas, E. Elizabeth Patton, Matthias Wilmanns, Panagis Filippakopoulos, Jean-Philippe Lambert, Eiríkur Steingrímsson, Davide Mazza, and Colin R. Goding. Acetylation reprograms MITF target selectivity and residence time. *Nature Communications*, 14(1):6051, September 2023. Number: 1 Publisher: Nature Publishing Group.

[8] Mariusz L. Hartman and Malgorzata Czyz. MITF in melanoma: mechanisms behind its expression and activity. *Cellular and molecular life sciences: CMLS*, 72(7):1249–1260, April 2015.

[9] Maria Colombino, Mariaelena Capone, Amelia Lissia, Antonio Cossu, Corrado Rubino, Vincenzo De Giorgi, Daniela Massi, Ester Fonsatti, Stefania Staibano, Oscar Nappi, Elena Pagani, Milena Casula, Antonella Manca, MariaCristina Sini, Renato Franco, Gerardo Botti, Corrado Caracò, Nicola Mozzillo, Paolo A. Ascierto, and Giuseppe Palmieri. BRAF/NRAS Mutation Frequencies Among Primary Tumors and Metastases in Patients With Melanoma. *Journal of Clinical Oncology*, 30(20):2522–2529, July 2012. Publisher: Wolters Kluwer.

[10] David Dankort, David P. Curley, Robert A. Cartlidge, Betsy Nelson, Anthony N. Karnezis, William E. Damsky, Mingjian J. You, Ronald A. DePinho, Martin McMahon, and Marcus Bosenberg. Braf(V600E) cooperates with Pten loss to induce metastatic melanoma. *Nature Genetics*, 41(5):544–552, May 2009.

[11] Joana B. Loureiro, Liliana Raimundo, Juliana Calheiros, Carla Carvalho, Valentina Barcherini, Nuno R. Lima, Célia Gomes, Maria Inês Almeida, Marco G. Alves, José Luís Costa, Maria M. M. Santos, and Lucília Saraiva. Targeting p53 for Melanoma Treatment: Counteracting Tumour Proliferation, Dissemination and Therapeutic Resistance. *Cancers*, 13(7):1648, April 2021.

[12] Weiyi Peng, Jie Qing Chen, Chengwen Liu, Shruti Malu, Caitlin Creasy, Michael T. Tetzlaff, Chunyu Xu, Jodi A. McKenzie, Chunlei Zhang, Xiaoxuan Liang, Leila J. Williams, Wanleng Deng, Guo Chen, Rina Mbofung, Alexander J. Lazar, Carlos A. Torres-Cabala, Zachary A. Cooper, Pei-Ling Chen, Trang N. Tieu, Stefani Spranger, Xiaoxing Yu, Chantale Bernatchez, Marie-Andree Forget, Cara Haymaker, Rodabe Amaria, Jennifer L. McQuade, Isabella C. Glitza, Tina Cascone, Haiyan S. Li, Lawrence N. Kwong, Timothy P. Heffernan, Jianhua Hu, Roland L. Bassett, Marcus W. Bosenberg, Scott E. Woodman, Willem W. Overwijk, Gregory Lizée, Jason Roszik, Thomas F. Gajewski, Jennifer A. Wargo, Jeffrey E. Gershenwald, Laszlo Radvanyi, Michael A. Davies, and Patrick Hwu. Loss of PTEN Promotes Resistance to T Cell-Mediated Immunotherapy. *Cancer Discovery*, 6(2):202–216, February 2016.

[13] C. Pritchard, L. Carragher, V. Aldridge, S. Giblett, H. Jin, C. Foster, C. Andreadi, and T. Kamata. Mouse models for BRAF-induced cancers. *Biochemical Society transactions*, 35(Pt 5):1329–1333, November 2007.

[14] Amanda D Bucheit, Guo Chen, Alan Siroy, Michael Tetzlaff, Russell Broaddus, Denai Milton, Patricia Fox, Roland Bassett, Patrick Hwu, Jeffrey E Gershenwald, Alexander J Lazar, and Michael A Davies. Complete loss of PTEN protein expression correlates with shorter time to brain metastasis and survival in stage IIIB/C melanoma patients with BRAFV600 mutations. *Clinical cancer research*, 20(21):5527–5536, November 2014.

[15] Jawad Fares, Mohamad Y. Fares, Hussein H. Khachfe, Hamza A. Salhab, and Youssef Fares. Molecular principles of metastasis: a hallmark of cancer revisited. *Signal Transduction and Targeted Therapy*, 5(1):1–17, March 2020. Number: 1 Publisher: Nature Publishing Group.

[16] Federica Catalanotti, Donavan T. Cheng, Alexander N. Shoushtari, Douglas B. Johnson, Katherine S. Panageas, Parisa Momtaz, Catherine Higham, Helen H. Won, James J. Harding, Taha Merghoub, Neal Rosen, Jeffrey A. Sosman, Michael F. Berger, Paul B. Chapman, and David B. Solit. PTEN Loss-of-Function Alterations Are Associated With Intrinsic Resistance to BRAF Inhibitors in Metastatic Melanoma. *JCO precision oncology*, 1:PO.16.00054, 2017.

[17] Thomas F. Gajewski, Leticia Corrales, Jason Williams, Brendan Horton, Ayelet Sivan, and Stefani Spranger. Cancer Immunotherapy Targets Based on Understanding the T Cell-Inflamed Versus Non-T Cell-Inflamed Tumor Microenvironment. *Advances in Experimental Medicine and Biology*, 1036:19–31, 2017.

[18] Jonathan A. Trujillo, Randy F. Sweis, Riyue Bao, and Jason J. Luke. T Cell-Inflamed versus Non-T Cell-Inflamed Tumors: A Conceptual Framework for Cancer Immunotherapy Drug Development and Combination Therapy Selection. *Cancer Immunology Research*, 6(9):990–1000, September 2018.

[19] Jason J. Luke, Riyue Bao, Randy F. Sweis, Stefani Spranger, and Thomas F. Gajewski. WNT/-catenin Pathway Activation Correlates with Immune Exclusion across Human Cancers. *Clinical Cancer Research: An Official Journal of the American Association for Cancer Research*, 25(10):3074–3083, May 2019.

[20] Helena Harlin, Yuru Meng, Amy C. Peterson, Yuanyuan Zha, Maria Tretiakova, Craig Slingluff, Mark McKee, and Thomas F. Gajewski. Chemokine Expression in Melanoma Metastases Associated with CD8+ T-Cell Recruitment. *Cancer Research*, 69(7):3077–3085, April 2009.

[21] Riyue Bao, Daniel Stapor, and Jason J. Luke. Molecular correlates and therapeutic targets in T cell-inflamed versus non-T cell-inflamed tumors across cancer types. *Genome Medicine*, 12(1):90, October 2020.

[22] Stefani Spranger, Robbert M. Spaapen, Yuanyuan Zha, Jason Williams, Yuru Meng, Thanh T. Ha, and Thomas F. Gajewski. Up-regulation of PD-L1, IDO, and T(regs) in the melanoma tumor microenvironment is driven by CD8(+) T cells. *Science Translational Medicine*, 5(200):200ra116, August 2013.

[23] Stefani Spranger, Daisy Dai, Brendan Horton, and Thomas F. Gajewski. Tumor-Residing Batf3 Dendritic Cells Are Required for Effector T Cell Trafficking and Adoptive T Cell Therapy. *Cancer Cell*, 31(5):711–723.e4, May 2017.

[24] Christina Pfirschke, Marie Siwicki, Hsin-Wei Liao, and Mikael J. Pittet. Tumor Microenvironment: No Effector T Cells without Dendritic Cells. *Cancer Cell*, 31(5):614–615, May 2017.

[25] Qiyao Yang, Ningning Guo, Yi Zhou, Jiejian Chen, Qichun Wei, and Min Han. The role of tumor-associated macrophages (TAMs) in tumor progression and relevant advance in targeted therapy. *Acta Pharmaceutica Sinica. B*, 10(11):2156–2170, November 2020.

[26] Anthos Christofides, Laura Strauss, Alan Yeo, Carol Cao, Alain Charest, and Vassiliki A. Boussiotis. The complex role of tumor-infiltrating macrophages. *Nature Immunology*, 23(8):1148–1156, August 2022. Publisher: Nature Publishing Group.

[27] Stefani Spranger, Riyue Bao, and Thomas F. Gajewski. Melanoma-intrinsic -catenin signalling prevents anti-tumour immunity. *Nature*, 523(7559):231–235, July 2015. Number: 7559 Publisher: Nature Publishing Group.

[28] Johanna A. Joyce and Douglas T. Fearon. T cell exclusion, immune privilege, and the tumor microenvironment. *Science (New York, N.Y.)*, 348(6230):74–80, April 2015.

[29] Satoshi Muto, Yuki Ozaki, Hikaru Yamaguchi, Hayato Mine, Hironori Takagi, Masayuki Watanabe, Takuya Inoue, Takumi Yamaura, Mitsuro Fukuhara, Naoyuki Okabe, Yuki Matsumura, Takeo Hasegawa, Jun Osugi, Mika Hoshino, Mitsunori Higuchi, Yutaka Shio, Hideaki Nanamiya, Jun-Ichi Imai, Takao Isogai, Shinya Watanabe, and Hiroyuki Suzuki. Tumor -catenin expression is associated with immune evasion in non-small cell lung cancer with high tumor mutation burden. *Oncology Letters*, 21(3):203, March 2021.

[30] Stefani Spranger and Thomas F. Gajewski. A new paradigm for tumor immune escape: -catenin-driven immune exclusion. *Journal for Immunotherapy of Cancer*, 3:43, September 2015.

[31] Ziying Lin, Lixia Huang, Shao Li Li, Jincui Gu, Xiaoxian Cui, and Yanbin Zhou. PTEN loss correlates with T cell exclusion across human cancers. *BMC Cancer*, 21(1):429, April 2021.

[32] Rita Cabrita, Shamik Mitra, Adriana Sanna, Henrik Ekedahl, Kristina Lövgren, Håkan Olsson, Christian Ingvar, Karolin Isaksson, Martin Lauss, Ana Carneiro, and Göran Jönsson. The Role of PTEN Loss in Immune Escape, Melanoma Prognosis and Therapy Response. *Cancers*, 12(3):742, March 2020.

[33] Mark Ayers, Jared Lunceford, Michael Nebozhyn, Erin Murphy, Andrey Loboda, David R. Kaufman, Andrew Albright, Jonathan D. Cheng, S. Peter Kang, Veena Shankaran, Sarina A. Piha-Paul, Jennifer Yearley, Tanguy Y. Seiwert, Antoni Ribas, and Terrill K. McClanahan. IFN--related mRNA profile predicts clinical response to PD-1 blockade. *The Journal of Clinical Investigation*, 127(8):2930–2940, August 2017.

[34] Paul C. Tumeh, Christina L. Harview, Jennifer H. Yearley, I. Peter Shintaku, Emma J. M. Taylor, Lidia Robert, Bartosz Chmielowski, Marko Spasic, Gina Henry, Voicu Ciobanu, Alisha N. West, Manuel Carmona, Christine Kivork, Elizabeth Seja, Grace Cherry, Antonio Gutierrez, Tristan R. Grogan, Christine Mateus, Gorana Tomasic, John A. Glaspy, Ryan O. Emerson, Harlan Robins, Robert H. Pierce, David A. Elashoff, Caroline Robert, and Antoni Ribas. PD-1 blockade induces responses by inhibiting adaptive immune resistance. *Nature*, 515(7528):568–571, November 2014.

[35] Ankur Tiwari, Tamas Oravecz, Laura A. Dillon, Antoine Italiano, Laurent Audoly, Wolf Hervé Fridman, and Guy Travis Clifton. Towards a consensus definition of immune exclusion in cancer. *Frontiers in Immunology*, 14, 2023.

[36] Tomas Valenta, George Hausmann, and Konrad Basler. The many faces and functions of -catenin. *The EMBO Journal*, 31(12):2714–2736, June 2012.

[37] Jiaqi Liu, Qing Xiao, Jiani Xiao, Chenxi Niu, Yuanyuan Li, Xiaojun Zhang, Zhengwei Zhou, Guang Shu, and Gang Yin. Wnt/-catenin signalling: function, biological mechanisms, and therapeutic opportunities. *Signal Transduction and Targeted Therapy*, 7(1):1–23, January 2022. Number: 1 Publisher: Nature Publishing Group.

[38] A. H. Huber, W. J. Nelson, and W. I. Weis. Three-dimensional structure of the armadillo repeat region of beta-catenin. *Cell*, 90(5):871–882, September 1997.

[39] Yi Xing, Ken-Ichi Takemaru, Jing Liu, Jason D. Berndt, Jie J. Zheng, Randall T. Moon, and Wenqing Xu. Crystal structure of a full-length beta-catenin. *Structure (London, England: 1993)*, 16(3):478–487, March 2008.

[40] Cara J. Gottardi and Barry M. Gumbiner. Distinct molecular forms of -catenin are targeted to adhesive or transcriptional complexes. *Journal of Cell Biology*, 167(2):339–349, October 2004.

[41] Xinrui Tian, Zhuola Liu, Bo Niu, Jianlin Zhang, Thian Kui Tan, So Ra Lee, Ye Zhao, David C. H. Harris, and Guoping Zheng. E-Cadherin/-Catenin Complex and the Epithelial Barrier. *Journal of Biomedicine and Biotechnology*, 2011:567305, 2011.

[42] Rabia Hayat, Maleeha Manzoor, and Ali Hussain. Wnt signaling pathway: A comprehensive review. *Cell Biology International*, 46(6):863–877, 2022. _eprint: https://onlinelibrary.wiley.com/doi/pdf/10.1002/cbin.11797.

[43] Jason Wray and Christine Hartmann. WNTing embryonic stem cells. *Trends in Cell Biology*, 22(3):159–168, March 2012.

[44] H. A. Baarsma and M. Königshoff. WNT-er is coming: WNT signalling in chronic lung diseases. *Thorax*, 72(8):746, August 2017. Publisher: BMJ Publishing Group.

[45] Paul F. Langton, Satoshi Kakugawa, and Jean-Paul Vincent. Making, Exporting, and Modulating Wnts. *Trends in Cell Biology*, 26(10):756–765, October 2016.

[46] Claudia Y. Janda, Luke T. Dang, Changjiang You, Junlei Chang, Wim de Lau, Zhendong A. Zhong, Kelley S. Yan, Owen Marecic, Dirk Siepe, Xingnan Li, James D. Moody, Bart O. Williams, Hans Clevers, Jacob Piehler, David Baker, Calvin J. Kuo, and K. Christopher Garcia. Surrogate Wnt agonists that phenocopy canonical Wnt/-catenin signaling. *Nature*, 545(7653):234–237, May 2017.

[47] Jennifer L. Stamos and William I. Weis. The -catenin destruction complex. *Cold Spring Harbor Perspectives in Biology*, 5(1):a007898, January 2013.

[48] Yeon-Su Lee, Yun Sung Cho, Geon Kook Lee, Sunghoon Lee, Young-Woo Kim, Sungwoong Jho, Hak-Min Kim, Seung-Hyun Hong, Jung-Ah Hwang, Sook-young Kim, Dongwan Hong, Il Ju Choi, Byung Chul Kim, Byoung-Chul Kim, Chul Hong Kim, Hansol Choi, Youngju Kim, Kyung Wook Kim, Gu Kong, Hyung Lae Kim, Jong Bhak, Seung Hoon Lee, and Jin Soo Lee. Genomic profile analysis of diffuse-type gastric cancers. *Genome Biology*, 15(4):R55, 2014.

[49] Lionel Larue and Véronique Delmas. The WNT/Beta-catenin pathway in melanoma. *Frontiers in Bioscience: A Journal and Virtual Library*, 11:733–742, January 2006.

[50] Karl Willert and Katherine A. Jones. Wnt signaling: is the party in the nucleus? *Genes & Development*, 20(11):1394–1404, June 2006. Company: Cold Spring Harbor Laboratory Press Distributor: Cold Spring Harbor Laboratory Press Institution: Cold Spring Harbor Laboratory Press Label: Cold Spring Harbor Laboratory Press Publisher: Cold Spring Harbor Lab.

[51] Nikolaos Doumpas, Franziska Lampart, Mark D Robinson, Antonio Lentini, Colm E Nestor, Claudio Cantù, and Konrad Basler. TCF/LEF dependent and independent transcriptional regulation of Wnt/catenin target genes. *The EMBO Journal*, 38(2):e98873, January 2019. Publisher: John Wiley & Sons, Ltd.

[52] Sachin Gopalkrishna Pai, Benedito A. Carneiro, Jose Mauricio Mota, Ricardo Costa, Caio Abner Leite, Romualdo Barroso-Sousa, Jason Benjamin Kaplan, Young Kwang Chae, and Francis Joseph Giles. Wnt/beta-catenin pathway: modulating anticancer immune response. *Journal of Hematology & Oncology*, 10(1):101, May 2017.

[53] Stefani Spranger, Brendan Horton, and Thomas F. Gajewski. Immune surveillance is thwarted by tumor-cell intrinsic beta-catenin signaling. *Journal for ImmunoTherapy of Cancer*, 3(Suppl 2):P418, December 2015. Publisher: BMJ Specialist Journals Section: Poster Presentation.

[54] T. Zhan, N. Rindtorff, and M. Boutros. Wnt signaling in cancer. *Oncogene*, 36(11):1461–1473, March 2017.

[55] V. Korinek, N. Barker, P. J. Morin, D. van Wichen, R. de Weger, K. W. Kinzler, B. Vogelstein, and H. Clevers. Constitutive transcriptional activation by a beta-catenin-Tcf complex in APC-/- colon carcinoma. *Science (New York, N.Y.)*, 275(5307):1784–1787, March 1997.

[56] Taj D. King, Mark J. Suto, and Yonghe Li. The Wnt/-catenin signaling pathway: A potential therapeutic target in the treatment of triple negative breast cancer. *Journal of cellular biochemistry*, 113(1):13–18, January 2012.

[57] Lidan Liu, Lifei Wang, and Xiujuan Li. The roles of HOXB8 through activating Wnt/-catenin and STAT3 signaling pathways in the growth, migration and invasion of ovarian cancer cells. *Cytotechnology*, 74(1):77–87, February 2022.

[58] Anna Gajos-Michniewicz and Malgorzata Czyz. WNT Signaling in Melanoma. *International Journal of Molecular Sciences*, 21(14):4852, January 2020. Number: 14 Publisher: Multidisciplinary Digital Publishing Institute.

[59] Nithya Krishnamurthy and Razelle Kurzrock. Targeting the Wnt/beta-catenin pathway in cancer: Update on effectors and inhibitors. *Cancer Treatment Reviews*, 62:50–60, January 2018. Publisher: Elsevier.

[60] Edward L. Korn, Ping-Yu Liu, Sandra J. Lee, Judith-Anne W. Chapman, Donna Niedzwiecki, Vera J. Suman, James Moon, Vernon K. Sondak, Michael B. Atkins,

Elizabeth A. Eisenhauer, Wendy Parulekar, Svetomir N. Markovic, Scott Saxman, and John M. Kirkwood. Meta-Analysis of Phase II Cooperative Group Trials in Metastatic Stage IV Melanoma to Determine Progression-Free and Overall Survival Benchmarks for Future Phase II Trials. *Journal of Clinical Oncology*, 26(4):527–534, February 2008. Publisher: Wolters Kluwer.

[61] Ryan J. Sullivan and Keith T. Flaherty. New Strategies in Melanoma: Entering the Era of Combinatorial Therapy. *Clinical Cancer Research*, 21(11):2424–2435, May 2015.

[62] Alicia M. Terando, Mark B. Faries, and Donald L. Morton. Vaccine therapy for melanoma: current status and future directions. *Vaccine*, 25 Suppl 2:B4–16, September 2007.

[63] Keith T. Flaherty. BRAF Inhibitors and Melanoma. *The Cancer Journal*, 17(6):505, December 2011.

[64] Helen Davies, Graham R. Bignell, Charles Cox, Philip Stephens, Sarah Edkins, Sheila Clegg, Jon Teague, Hayley Woffendin, Mathew J. Garnett, William Bottomley, Neil Davis, Ed Dicks, Rebecca Ewing, Yvonne Floyd, Kristian Gray, Sarah Hall, Rachel Hawes, Jaime Hughes, Vivian Kosmidou, Andrew Menzies, Catherine Mould, Adrian Parker, Claire Stevens, Stephen Watt, Steven Hooper, Rebecca Wilson, Hiran Jayatilake, Barry A. Gusterson, Colin Cooper, Janet Shipley, Darren Hargrave, Katherine Pritchard-Jones, Norman Maitland, Georgia Chenevix-Trench, Gregory J. Riggins, Darell D. Bigner, Giuseppe Palmieri, Antonio Cossu, Adrienne Flanagan, Andrew Nicholson, Judy W. C. Ho, Suet Y. Leung, Siu T. Yuen, Barbara L. Weber, Hilliard F. Seigler, Timothy L. Darrow, Hugh Paterson, Richard Marais, Christopher J. Marshall, Richard Wooster, Michael R. Stratton, and P. Andrew Futreal. Mutations of the BRAF gene in human cancer. *Nature*, 417(6892):949–954, June 2002. Publisher: Nature Publishing Group.

[65] Claudia Wellbrock, Lesley Ogilvie, Douglas Hedley, Maria Karasarides, Jan Martin, Dan Niculescu-Duvaz, Caroline J. Springer, and Richard Marais. V599EB-RAF is an Oncogene in Melanocytes. *Cancer Research*, 64(7):2338–2342, April 2004.

[66] Muna Al Hashmi, Konduru S. Sastry, Lee Silcock, Lotfi Chouchane, Valentina Mattei, Nicola James, Rebecca Mathew, Davide Bedognetti, Valeria De Giorgi, Daniela Murtas, Wei Liu, Aouatef Chouchane, Ramzi Temanni, Barbara Seliger, Ena Wang, Francesco M. Marincola, and Sara Tomei. Differential responsiveness to BRAF inhibitors of melanoma cell lines BRAF V600E-mutated. *Journal of Translational Medicine*, 18:192, May 2020.

[67] Leisl M. Packer, Philip East, Jorge S. Reis-Filho, and Richard Marais. Identification of direct transcriptional targets of (V600E)BRAF/MEK signalling in melanoma. *Pigment Cell & Melanoma Research*, 22(6):785–798, December 2009.

[68] Paola Savoia, Elisa Zavattaro, and Ottavio Cremona. Clinical Implications of Acquired BRAF Inhibitors Resistance in Melanoma. *International Journal of Molecular Sciences*, 21(24):9730, December 2020.

[69] Chapman Paul B., Hauschild Axel, Robert Caroline, Haanen John B., Ascierto Paolo, Larkin James, Dummer Reinhard, Garbe Claus, Testori Alessandro, Maio Michele, Hogg David, Lorigan Paul, Lebbe Celeste, Jouary Thomas, Schadendorf Dirk, Ribas Antoni, O'Day Steven J., Sosman Jeffrey A., Kirkwood John M., Eggermont Alexander M.M., Dreno Brigitte, Nolop Keith, Li Jiang, Nelson Betty, Hou Jeannie, Lee Richard J., Flaherty Keith T., and McArthur Grant A. Improved Survival with Vemurafenib in Melanoma with BRAF V600E Mutation. *New England Journal of Medicine*, 364(26):2507–2516, 2011. Publisher: Massachusetts Medical Society _eprint: https://www.nejm.org/doi/pdf/10.1056/NEJMoa1103782.

[70] Keith T. Flaherty, Caroline Robert, Peter Hersey, Paul Nathan, Claus Garbe, Mohammed Milhem, Lev V. Demidov, Jessica C. Hassel, Piotr Rutkowski, Peter Mohr, Reinhard Dummer, Uwe Trefzer, James M.G. Larkin, Jochen Utikal, Brigitte Dreno, Marta Nyakas, Mark R. Middleton, Jürgen C. Becker, Michelle Casey, Laurie J. Sherman, Frank S. Wu, Daniele Ouellet, Anne-Marie Martin, Kiran Patel, and Dirk Schadendorf. Improved Survival with MEK Inhibition in BRAF-Mutated Melanoma. *New England Journal of Medicine*, 367(2):107–114, July 2012. Publisher: Massachusetts Medical Society _eprint: https://doi.org/10.1056/NEJMoa1203421.

[71] Keith T. Flaherty, Jeffery R. Infante, Adil Daud, Rene Gonzalez, Richard F. Kefford, Jeffrey Sosman, Omid Hamid, Lynn Schuchter, Jonathan Cebon, Nageatte Ibrahim, Ragini Kudchadkar, Howard A. Burris, Gerald Falchook, Alain Algazi, Karl Lewis, Georgina V. Long, Igor Puzanov, Peter Lebowitz, Ajay Singh, Shonda Little, Peng Sun, Alicia Allred, Daniele Ouellet, Kevin B. Kim, Kiran Patel, and Jeffrey Weber. Combined BRAF and MEK inhibition in melanoma with BRAF V600 mutations. *The New England Journal of Medicine*, 367(18):1694–1703, November 2012.

[72] Joseph Kattan, Clarisse Kattan, Fadi Farhat, and Tarek Assi. Overcoming the resistance to BRAF inhibitor by the double BRAF and MEK inhibitions in advanced melanoma: a case report. *Anti-Cancer Drugs*, 30(10):1052–1054, November 2019.

[73] Jack McCain. The MAPK (ERK) Pathway. *Pharmacy and Therapeutics*, 38(2):96–108, February 2013.

[74] Taku Fujimura, Takanori Hidaka, Yumi Kambayashi, and Setsuya Aiba. BRAF kinase inhibitors for treatment of melanoma: developments from early-stage animal studies to Phase II clinical trials. *Expert Opinion on Investigational Drugs*, 28(2):143–148, February 2019.

[75] Dana R. Leach, Matthew F. Krummel, and James P. Allison. Enhancement of Antitumor Immunity by CTLA-4 Blockade. *Science*, 271(5256):1734–1736, March 1996. Publisher: American Association for the Advancement of Science.

[76] Yi-Fu Yang, Jian-Ping Zou, Jie Mu, Rishani Wijesuriya, Shiro Ono, Theresa Walunas, Jeffrey Bluestone, Hiromi Fujiwara, and Toshiyuki Hamaoka. Enhanced Induction of Antitumor T-Cell Responses by Cytotoxic T Lymphocyte-associated Molecule-4 Blockade: The Effect Is Manifested Only at the Restricted Tumor-bearing Stages1. *Cancer Research*, 57(18):4036–4041, September 1997.

[77] Karl S Peggs, Sergio A Quezada, Alan J Korman, and James P Allison. Principles and use of anti-CTLA4 antibody in human cancer immunotherapy. *Current Opinion in Immunology*, 18(2):206–213, April 2006.

[78] Spencer C. Wei, Jacob H. Levine, Alexandria P. Cogdill, Yang Zhao, Nana-Ama A. S. Anang, Miles C. Andrews, Padmanee Sharma, Jing Wang, Jennifer A. Wargo, Dana Peer, and James P. Allison. Distinct Cellular Mechanisms Underlie Anti-CTLA-4 and Anti-PD-1 Checkpoint Blockade. *Cell*, 170(6):1120–1133.e17, September 2017.

[79] Spencer C. Wei, Colm R. Duffy, and James P. Allison. Fundamental Mechanisms of Immune Checkpoint Blockade Therapy. *Cancer Discovery*, 8(9):1069–1086, September 2018.

[80] Peter A. Prieto, James C. Yang, Richard M. Sherry, Marybeth S. Hughes, Udai S. Kammula, Donald E. White, Catherine L. Levy, Steven A. Rosenberg, and Giao Q. Phan. CTLA-4 Blockade with Ipilimumab: Long-term Follow-up of 177 Patients with Metastatic Melanoma. *Clinical Cancer Research*, 18(7):2039–2047, April 2012.

[81] Yoshiko Iwai, Junzo Hamanishi, Kenji Chamoto, and Tasuku Honjo. Cancer immunotherapies targeting the PD-1 signaling pathway. *Journal of Biomedical Science*, 24(1):26, April 2017.

[82] Yoshiko Iwai, Masayoshi Ishida, Yoshimasa Tanaka, Taku Okazaki, Tasuku Honjo, and Nagahiro Minato. Involvement of PD-L1 on tumor cells in the escape from host immune system and tumor immunotherapy by PD-L1 blockade. *Proceedings of the National Academy of Sciences of the United States of America*, 99(19):12293–12297, September 2002.

[83] B. Paiva, A. Azpilikueta, N. Puig, E. M. Ocio, R. Sharma, B. O. Oyajobi, S. Labiano, L. San-Segundo, A. Rodriguez, I. Aires-Mejia, I. Rodriguez, F. Escalante, A. G. de Coca, A. Barez, J. F. San Miguel, and I. Melero. PD-L1/PD-1 presence in the tumor microenvironment and activity of PD-1 blockade in multiple myeloma. *Leukemia*, 29(10):2110–2113, October 2015. Number: 10 Publisher: Nature Publishing Group.

[84] Anand Rotte. Combination of CTLA-4 and PD-1 blockers for treatment of cancer. *Journal of Experimental & Clinical Cancer Research*, 38(1):255, June 2019.

[85] Jedd D. Wolchok, Harriet Kluger, Margaret K. Callahan, Michael A. Postow, Naiyer A. Rizvi, Alexander M. Lesokhin, Neil H. Segal, Charlotte E. Ariyan, Ruth-Ann Gordon, Kathleen Reed, Matthew M. Burke, Anne Caldwell, Stephanie A. Kronenberg, Blessing U. Agunwamba, Xiaoling Zhang, Israel Lowy, Hector David Inzunza, William

Feely, Christine E. Horak, Quan Hong, Alan J. Korman, Jon M. Wigginton, Ashok Gupta, and Mario Sznol. Nivolumab plus ipilimumab in advanced melanoma. *The New England Journal of Medicine*, 369(2):122–133, July 2013.

[86] Su Yin Lim, Elena Shklovskaya, Jenny H. Lee, Bernadette Pedersen, Ashleigh Stewart, Zizhen Ming, Mal Irvine, Brindha Shivalingam, Robyn P. M. Saw, Alexander M. Menzies, Matteo S. Carlino, Richard A. Scolyer, Georgina V. Long, and Helen Rizos. The molecular and functional landscape of resistance to immune checkpoint blockade in melanoma. *Nature Communications*, 14:1516, March 2023.

[87] Stefani Spranger and Thomas F. Gajewski. Impact of oncogenic pathways on evasion of antitumour immune responses. *Nature Reviews. Cancer*, 18(3):139–147, March 2018.

[88] Vyara Matson, Jessica Fessler, Riyue Bao, Tara Chongsuwat, Yuanyuan Zha, Maria-Luisa Alegre, Jason J. Luke, and Thomas F. Gajewski. The commensal microbiome is associated with antiPD-1 efficacy in metastatic melanoma patients. *Science*, 359(6371):104–108, January 2018.

[89] Vyara Matson and Thomas F. Gajewski. Dietary modulation of the gut microbiome as an immunoregulatory intervention. *Cancer Cell*, 40(3):246–248, March 2022. Publisher: Elsevier.

[90] Jesse M. Zaretsky, Angel Garcia-Diaz, Daniel S. Shin, Helena Escuin-Ordinas, Willy Hugo, Siwen Hu-Lieskovan, Davis Y. Torrejon, Gabriel Abril-Rodriguez, Salemiz Sandoval, Lucas Barthly, Justin Saco, Blanca Homet Moreno, Riccardo Mezzadra, Bartosz Chmielowski, Kathleen Ruchalski, I. Peter Shintaku, Phillip J. Sanchez, Cristina Puig-Saus, Grace Cherry, Elizabeth Seja, Xiangju Kong, Jia Pang, Beata Berent-Maoz, Begoña Comin-Anduix, Thomas G. Graeber, Paul C. Tumeh, Ton N. M. Schumacher, Roger S. Lo, and Antoni Ribas. Mutations Associated with Acquired Resistance to PD-1 Blockade in Melanoma. *The New England Journal of Medicine*, 375(9):819–829, September 2016.

[91] Moshe Sade-Feldman, Yunxin J. Jiao, Jonathan H. Chen, Michael S. Rooney, Michal Barzily-Rokni, Jean-Pierre Eliane, Stacey L. Bjorgaard, Marc R. Hammond, Hans Vitzthum, Shauna M. Blackmon, Dennie T. Frederick, Mehlika Hazar-Rethinam, Brandon A. Nadres, Emily E. Van Seventer, Sachet A. Shukla, Keren Yizhak, John P. Ray, Daniel Rosebrock, Dimitri Livitz, Viktor Adalsteinsson, Gad Getz, Lyn M. Duncan, Bo Li, Ryan B. Corcoran, Donald P. Lawrence, Anat Stemmer-Rachamimov, Genevieve M. Boland, Dan A. Landau, Keith T. Flaherty, Ryan J. Sullivan, and Nir Hacohen. Resistance to checkpoint blockade therapy through inactivation of antigen presentation. *Nature Communications*, 8(1):1136, October 2017.

[92] Cheng Wang, Cheng Ma, Lihong Gong, Yuqin Guo, Ke Fu, Yafang Zhang, Honglin Zhou, and Yunxia Li. Macrophage Polarization and Its Role in Liver Disease. *Frontiers in Immunology*, 12:803037, December 2021.

[93] Abbas Shapouri-Moghaddam, Saeed Mohammadian, Hossein Vazini, Mahdi Taghadosi, Seyed-Alireza Esmaeili, Fatemeh Mardani, Bita Seifi, Asadollah Mohammadi, Jalil T. Afshari, and Amirhossein Sahebkar. Macrophage plasticity, polarization, and function in health and disease. *Journal of Cellular Physiology*, 233(9):6425–6440, September 2018.

[94] Andrew J. Fleetwood, Toby Lawrence, John A. Hamilton, and Andrew D. Cook. Granulocyte-macrophage colony-stimulating factor (CSF) and macrophage CSF-dependent macrophage phenotypes display differences in cytokine profiles and transcription factor activities: implications for CSF blockade in inflammation. *Journal of Immunology (Baltimore, Md.: 1950)*, 178(8):5245–5252, April 2007.

[95] Klaus Ley, Norbert Gerdes, and Holger Winkels. How co-stimulatory and co-inhibitory pathways shape atherosclerosis. *Arteriosclerosis, thrombosis, and vascular biology*, 37(5):764–777, May 2017.

[96] Jörg Reutershan, Margaret A. Morris, Tracy L. Burcin, David F. Smith, Daniel Chang, Mary S. Saprito, and Klaus Ley. Critical role of endothelial CXCR2 in LPS-induced neutrophil migration into the lung. *The Journal of Clinical Investigation*, 116(3):695–702, March 2006.

[97] Jolanta Maria Dzik. Evolutionary roots of arginase expression and regulation. *Frontiers in Immunology*, 5:544, 2014.

[98] Miguel Relloso, Amaya Puig-Kröger, Oscar Muñiz Pello, José Luis Rodríguez-Fernández, Gonzalo de la Rosa, Natividad Longo, Joaquín Navarro, Mari Angeles Muñoz-Fernández, Paloma Sánchez-Mateos, and Angel L. Corbí. DC-SIGN (CD209) expression is IL-4 dependent and is negatively regulated by IFN, TGF-beta, and anti-inflammatory agents. *Journal of Immunology (Baltimore, Md.: 1950)*, 168(6):2634–2643, March 2002.

[99] F. Porcheray, S. Viaud, A.-C. Rimaniol, C. Léone, B. Samah, N. Dereuddre-Bosquet, D. Dormont, and G. Gras. Macrophage activation switching: an asset for the resolution of inflammation. *Clinical and Experimental Immunology*, 142(3):481–489, December 2005.

[100] Sara Tucci, Ulrich Floegel, Frauke Beermann, Sidney Behringer, and Ute Spiekerkoetter. Triheptanoin: long-term effects in the very long-chain acyl-CoA dehydrogenase-deficient mouse. *Journal of Lipid Research*, 58(1):196–207, January 2017.

[101] Zhaonian Hao, Ruyuan Li, Yuanyuan Wang, Shuangying Li, Zhenya Hong, and Zhiqiang Han. Landscape of Myeloid-derived Suppressor Cell in Tumor Immunotherapy. *Biomarker Research*, 9(1):77, October 2021.

[102] Jinpu Yu, Weijiao Du, Fang Yan, Yue Wang, Hui Li, Shui Cao, Wenwen Yu, Chun Shen, Juntian Liu, and Xiubao Ren. Myeloid-derived suppressor cells suppress antitumor immune responses through IDO expression and correlate with lymph node

metastasis in patients with breast cancer. *Journal of Immunology (Baltimore, Md.: 1950)*, 190(7):3783–3797, April 2013.

[103] Paolo Serafini, Stephanie Mgebroff, Kimberly Noonan, and Ivan Borrello. Myeloid-derived suppressor cells promote cross-tolerance in B-cell lymphoma by expanding regulatory T cells. *Cancer Research*, 68(13):5439–5449, July 2008.

[104] Yosuke Togashi and Hiroyoshi Nishikawa. Regulatory T Cells: Molecular and Cellular Basis for Immunoregulation. *Current Topics in Microbiology and Immunology*, 410:3–27, 2017.

[105] Marco De Simone, Alberto Arrigoni, Grazisa Rossetti, Paola Gruarin, Valeria Ranzani, Claudia Politano, Raoul J. P. Bonnal, Elena Provasi, Maria Lucia Sarnicola, Ilaria Panzeri, Monica Moro, Mariacristina Crosti, Saveria Mazzara, Valentina Vaira, Silvano Bosari, Alessandro Palleschi, Luigi Santambrogio, Giorgio Bovo, Nicola Zucchini, Mauro Totis, Luca Gianotti, Giancarlo Cesana, Roberto A. Perego, Nirvana Maroni, Andrea Pisani Ceretti, Enrico Opocher, Raffaele De Francesco, Jens Geginat, Hendrik G. Stunnenberg, Sergio Abrignani, and Massimiliano Pagani. Transcriptional Landscape of Human Tissue Lymphocytes Unveils Uniqueness of Tumor-Infiltrating T Regulatory Cells. *Immunity*, 45(5):1135–1147, November 2016.

[106] Daisuke Sugiyama, Hiroyoshi Nishikawa, Yuka Maeda, Megumi Nishioka, Atsushi Tanemura, Ichiro Katayama, Sachiko Ezoe, Yuzuru Kanakura, Eiichi Sato, Yasuo Fukumori, Julia Karbach, Elke Jäger, and Shimon Sakaguchi. Anti-CCR4 mAb selectively depletes effector-type FoxP3+CD4+ regulatory T cells, evoking antitumor immune responses in humans. *Proceedings of the National Academy of Sciences of the United States of America*, 110(44):17945–17950, October 2013.

[107] Wolf Herman Fridman, Franck Pagès, Catherine Sautès-Fridman, and Jérôme Galon. The immune contexture in human tumours: impact on clinical outcome. *Nature Reviews. Cancer*, 12(4):298–306, March 2012.

[108] Rushikesh S. Joshi, Samanvi S. Kanugula, Sweta Sudhir, Matheus P. Pereira, Saket Jain, and Manish K. Aghi. The Role of Cancer-Associated Fibroblasts in Tumor Progression. *Cancers*, 13(6):1399, March 2021.

[109] Fei Xing, Jamila Saidou, and Kounosuke Watabe. Cancer associated fibroblasts (CAFs) in tumor microenvironment. *Frontiers in Bioscience (Landmark Edition)*, 15(1):166–179, January 2010.

[110] Barbara Érsek, Pálma Silló, Ugur Cakir, Viktor Molnár, András Bencsik, Balázs Mayer, Eva Mezey, Sarolta Kárpáti, Zoltán Pós, and Krisztián Németh. Melanoma-associated fibroblasts impair CD8+T cell function and modify expression of immune checkpoint regulators via increased arginase activity. *Cellular and molecular life sciences: CMLS*, 78(2):661–673, January 2021.

[111] Luca Cassetta and Jeffrey W. Pollard. A timeline of tumour-associated macrophage biology. *Nature Reviews Cancer*, 23(4):238–257, April 2023. Publisher: Nature Publishing Group.

[112] Jeffrey W. Pollard. Trophic macrophages in development and disease. *Nature Reviews. Immunology*, 9(4):259–270, April 2009.

[113] Thomas A. Wynn, Ajay Chawla, and Jeffrey W. Pollard. Macrophage biology in development, homeostasis and disease. *Nature*, 496(7446):445–455, April 2013.

[114] Frances R. Balkwill and Alberto Mantovani. Cancer-related inflammation: common themes and therapeutic opportunities. *Seminars in Cancer Biology*, 22(1):33–40, February 2012.

[115] Inhibition of Mac-1 (CD11b/CD18) enhances tumor response to radiation by reducing myeloid cell recruitment - PubMed.

[116] Bin-Zhi Qian and Jeffrey W. Pollard. Macrophage diversity enhances tumor progression and metastasis. *Cell*, 141(1):39–51, April 2010.

[117] Kai Kessenbrock, Vicki Plaks, and Zena Werb. Matrix metalloproteinases: regulators of the tumor microenvironment. *Cell*, 141(1):52–67, April 2010.

[118] Douglas Hanahan and Lisa M. Coussens. Accessories to the crime: functions of cells recruited to the tumor microenvironment. *Cancer Cell*, 21(3):309–322, March 2012.

[119] Craig Murdoch, Munitta Muthana, Seth B. Coffelt, and Claire E. Lewis. The role of myeloid cells in the promotion of tumour angiogenesis. *Nature Reviews. Cancer*, 8(8):618–631, August 2008.

[120] Rosandra N. Kaplan, Rebecca D. Riba, Stergios Zacharoulis, Anna H. Bramley, Loïc Vincent, Carla Costa, Daniel D. MacDonald, David K. Jin, Koji Shido, Scott A. Kerns, Zhenping Zhu, Daniel Hicklin, Yan Wu, Jeffrey L. Port, Nasser Altorki, Elisa R. Port, Davide Ruggero, Sergey V. Shmelkov, Kristian K. Jensen, Shahin Rafii, and David Lyden. VEGFR1-positive haematopoietic bone marrow progenitors initiate the premetastatic niche. *Nature*, 438(7069):820–827, December 2005.

[121] Bethan Psaila and David Lyden. The Metastatic Niche: Adapting the Foreign Soil. *Nature reviews. Cancer*, 9(4):285–293, April 2009.

[122] Sachie Hiratsuka, Akira Watanabe, Hiroyuki Aburatani, and Yoshiro Maru. Tumour-mediated upregulation of chemoattractants and recruitment of myeloid cells predetermines lung metastasis. *Nature Cell Biology*, 8(12):1369–1375, December 2006.

[123] Yu Zhu, Brett L. Knolhoff, Melissa A. Meyer, Timothy M. Nywening, Brian L. West, Jingqin Luo, Andrea Wang-Gillam, S. Peter Goedegebuure, David C. Linehan, and David G. DeNardo. CSF1/CSF1R blockade reprograms tumor-infiltrating

macrophages and improves response to T-cell checkpoint immunotherapy in pancreatic cancer models. *Cancer Research*, 74(18):5057–5069, September 2014.

[124] Christina Pfirschke, Rapolas Zilionis, Camilla Engblom, Marius Messemaker, Angela E. Zou, Steffen Rickelt, Nicolas A. Gort-Freitas, Yunkang Lin, Ruben Bill, Marie Siwicki, Jeremy Gungabeesoon, Melissa M. Sprachman, Angela N. Marquard, Christopher B. Rodell, Michael F. Cuccarese, Jeremy Quintana, Maaz S. Ahmed, Rainer H. Kohler, Virginia Savova, Ralph Weissleder, Allon M. Klein, and Mikael J. Pittet. Macrophage-Targeted Therapy Unlocks Antitumoral Cross-talk between IFN-Secreting Lymphocytes and IL12-Producing Dendritic Cells. *Cancer Immunology Research*, 10(1):40–55, January 2022.

[125] Da-Ke Li and Wen Wang. Characteristics and clinical trial results of agonistic anti-CD40 antibodies in the treatment of malignancies. *Oncology Letters*, 20(5):176, November 2020.

[126] Abhishek S. Kashyap, Martina Schmittnaegel, Nicolò Rigamonti, Daniela Pais-Ferreira, Philipp Mueller, Melanie Buchi, Chia-Huey Ooi, Matthias Kreuzaler, Petra Hirschmann, Alan Guichard, Natascha Rieder, Ruben Bill, Frank Herting, Yvonne Kienast, Stefan Dirnhofer, Christian Klein, Sabine Hoves, Carola H. Ries, Emily Corse, Michele De Palma, and Alfred Zippelius. Optimized antiangiogenic reprogramming of the tumor microenvironment potentiates CD40 immunotherapy. *Proceedings of the National Academy of Sciences of the United States of America*, 117(1):541–551, January 2020.

[127] Gregory L. Beatty, Elena G. Chiorean, Matthew P. Fishman, Babak Saboury, Ursina R. Teitelbaum, Weijing Sun, Richard D. Huhn, Wenru Song, Dongguang Li, Leslie L. Sharp, Drew A. Torigian, Peter J. O'Dwyer, and Robert H. Vonderheide. CD40 agonists alter tumor stroma and show efficacy against pancreatic carcinoma in mice and humans. *Science (New York, N.Y.)*, 331(6024):1612–1616, March 2011.

[128] Sabine Hoves, Chia-Huey Ooi, Carsten Wolter, Hadassah Sade, Stefan Bissinger, Martina Schmittnaegel, Oliver Ast, Anna M. Giusti, Katharina Wartha, Valeria Runza, Wei Xu, Yvonne Kienast, Michael A. Cannarile, Hyam Levitsky, Solange Romagnoli, Michele De Palma, Dominik Rüttinger, and Carola H. Ries. Rapid activation of tumor-associated macrophages boosts preexisting tumor immunity. *The Journal of Experimental Medicine*, 215(3):859–876, March 2018.

[129] Christoph Hafemeister and Rahul Satija. Normalization and variance stabilization of single-cell RNA-seq data using regularized negative binomial regression. *Genome Biology*, 20(1):296, December 2019.

[130] Akihiro Hirata, Jochen Utikal, Satoshi Yamashita, Hitomi Aoki, Akira Watanabe, Takuya Yamamoto, Hideyuki Okano, Nabeel Bardeesy, Takahiro Kunisada, Toshikazu Ushijima, Akira Hara, Rudolf Jaenisch, Konrad Hochedlinger, and Yasuhiro Yamada. Dose-dependent roles for canonical Wnt signalling in de novo crypt formation and

cell cycle properties of the colonic epithelium. *Development (Cambridge, England)*, 140(1):66–75, January 2013.

[131] Andrea Ziblat, Brendan L. Horton, Emily F. Higgs, Ken Hatogai, Anna Martinez, Jason W. Shapiro, Danny E. C. Kim, YuanYuan Zha, Randy F. Sweis, and Thomas F. Gajewski. Batf3+ DCs and the 4-1BB/4-1BBL axis are required at the effector phase in the tumor microenvironment for PD-1/PD-L1 blockade efficacy. *Cell Reports*, 43(5):114141, May 2024.

[132] Caihong Wang, Jingjing Yan, Pan Yin, Liming Gui, Lu Ji, Bin Ma, and Wei-Qiang Gao. -Catenin inhibition shapes tumor immunity and synergizes with immunotherapy in colorectal cancer. *Oncoimmunology*, 9(1):1809947.

[133] Junli Xue, Xuetao Yu, Liqiong Xue, Xiaoxiao Ge, Wei Zhao, and Wei Peng. Intrinsic -catenin signaling suppresses CD8+ T-cell infiltration in colorectal cancer. *Biomedicine & Pharmacotherapy = Biomedecine & Pharmacotherapie*, 115:108921, July 2019.

[134] Xin Li, Yanwei Xiang, Fulun Li, Chengqian Yin, Bin Li, and Xisong Ke. WNT/-Catenin Signaling Pathway Regulating T Cell-Inflammation in the Tumor Microenvironment. *Frontiers in Immunology*, 10:2293, 2019.

[135] Zachary Steinhart and Stephane Angers. Wnt signaling in development and tissue homeostasis. *Development (Cambridge, England)*, 145(11):dev146589, June 2018.

[136] Xun Zhang, Nazhen Dong, and Xiaoyan Hu. Wnt/-catenin Signaling Inhibitors. *Current Topics in Medicinal Chemistry*, 23(10):880–896, 2023.

[137] Ann Neiheisel, Manpreet Kaur, Nancy Ma, Patty Havard, and Anitha K. Shenoy. Wnt pathway modulators in cancer therapeutics: An update on completed and ongoing clinical trials. *International Journal of Cancer*, 150(5):727–740, 2022. _eprint: https://onlinelibrary.wiley.com/doi/pdf/10.1002/ijc.33811.

[138] Ya Zhang and Xin Wang. Targeting the Wnt/-catenin signaling pathway in cancer. *Journal of Hematology & Oncology*, 13(1):165, December 2020.

[139] Sewoon Kim and Sunjoo Jeong. Mutation Hotspots in the -Catenin Gene: Lessons from the Human Cancer Genome Databases. *Molecules and Cells*, 42(1):8–16, January 2019.

[140] Martina Severa, Sabina A. Islam, Stephen N. Waggoner, Zhaozhao Jiang, Nancy D. Kim, Glennice Ryan, Evelyn Kurt-Jones, Israel Charo, Daniel R. Caffrey, Victor L. Boyartchuk, Andrew D. Luster, and Katherine A. Fitzgerald. The transcriptional repressor BLIMP1 curbs host defenses by suppressing expression of the chemokine CCL8. *Journal of Immunology (Baltimore, Md.: 1950)*, 192(5):2291–2304, March 2014.

[141] Jie Ji, Peiru Wang, Qian Zhou, Lude Zhu, Haiyan Zhang, Yunfeng Zhang, Zhe Zheng, Anil Kumar Bhatta, Goulong Zhang, and Xiuli Wang. CCL8 enhances sensitivity of cutaneous squamous cell carcinoma to photodynamic therapy by recruiting M1 macrophages. *Photodiagnosis and Photodynamic Therapy*, 26:235–243, June 2019.

[142] Peipei Yang, Wanrong Chen, Hua Xu, Junhan Yang, Jinghang Jiang, Yunhui Jiang, and Ganglin Xu. Correlation of CCL8 expression with immune cell infiltration of skin cutaneous melanoma: potential as a prognostic indicator and therapeutic pathway. *Cancer Cell International*, 21(1):635, November 2021.

[143] Tsukasa Hori, Yasuyoshi Naishiro, Hitoshi Sohma, Nobuhiro Suzuki, Naoki Hatakeyama, Masaki Yamamoto, Tomoko Sonoda, Yuka Mizue, Kohzoh Imai, Hiroyuki Tsutsumi, and Yasuo Kokai. CCL8 is a potential molecular candidate for the diagnosis of graft-versus-host disease. *Blood*, 111(8):4403–4412, April 2008.

[144] Keita Igarashi, Norio Takei, Tsukasa Hori, Masaki Yamamoto, and Yasuo Kokai. CCL8 Deficiency in Host Strongly Inhibits Early Mortality and Morbidity of Graft-Versus-Host Disease in Mice. *Blood*, 124(21):1096, December 2014.

[145] E. Farmaki, I. Chatzistamou, V. Kaza, and H. Kiaris. A CCL8 gradient drives breast cancer cell dissemination. *Oncogene*, 35(49):6309–6318, December 2016.

[146] E. C. Halvorsen, M. J. Hamilton, A. Young, B. J. Wadsworth, N. E. LePard, H. N. Lee, N. Firmino, J. L. Collier, and K. L. Bennewith. Maraviroc decreases CCL8-mediated migration of CCR5+ regulatory T cells and reduces metastatic tumor growth in the lungs. *OncoImmunology*, 5(6):e1150398, June 2016. Publisher: Taylor & Francis _eprint: https://doi.org/10.1080/2162402X.2016.1150398.

[147] Luca Cassetta, Stamatina Fragkogianni, Andrew H. Sims, Agnieszka Swierczak, Lesley M. Forrester, Hui Zhang, Daniel Y. H. Soong, Tiziana Cotechini, Pavana Anur, Elaine Y. Lin, Antonella Fidanza, Martha Lopez-Yrigoyen, Michael R. Millar, Alexandra Urman, Zhichao Ai, Paul T. Spellman, E. Shelley Hwang, J. Michael Dixon, Lisa Wiechmann, Lisa M. Coussens, Harriet O. Smith, and Jeffrey W. Pollard. Human Tumor-Associated Macrophage and Monocyte Transcriptional Landscapes Reveal Cancer-Specific Reprogramming, Biomarkers, and Therapeutic Targets. *Cancer Cell*, 35(4):588–602.e10, April 2019.

[148] Elena Farmaki, Vimala Kaza, Ioulia Chatzistamou, and Hippokratis Kiaris. CCL8 Promotes Postpartum Breast Cancer by Recruiting M2 Macrophages. *iScience*, 23(6):101217, June 2020.

[149] Hyung Sook Kim, Hong Kyung Lee, Kihyeon Kim, Gi Beom Ahn, Min Sung Kim, Tae Yong Lee, Dong Ju Son, Youngsoo Kim, Jin Tae Hong, and Sang-Bae Han. Mesenchymal stem cells enhance CCL8 expression by podocytes in lupus-prone MRL.Faslpr mice. *Scientific Reports*, 13(1):13074, August 2023. Publisher: Nature Publishing Group.

[150] Xiaoli Lou, Ke Zhao, Jingze Xu, Lixiong Shuai, Hui Niu, Zhifei Cao, Juan Wang, and Yongsheng Zhang. CCL8 as a promising prognostic factor in diffuse large B-cell lymphoma via M2 macrophage interactions: A bioinformatic analysis of the tumor microenvironment. *Frontiers in Immunology*, 13, 2022.

[151] Antonio Sica. Macrophages give Gas(6) to cancer. *Blood*, 115(11):2122–2123, March 2010.

[152] Guiling Wu, Zhiqiang Ma, Yicheng Cheng, Wei Hu, Chao Deng, Shuai Jiang, Tian Li, Fulin Chen, and Yang Yang. Targeting Gas6/TAM in cancer cells and tumor microenvironment. *Molecular Cancer*, 17(1):20, January 2018.

[153] Kayla V. Myers, Sarah R. Amend, and Kenneth J. Pienta. Targeting Tyro3, Axl and MerTK (TAM receptors): implications for macrophages in the tumor microenvironment. *Molecular Cancer*, 18(1):94, May 2019.

[154] Angelica M. Gomes, Emily C. Carron, Kylie L. Mills, Alexa M. Dow, Zane Gray, Christopher R. Fecca, Meredith A. Lakey, Peter Carmeliet, Frances Kittrell, Daniel Medina, and Heather L. Machado. Stromal Gas6 promotes the progression of premalignant mammary cells. *Oncogene*, 38(14):2437–2450, April 2019. Publisher: Nature Publishing Group.

[155] Saroj Nepal, Chinnaswamy Tiruppathi, Yoshikazu Tsukasaki, Joseph Farahany, Manish Mittal, Jalees Rehman, Darwin J. Prockop, and Asrar B. Malik. STAT6 induces expression of Gas6 in macrophages to clear apoptotic neutrophils and resolve inflammation. *Proceedings of the National Academy of Sciences of the United States of America*, 116(33):16513–16518, August 2019.

[156] Lucy Ireland, Teifion Luckett, Michael C. Schmid, and Ainhoa Mielgo. Blockade of Stromal Gas6 Alters Cancer Cell Plasticity, Activates NK Cells, and Inhibits Pancreatic Cancer Metastasis. *Frontiers in Immunology*, 11:297, February 2020.

[157] Yihui Shao, Yang Li, Yan Liu, Shuolin Zhu, Jianing Wu, Ke Ma, Guoqi Li, Shan Huang, Haichu Wen, Congcong Zhang, Xin-liang Ma, Ping Li, Jie Du, and Yulin Li. ATF3 coordinates the survival and proliferation of cardiac macrophages and protects against ischemiareperfusion injury. *Nature Cardiovascular Research*, 3(1):28–45, January 2024. Publisher: Nature Publishing Group.